To keep or not to keep: The molecular mechanisms of activity-dependent synapse refinement

HARVARD UNIVERSITY
Graduate School of Arts and Sciences

DISSERTATION ACCEPTANCE CERTIFICATE

The undersigned, appointed by the

Division of Medical Sciences

Program in Neuroscience

have examined a dissertation entitled

To keep or not to keep: The molecular mechanisms of activity-dependent synaptic refinement

presented by Sivapratha Nagappan Chettiar

candidate for the degree of Doctor of Philosophy and hereby certify that it is worthy of acceptance.

Signature: _____

Typed Name: Dr. Joshua Sanes

Signature: Michael Greenberg (Aug 26, 2020 16:03 EDT)

Typed Name: Dr. Michael Greenberg

Signature: Thomas Schwarz (Aug 29, 2020 16:23 EDT)

Typed Name: Dr. Thomas Schwarz

Signature: _____

Typed Name: Dr. Carol Mason

Date: August 25, 2020

To keep or not to keep: The molecular mechanisms of activity-dependent synapse refinement

A dissertation presented

by

Sivapratha Nagappan Chettiar

to

The Division of Medical Sciences

in partial fulfillment of the requirements

for the degree of

Doctor of Philosophy

in the subject of

Neuroscience

Harvard University

Cambridge, Massachusetts

August 2020

Dissertation Advisor: Dr. Hisashi Umemori Sivapratha Nagappan Chettiar

To keep or not to keep:

The molecular mechanisms of activity-dependent synapse refinement

Abstract

To establish efficient neural networks, neurons selectively *strengthen active* synapses and *eliminate inactive* ones through a neuronal activity-dependent developmental process known as *synaptic refinement*. Aberrant synaptic refinement underlies several neuropsychiatric disorders. However, the molecular mechanisms that detect neuronal activity and accordingly determine synaptic connectivity remain to be elucidated.

Active synapses undergo synapse maturation, a process regulated by the transmembrane protein, SIRPα. In the presence of synaptic activity, SIRPα's ectodomain is cleaved and released to strengthen synapses. I determined *how SIRPα detects synaptic activity to function at and strengthen active synapses*. I showed that SIRPα tyrosine-phosphorylation, which is driven by neuronal activity, drives SIRPα cleavage, which in turn, stabilizes synapses in an activity-dependent manner. This work identified a new role for SIRPα phosphorylation and established a novel mechanism through which neuronal activity regulates SIRPα function to promote proper refinement.

Inactive synapses are eliminated. We demonstrated that inactive synapses in the brain are eliminated only when there are active connections to compete with. This suggests that active connections send *'punishment'* signals that trigger *'elimination'* signals within inactive synapses and instruct them to leave. However, *the molecular signals that determine inactive synapse elimination are unknown.* Here, we identified the tyrosine kinases, Pyk2 and JAK2 as

determinants of inactive synapse elimination. I showed that Pyk2 is necessary for functional and structural synaptic elimination, and is activated at inactive synapses, but only in the presence of other active ones. JAK2, a Pyk2-interacting kinase activated at inactive synapses, is necessary and sufficient for synaptic elimination. This work uncovered key mechanisms that dictate the elimination of inactive synapses.

Finally, I reasoned that *'punishment'* signals that drive the elimination of inactive synapses may target other active synapses as well. To prevent the elimination of active synapses, I proposed that a *'stabilization'* signal *signals at and protects active synapses*. I hypothesized that signals that strengthen active synapses, i.e. SIRPα, may also stabilize them. Indeed, we showed that SIRPα suppresses Pyk2/JAK2 activation and prevents synaptic elimination. Together, this work established the molecular bridges that link neuronal activity to synaptic connectivity, thus, furthering our understanding of brain development and function.

Acknowledgements

I have been exceedingly fortunate to have had an incredible amount of scientific, non-scientific and life-in-general support throughout my graduate career. For this, I am grateful.

The person I am most thankful for is Hisashi Umemori, my PhD mentor for all his help, mentorship and support. Working with Hisashi has helped me grow into the person and scientist I am today. I am grateful to Hisashi for teaching me that learning how to think is more important (slightly) than producing data; for making me ask five questions in lab meetings, which has made me a better and bolder communicator; for weekly meetings that I always left feeling more motivated; for large amounts of technical advice that included a late night, weekend Western blot tutorial; and for (Pyk)ing me to join the lab, patiently helping me through my failures and celebrating my successes. I am also thankful to Hisashi for creating a really great scientific environment in the lab.

I have to say a special thank you to three postdocs in the lab, Masahiro Yasuda, Erin M. Johnson-Venkatesh, and Akiko Terauchi. Masa – for letting me join you on this exciting scientific adventure into activity-dependent synaptic refinement; for sharing your technical expertise; and for teaching me that many things that are broken, can often be fixed, with some creativity. Erin – for patiently teaching me electrophysiology and letting me use your precious rig; for being a warm friend, mentor and cheerleader scientifically and personally; and for letting me “borrow” your fantastic kids when I just needed to be a kid again. Akiko – for being the lab “mom” with an incredible level of organization and meticulousness; for readily having answers to any question and mice for experiments; and for the constant supply of Kit Kats. I also want to acknowledge members of the Umemori lab, past and present, for feedback, support and lunch/coffee dates.

I would like to thank my Dissertation Advisory Committee – Joshua Sanes, Chinfei Chen, and Matthew Pecot. I truly enjoyed the discussions during my DAC meetings and the feedback and suggestions have helped me grow as a scientist. Josh, Chinfei and Matt’s support often left me feeling more confident, excited and focused after my DAC meetings. I also thank my Defense

Advisory Committee – Michael Greenberg, Thomas Schwarz, Carol Mason (Columbia University) and Josh, for staying on as the chair. I also thank my Student Advisory Committee member, Rachel Wilson, for helping me be an adult.

Thank you to the Program in Neuroscience – directors: Rosalind Segal, John Assad and David Ginty, and administrators: Karen Harmin and Susan Jackson – for welcoming me into this program and creating a supportive environment and community for all students.

I have also been fortunate to have had a strong network of peers and friends. To Jennifer Helble – for being my grad school partner and gym buddy; for making Boston into an adventure. To Dhiral Chheda, Michael Walsh, Aubrie Soucy, Imelda Ko, Kamini Iyer, Sindana Ilango, Pooja Jaeel, Divya Narayanan, Nicholas Silva – for all the support, advice and fun. To my Assuntarians – for making home always feel like home.

Last, but certainly not least, I must thank my family, without whom, I would not be here today. Living across an ocean from one another for over a decade has not been easy. It'll be difficult to express my gratitude for all the sacrifice. To my uncle, Asok – for teaching me how to see the humor even when things aren't going great. To my Appa and Amma – for the never-ending amount of love and support; for allowing me to dream big; for teaching me the importance of learning, thinking and being creative; for teaching me that "when the going gets tough, the tough get going"; and for always keeping me grounded. To my sister, Shivathmihai – for always being there for me; for being my best friend; and for inspiring me to be a better human.

Table of contents

Listing of figures

To Nagappan Chettiar Rengasamy, Suseela Malakolunthu and Shivathmihai Nagappan

My Appa, Amma and favorite sister

Chapter 1.

General introduction and background

Parts of this chapter are adapted from a published review I wrote with Erin M. Johnson-Venkatesh and Hisashi Umemori. Nagappan-Chettiar, S., Johnson-Venkatesh, E. M., Umemori, H. (2017). Neurosci Res. ***116****, 60-69.*

1.1 General introduction

Neuronal activity is at the heart of information transfer and processing in the brain. Neuronal activity, in the form of synaptic transmission, also regulates the development, strength, and remodeling of neuronal networks. Impaired development and function of neuronal networks underlies a number of devastating neurological and psychiatric disorders. Thus, an important question is how neuronal activity is detected and then converted into the molecular signals that regulate neuronal network connectivity and function. In this thesis, I address this key question by focusing on the role of neuronal activity during excitatory synaptic development.

Synapses are highly specialized nodes within the neuronal network that facilitate information transfer between presynaptic nerve terminals and their postsynaptic targets. This information transfer occurs via chemical transmission in the form of neurotransmitter release. The most prominent of synapses in the brain are the excitatory glutamatergic synapses. These are synapses that signal via the release of the neurotransmitter, glutamate, to drive the excitation of the postsynaptic target. In order for the brain to function efficiently, synapses and synaptic networks have to develop in a highly precise and organized manner. Aberrant excitatory synaptic connectivity is implicated in a number of neuropsychiatric diseases including autism spectrum disorders (ASD) and schizophrenia (Tang et al., 2014; Sekar et al., 2016; Sellgren et al., 2019). Thus, it is critical that we establish a comprehensive understanding of how synaptic networks are developed.

Synapses develop via multiple stages: 1) axon elongation and targeting, 2) synaptic differentiation, and 3) synaptic refinement, which includes both the maturation of active synapses and the elimination of inactive ones. After completing these developmental stages, synapses are maintained into adulthood (Sanes and Lichtman, 1999; Fox and Umemori, 2006; Johnson-Venkatesh and Umemori, 2010). The first two stages of synapse development are thought to be largely neuronal activity independent. However, the final stage of synaptic refinement is orchestrated by neuronal activity (Fig. 1.1). *Here, I focus on the synaptic refinement stage and determine the molecular switches that detect neuronal activity and appropriately turn on the signals that regulate synaptic refinement. Specifically, I ask how neurons detect different levels of synaptic activity and determine which synapses to strengthen and stabilize and which ones to eliminate.*

1.2 Synaptic refinement – A critical stage of neural network development

The brain is a remarkable organ with the capacity to be modified by and adapt to the changing external environment we experience. This adaptability is especially critical for brain development, where synaptic networks optimize the connections they form based on the surrounding environment. Pioneering work by Hubel and Wiesel demonstrated that during synaptic refinement, sensory experience shapes and refines synaptic networks in the developing visual system (Hubel and Wiesel, 1970; Hubel et al., 1977). This work and work done in other regions of the nervous system established that the process of synaptic refinement finetunes the developing brain such that some connections are eliminated, while the remaining connections are stabilized and strengthened to form the mature synaptic networks of the adult brain (Katz and Shatz, 1996; Sanes and Lichtman, 1999). Synaptic refinement is a key feature of the developing human brain. Electron micrographs of human brain tissue showed that synaptic density peaks in the human cortex from 1-5 years of age and decreases during adolescence to reach a stable density that is maintained into adulthood (Huttenlocher, 1979). Impaired synaptic refinement leads

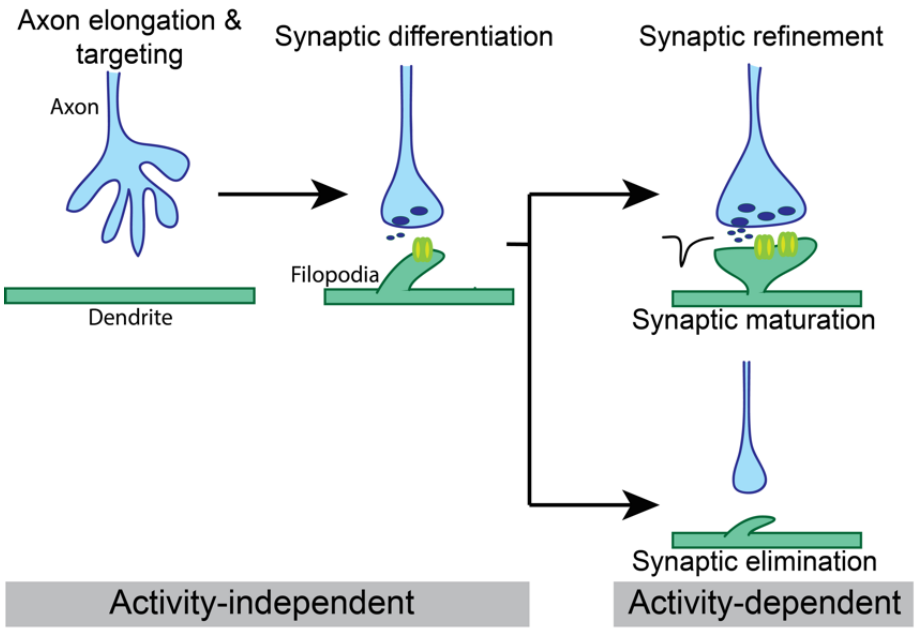

FIGURE 1.1. Stages of excitatory synaptic development.

Synaptic development occurs in distinct steps.

During the *axon elongation and targeting* stage, a newly differentiated neuron extends its axon. This axon elongation is often led by a highly dynamic growth cone that detects extracellular cues to identify its appropriate target (in the brain, this is often a neuronal dendrite).

Upon contacting its target, *synaptic differentiation* occurs. The growth cone becomes a presynaptic terminal with neurotransmitter release machinery and the dendrite forms a postsynaptic terminal that contains neurotransmitter receptors and machinery to process the signals received. Often, this stage produces more synapses than what is needed for and found in a functional adult brain.

The *synaptic refinement* process removes the excess synapses produced (*synaptic elimination*) and strengthens remaining ones (*synaptic maturation*). Synaptic refinement is regulated by neuronal activity and includes both the maturation of active synapses and the elimination of inactive ones.

to a range of neuropsychiatric disorders, including ASD and schizophrenia, further highlighting the importance of this process (Noutel et al., 2011; Tang et al., 2014; Sekar et al., 2016; Sellgren et al., 2019).

While the molecular mechanisms underlying synaptic refinement in the brain remain to be elucidated, work done in our lab and by others have established that this process is dependent on neuronal activity (Sretavan et al., 1984, Penn et al., 1998; Buffelli et al., 2003; Kano and Hashimoto, 2009; Yasuda et al., 2011). In general, during the process of activity-dependent synaptic refinement active, functional inputs are strengthened while inactive, non-functional inputs are eliminated (*activity-dependent*; Fig. 1.2 A, C and D).

Synaptic elimination is also considered to be a competition between active and inactive inputs for postsynaptic territory and resources. When all inputs are equal, no *'winning'* or *'losing'* input, all inputs remain (*competition-dependent*; Fig. 1.2 B; Penn et al., 1998; Yasuda et al., 2011). When a *subset* of inputs is inactive, the inactive inputs are eliminated. Contrarily, when *all* inputs are inactive, elimination does not occur (Yasuda et al., 2011). This suggests that active connections send a *'punishment'* signal to inactive ones and destabilize them by triggering *'elimination'* signals within inactive synapses (Fig. 1.2 D).

Recent studies have begun to uncover the *'maturation'* signals and mechanisms regulating active synapse strengthening (Toth et al., 2013; Kakegawa et al., 2015; Cheadle et al., 2018). *However, much less is known about the 'elimination' and 'punishment' signals, and how these signals coordinate to precisely regulate synaptic refinement. Additionally, the mechanisms by which neuronal activity regulates these signals remain to be elucidated*.

1.3 Synaptic maturation and the role of activity-dependent proteolytic cleavage of SIRPα

During the refinement process, active and functional synapses undergo maturation, while inactive and non-functional ones are eliminated. During synaptic maturation, immature synapses,

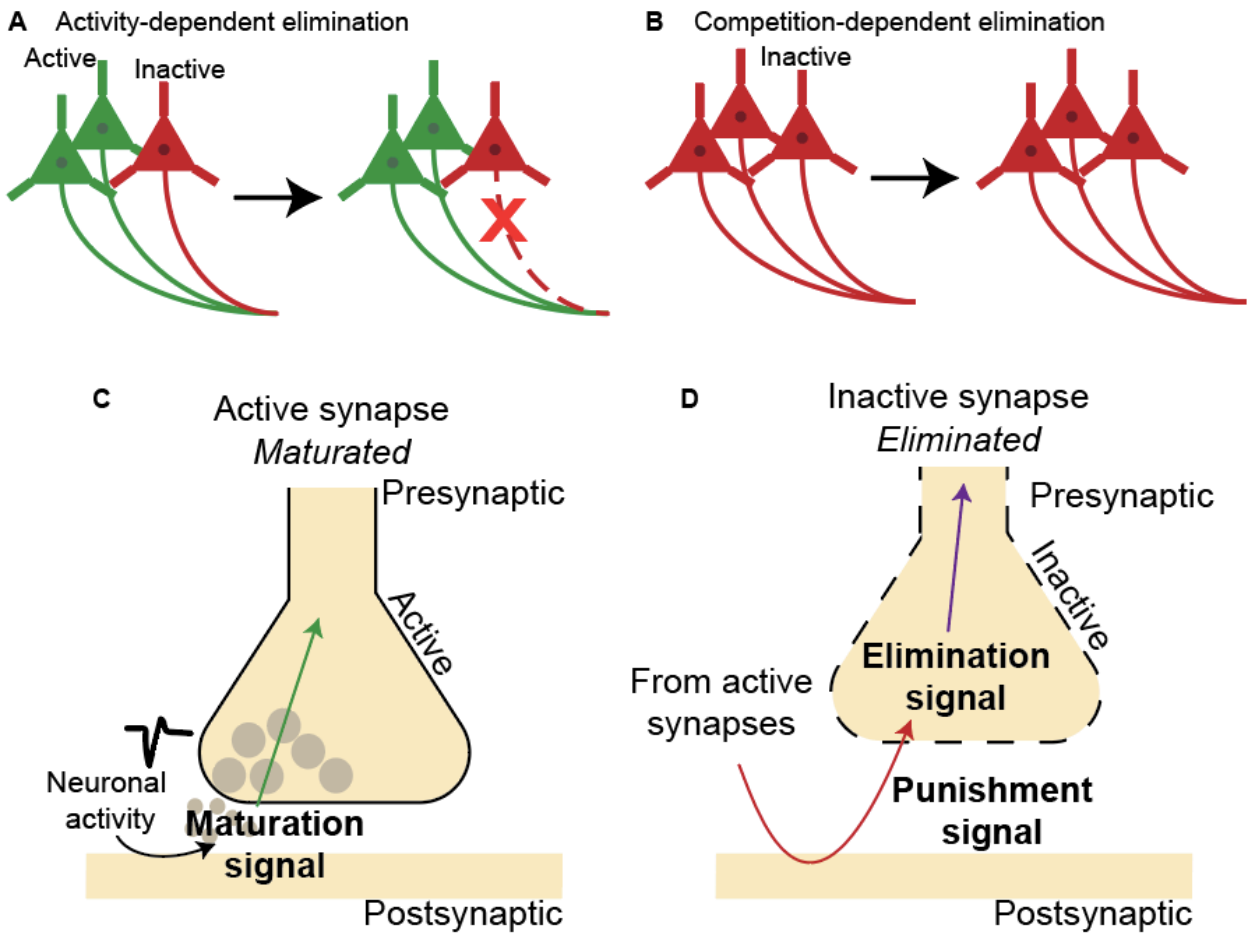

FIGURE 1.2. Proposed model of the mechanisms of active synapse maturation and inactive synapse elimination.

Schematic depicting the means by which neuronal activity regulates synaptic maturation and synaptic elimination

(A) Activity-dependent elimination. When a subset of connections is inactivated, inactive connections are eliminated.

(B) Competition-dependent elimination. When all connections are inactivated, inactive connections are maintained although they are inactive.

(C) Active synapses are strengthened by *'maturation'* signals (green arrow) that signal at active synapses.

(D) Inactive synapses are eliminated in an activity and competition-dependent manner. *'Punishment'* signals (red arrow) sent by active connections activate *'elimination'* signals (purple arrow) within inactive connections driving the removal of these inactive inputs.

formed during the synaptic differentiation stage, undergo structural and functional reorganization to form mature synapses. Relative to the immature synapse, the mature excitatory synapse is characterized by increases in the number of glutamatergic vesicles in the presynaptic terminal and neurotransmitter receptors in the postsynaptic density (PSD). Additionally, both the active zone and PSD widen, and immature, dendritic filopodia morph into mature, mushroom-like spines (Fiala et al., 1998; Li and Sheng, 2003; Yuste and Bonhoeffer, 2004). Synaptic maturation can also involve an increase in the ratio of AMPA to NMDA receptors, changes to NMDA receptor subunits, and changes to the types of presynaptic calcium channels (Reviewed in Yasuda and Umemori, 2009).

Synaptic maturation, like many other stages of synaptic development and function, is heavily orchestrated by a class of proteins known as cell adhesion molecules (CAMs). CAMs span the synaptic cleft and allow trans-synaptic communication between pre and postsynaptic terminals. This trans-synaptic signaling serves two critical roles during activity-dependent synapse maturation. 1) Trans-synaptic signaling promotes the coordinated development of the pre and postsynaptic terminals to ensure efficient synaptic transmission. 2) Trans-synaptic signaling communicates the synaptic activity and excitability levels of the pre and postsynaptic neurons allowing each synaptic partner to make appropriate modifications. Several CAMs have been implicated in synaptic maturation (Varoqueaux et al., 2006; Matsuno et al., 2006; Toth et al., 2013). In this thesis, I will focus on **Signal Regulatory Protein-α (SIRPα)** (Chapter 2).

SIRPα is a member of the immunoglobulin (Ig) superfamily transmembrane proteins. The extracellular domain of SIRPα has three Ig domains while the intracellular domain of SIRPα has four tyrosine residues that form putative immunoreceptor tyrosine-based inhibition motifs. SIRPα has predominantly been studied in the immune system where it allows recognition and prevents phagocytosis of “self” cells. In the brain, recent work has implicated SIRPα as a key regulator of synaptic refinement (Fig. 1.3; Toth et al., 2013; Lehrman et al., 2018).

SIRPα was identified through a screen where synaptogenic molecules were purified from developing mouse brains using a synapse formation assay in cultured neurons (Umemori and Sanes, 2008). SIRPα is highly expressed in neurons during development where it is enriched at excitatory postsynaptic terminals. In the hippocampus, the temporally regulated deletion of SIRPα demonstrated that SIRPα is critical during the synaptic refinement stage and not during synapse differentiation or maintenance. Perturbations to SIRPα function results in fewer and less mature presynaptic terminals while the overexpression of SIRPα drives presynaptic maturation (Toth et al., 2013).

Importantly, SIRPα drives synapse maturation only in the presence of neuronal activity. The synaptic maturation driven by the overexpression of SIRPα is suppressed when neuronal excitability and synaptic transmission is suppressed (Fig. 1.3; Toth et al., 2013). This raises the question as to how neuronal activity regulates SIRPα function. There are a number of ways by which neuronal activity alters molecular signals within the cell. These include gene transcription, protein translation as well as the modification of existing proteins. In the case of SIRPα, it is shown that SIRPα undergoes activity-dependent proteolytic cleavage. The proteolytic cleavage of SIRPα allows the release of a cleaved extracellular fragment, that binds to SIRPα's presynaptic receptor, CD47, to signal presynaptic maturation (Toth et al., 2013). Proteolytic cleavage as a mechanism to detect neuronal activity and turn on appropriate synaptic signals is discussed further below.

1.3.1 Proteolytic cleavage of CAMs in activity-dependent synaptic regulation

Proteolytic cleavage is the process by which proteins are cut into fragments in a rapid and sequence-specific manner by enzymes known as proteases. The two major classes of extracellular proteases that have been heavily linked to brain development and function are Matrix

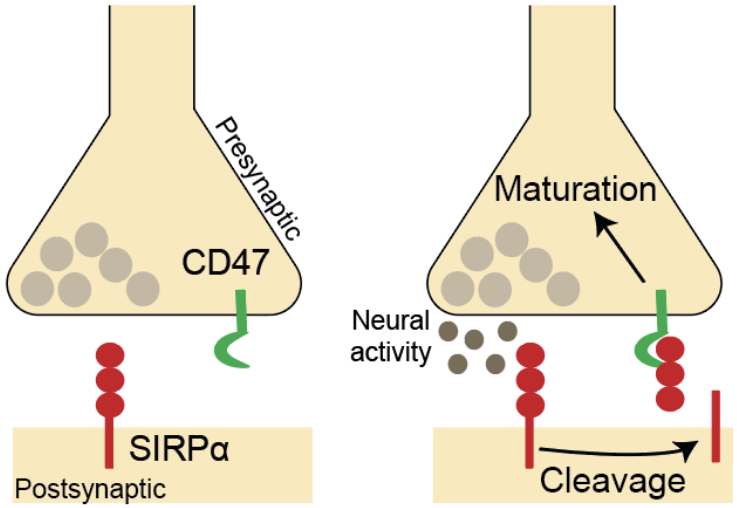

FIGURE 1.3. Activity-dependent ectodomain cleavage of SIRPα drives presynaptic maturation.

The extracellular domain of the postsynaptically expressed, transmembrane protein, SIRPα is cleaved and shed in an activity-dependent manner. The cleaved SIRPα ectodomain retrogradely signals presynaptic maturation by interacting with CD47 (Toth et al., 2013).

Metalloproteinases (MMPs) and A Disintegrin and Metalloproteinases (ADAMs). A number of *in vivo* studies demonstrate the clear importance of these proteases in both synapse development and function (Nagy et al., 2006; Michaluk et al., 2011; Zhuang et al., 2015; reviewed in Sonderegger and Matsumoto-Miyai, 2014).

There are several reasons why the proteolytic cleavage of CAMs is an effective regulator of activity-dependent signaling. 1) Numerous CAMs undergo proteolytic cleavage in an activity-dependent manner in the developing as well as the adult brain (summarized in Nagappan-Chettiar et al., 2017). 2) Proteolytic cleavage can activate or inactivate CAM-mediated signaling and also generate novel, bioactive fragments to influence a broad range of signaling pathways. 3) In response to synaptic transmission, activity-dependent CAM cleavage can occur rapidly (seconds to a few minutes) and in a spatially restricted manner (Conant et al., 2010; Peixoto et al., 2012).

During the activity-dependent stage of synaptic refinement, activity-dependent proteolytic cleavage occurs. Cleavage of CAMs, in response to neuronal activity, plays three distinct, but coordinated roles in orchestrating the structural and functional maturation of active synapses during synaptic refinement. Namely, proteolytic cleavage 1) creates a permissive environment for maturation by switching off signals that prevent maturation (e.g.: ICAM-5; Benson et al., 1998; Matsuno et al., 2006; Tian et al., 2007; Ning et al., 2013); 2) drives maturation by switching on maturation-promoting signals and (e.g.: SIRPα; Toth et al., 2013); 3) restricts synaptic maturation to maintain synapses at a stable state once the synapse is sufficiently mature (e.g.: Neuroligin-1 and Neuroligin-3; Suzuki et al., 2012; Peixoto et al., 2012; Bemben et al., 2019).

In the case of SIRPα, proteolytic cleavage drives synaptic maturation specifically at active synapses by sending a maturation-promoting signal. The extracellular domain of SIRPα is cleaved and released from neurons in response to neuronal activation. The bath application of the soluble, extracellular fragment of SIRPα to cultured hippocampal or motor neurons is sufficient to increase presynaptic vesicle clustering and the frequency of miniature excitatory postsynaptic

currents (Umemori and Sanes, 2008; Toth et al., 2013). Synapse maturation by SIRPα requires both neuronal activity and proteolytic cleavage, because 1) the overexpression of the cleavable, full-length SIRPα in cultured neurons drives synapse maturation while the overexpression of a non-cleavable mutant does not and 2) the blockade of neuronal activity deters the maturation-promoting effect of SIRPα overexpression. These suggest that the cleavage of SIRPα ectodomain by neuronal activity is necessary for SIRPα-dependent synaptic maturation (Toth et al., 2013).

Proteolytic cleavage of SIRPα may be necessary for SIRPα to bind its receptor, CD47 because of the physical distance between the two molecules. SIRPα is expressed postsynaptically, while CD47 is primarily expressed presynaptically. Crystal structure modeling of SIRPα-CD47 demonstrates that the size of this complex is smaller than the width of the synaptic cleft suggesting that direct interaction between the two molecules across the cleft is unlikely (Hatherly et al., 2008). Therefore, SIRPα can only bind CD47 after it is cleaved and released, allowing it to translocate across the synaptic cleft. This process allows SIRPα-CD47 to send maturation signals specifically at active, functional synapses where neuronal activity cleaves the extracellular domain of SIRPα.

Work done in the lab so far has shown that the extracellular domain of SIRPα is cleaved and released in a neuronal activity-dependent manner. This cleaved fragment then acts as a retrograde signal to induce presynaptic maturation (Fig. 1.3; Toth et al., 2013). However, *how SIRPα detects synaptic activity to promote its ectodomain cleavage and, ultimately, synapse maturation is not known*. This is addressed in chapter 2.

1.4 Synaptic elimination and non-receptor tyrosine kinases as candidate *'elimination'* signals

Synaptic elimination removes excess, non-functional synapses to sculpt the efficient synaptic connectivity of the adult brain. In the brain, elimination can take two forms: 1) structural elimination; 2) functional elimination. The structural elimination of inputs often involves the pruning of synapses and the retraction of axons. The overproduction and subsequent removal of axons is seen in the visual system and cerebellum as well as in the corpus callosum, the largest fiber bundle in the brain (LaMantia and Rakic,1990; Kano and Hashimoto, 2009). In contrast to the axon retraction seen in structural elimination, functional synaptic elimination involves changes in the size and distribution of presynaptic boutons that correspond to changes in synaptic function. This is seen during the later stages of refinement in the visual thalamus where axons are not removed, but instead presynaptic boutons cluster, become larger and undergo dynamic spatial redistribution during synaptic refinement (Hong et al., 2014).

Synaptic elimination occurs in an activity and competition-dependent manner. Inactive inputs are preferentially eliminated only in the presence of active ones. This activity and competition-dependence of synaptic elimination suggests that active connections send a *'punishment'* signal to inactive ones and instruct them to leave by triggering *'elimination'* signals within inactive synapses (Fig. 1.2). However, *the molecular mechanisms and signals that read out synaptic activity and accordingly drive synaptic elimination in the brain are largely unknown.*

Several molecules have been implicated as regulators of developmental synaptic elimination (summarized in Table 1.1). One group of these molecules signal within the postsynaptic neuron to drive elimination. In the visual system, major histocompatibility complex class 1 (MHC1) proteins and the MHC1 receptor, PirB, Fn14, Methyl-CpG-binding protein 2 (MeCP2) and Stargazin regulate synaptic refinement (Huh et al., 2000; Datwani et al., 2008; Noutel et al., 2011; Louros et al., 2014; Cheadle et al., 2018). Of these, MHC1 is the most studied in refinement and it has been shown that the loss of function of MHC1 results in impaired synaptic

elimination and disrupted eye-specific segregation of retinal axons, a process that involves synaptic pruning, in the visual thalamus (Huh et al., 2000; Datwani et al., 2008; Lee et al., 2014). MHC1 localizes to the postsynaptic terminal, where it regulates postsynaptic excitatory neurotransmitter receptors (Goddard et al., 2007; Lee et al., 2014). Accordingly, the loss of PirB results in an increase in spine density and stability (Djurisic et al., 2013). In the cerebellum, phospholipase Cβ4 (PLCβ4), protein kinase Cγ (PKCγ), and Arc/Arg3.1 signal within the postsynaptic Purkinje cell to regulate the elimination of the presynaptic climbing fibers. Purkinje cell-specific disruption of these proteins impairs climbing fiber elimination (Kano et al., 1995; Kano et al., 1998; Mikuni et al., 2013). Postsynaptic mGluR1 to PKCγ signaling also regulates the elimination of presynaptic parallel fiber inputs on proximal Purkinje cell dendrites to create climbing fiber and parallel fiber-specific territories (Ichikawa et al., 2016).

Another group of these molecules are thought to be the executors of synapse elimination by way of microglial or astrocytic engulfment. Microglia, the resident immune cells in the brain, and astrocytes have been shown to be important for synaptic pruning. Microglia and astrocytes act by engulfing and removing excess synapses. Complement proteins localize to and label excess synapses for removal by microglial engulfment (Stevens et al., 2007; Schafer et al., 2012). The astrocytic receptors, MERTK and MEGF10 also promote synapse elimination by driving astrocytic engulfment of less active inputs (Chung et al., 2013).

These molecules play critical roles in synaptic elimination. *However, the identity of the 'elimination' signal, the decision-making molecule within the presynaptic neuron that detects levels of synaptic activity and determines whether the synapse should be eliminated, is unknown.* Based on the activity and competition-dependence of synapse elimination (as illustrated in Fig. 1.2), the *'elimination'* signal should satisfy three criteria. 1) The *'elimination'* signal should be presynaptically localized and/or signal within the presynaptic neuron. 2) The activation of the *'elimination'* signal should be activity-dependent. Specifically, this signal should be active at

TABLE 1.1. List of signaling molecules that promote synapse elimination in the developing brain and their proposed mechanisms of action.

Molecule	Effect on synapse elimination (Loss of function)	Mechanism of action	Reference
Retinogeniculate system			
MHC1-PirB	Impaired functional refinement of RGC inputs; Less eye-specific segregation	Regulates postsynaptic neurotransmitter receptors	Huh et al., 2000; Datwani et al., 2008; Lee et al., 2014
Fn14	Impaired functional refinement of RGC inputs	Signals within the postsynaptic relay neuron	Cheadle et al., 2018
MeCP2	Impaired functional refinement of RGC inputs; Less eye-specific segregation	Unknown	Noutel et al., 2011
Stargazin	Impaired functional refinement of RGC inputs	Regulates postsynaptic neurotransmitter receptors	Louros et al., 2014
Complement proteins	Less eye-specific segregation	Drives microglial engulfment of excess synapses	Stevens et al., 2007; Schafer et al., 2012
MERTK/ MEGF10	Impaired functional refinement of RGC inputs; Less eye-specific segregation	Localized on astrocytes; Drives astrocytic engulfment of less active synapses	Chung et al. 2013
Cerebellum			
PLCβ4	Purkinje cells remain multiply innervated by climbing fibers	Signals within the postsynaptic Purkinje cell; regulates PKCγ	Kano et al., 1998
mGluR1 - PKCγ	Purkinje cells remain multiply innervated by climbing fibers; impaired parallel fiber elimination	Signals within the postsynaptic Purkinje cell	Kano et al., 1995; Ichikawa et al., 2016
Sema7A-PlxnC1	Purkinje cells remain multiply innervated by climbing fibers	Signals retrogradely from the Purkinje cell	Uesaka et al., 2014
Arc/Arg3.1	Purkinje cells remain multiply innervated by climbing fibers	Signals within the postsynaptic Purkinje cell	Mikuni et al., 2013
BDNF-TrkB	Purkinje cells remain multiply innervated by climbing fibers	Signals retrogradely from the Purkinje cell	Johnson, et al., 2007; Choo et al., 2017

inactive synapses, but only in the presence of other active synapses. 3) Activation of the *'elimination'* signal should drive the modification of synaptic structure or function, ultimately leading to synaptic elimination.

To identify candidate *'elimination'* signals, we performed an RNAseq screen based on the reasoning that molecules that determine the elimination of inactive connections will be differentially expressed by active and inactive neurons just prior to developmental synaptic elimination. Through such a screen (see Chapter 3), we identified **Protein tyrosine kinase 2β (Pyk2)**, a non-receptor tyrosine kinase (NRTK) as a candidate *'elimination'* signal. We subsequently identified a Pyk2 interacting NRTK, **Janus kinase 2 (JAK2)**, as a critical regulator of synaptic elimination. In chapter 3, we determined the role of these NRTKs in developmental synapse elimination and established how neuronal activity regulates Pyk2 and JAK2.

1.4.1 Non-receptor tyrosine kinases – Pyk2 and JAK2 as candidate *'elimination'* signals

NRTKs are tightly regulated, intracellular, cytoplasmic or membrane bound proteins involved in the intracellular transduction of signals, often via the tyrosine phosphorylation of substrate proteins, in response to extracellular cues. There are nine subfamilies of NRTKs and a number of them have been linked to brain development and function (Grant et al., 1992; Lu et al., 1998; Nicolas et al., 2012; Hsin et al., 2010). There are several reasons why NRTKs can serve as effective regulators of activity-dependent signaling. 1) Numerous NRTKs are activated and signal in an activity-dependent manner (Lu et al., 1998; Huang et al., 2001; Hsin et al., 2010; Nicolas et al., 2012). 2) NRTK activation can convert extracellular cues (like synaptic transmission) to intracellular signals that function in both a local and neuron-wide manner (Faure et al., 2007; Nicolas et al., 2012). 3) In response to synaptic transmission or stimulation, NRTK activation, and the subsequent tyrosine phosphorylation of its substrates can occur rapidly (seconds to a few minutes) and in a spatially restricted manner (Bading and Greenberg, 1991;

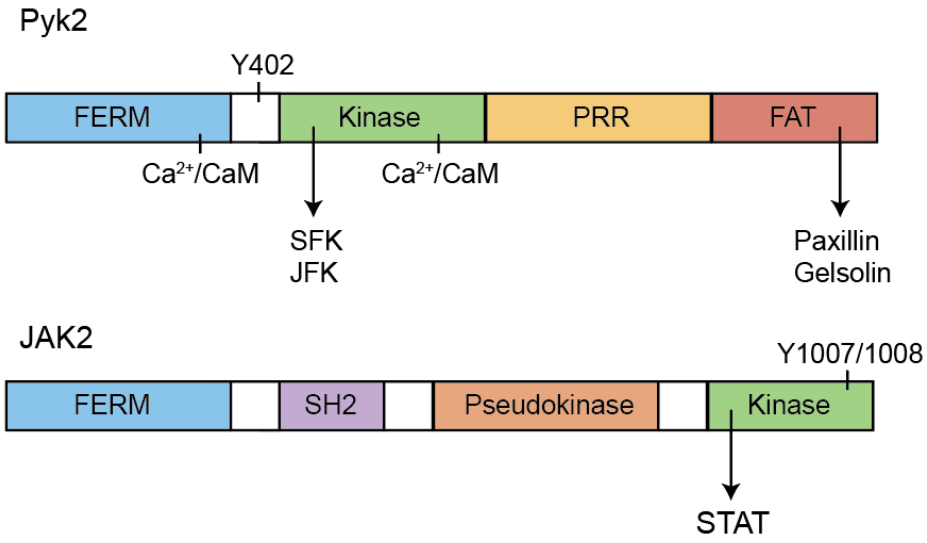

FIGURE 1.4. Protein structure of Pyk2 and JAK2 non-receptor tyrosine kinases.

(Top) Protein structural domains and interacting partners of Pyk2. Pyk2 activation is regulated by changes in levels of intracellular calcium. Calcium/calmodulin (Ca^{2+}/CaM) interacting sites are indicated. Y402 indicates the autophosphorylation site on Pyk2. Pyk2 is phosphorylated at this site upon activation. Once activated, Pyk2 signals via the activation of Pyk2 interacting kinases, often from the Src family kinases (SFK) or JAK family kinases (JFK). Pyk2 can also regulate the cytoskeleton via the regulation of actin-modulating proteins, paxillin and gelsolin.

(Bottom) Protein structural domains and interacting partner of JAK2. Y1007/1008 indicates the autophosphorylation sites on JAK2. JAK2 is phosphorylated at this site upon activation. Once activated, JAK2 activates STATs (signal transducers and activators of transcription) which then regulates transcription.

Protein domains: 4.1 protein-ezrin-radixin-moesin (FERM); proline-rich region (PRR); focal adhesion targeting (FAT); Src homology 2 (SH2).

Ting et al., 2001; Corvol et al., 2005). In this thesis (Chapter 3), we focus on two NRTKs, Pyk2 and JAK2 as candidate *'elimination'* signals**.**

Pyk2, a member of focal adhesion kinase family (Fig. 1.4 top), and JAK2, a member of the JAK kinase family (Fig. 1.4 bottom), are abundantly expressed in the brain and localize to excitatory synaptic terminals (De-Fraja et al., 1998; Menegon et al., 1999; Murata et al., 2000; Giralt et al., 2017). An interesting feature of Pyk2 is that Pyk2 is activated in response to stimuli that elevate intracellular calcium concentrations (Lev et al., 1995). It is thought that calcium/calmodulin binds Pyk2 and releases the Pyk2 kinase domain from autoinhibition, thereby activating Pyk2 (Xie et al., 2008; Kohno et al., 2008). The calcium-dependence of Pyk2 activation drove a series of studies implicating Pyk2 in the activity-dependent process of synaptic plasticity. Pyk2 is activated by and is necessary for the induction of both long-term potentiation (LTP) and long-term depression (LTD; Huang et al., 2001; Bartos et al., 2010; Hsin et al., 2010; Giralt et al., 2017; Salazar et al., 2019). More recent work has determined that JAK2 is also activated by and is necessary for the induction of LTD (Nicolas et al., 2012) This suggests that both Pyk2 and JAK2 can read-out neuronal activity and appropriately modify synapses. This makes Pyk2 and JAK2 ideal candidate *'elimination'* signals.

Aside from adult plasticity, both Pyk2 and JAK2 have been studied in the context of disease. Pyk2 has been identified as a risk gene in genetic studies of Alzheimer's disease (AD; Lambert et al., 2013). Pyk2 is necessary for synapse loss and functional deficits in mouse models of AD (Salazar et al., 2019; Lee et al., 2019). JAK2 signaling is necessary for inflammatory disorder-driven synapse loss. The pharmacological suppression of JAK2 signaling in a mouse model of encephalitis rescued the synapse loss associated with the disease (Di Liberto et al., 2018). These findings suggest that Pyk2 and JAK2 can regulate synapse loss, albeit under disease conditions, further supporting the notion that Pyk2 and JAK2 may serve as *'elimination'* signals during developmental synaptic refinement.

1.5 Synaptic stabilization - Protecting active synapses from elimination

Building an efficient synaptic network involves a fine balance of strengthening necessary synapses and breaking down unnecessary ones. This fine balance implies the need for precise coordination and crosstalk between the signals that strengthen and eliminate synapses. Thinking about this mechanistically, the competition-dependence of synaptic refinement suggests that active synapses send out a *'punishment'* signal that activates *'elimination'* signals within inactive synapses. These *'elimination'* signals drive the removal of inactive synapses (Fig. 1.2). However, many brain regions are densely packed with synapses of different levels of synaptic activity in close proximity to one another. Therefore, a logical extension of the model proposed in Fig. 1.2 is that the *'punishment'* signal may also target other synapses that are active and need to be maintained. Thus, there must be a protective, *'stabilization'* signal that signals locally and preferentially at active synapses to counteract the *'punishment'* as well as *'elimination'* signals and prevent these synapses from being eliminated (Fig. 1.5). *However, the identity of the 'stabilization' signal in the brain remains to be elucidated.*

The *'stabilization'* signal can protect active synapses at three levels: 1) It may prevent active synapses from receiving the *'punishment'* signal; 2) It could switch off the *'elimination'* signal; and 3) It may suppress molecules downstream of the *'elimination'* signal that carry out synaptic removal. Ultimately, the '*stabilization*' signaling should stabilize and protect active synapses from elimination.

In order to identify the *'stabilization'* signal, I reasoned that molecules that promote synapse maturation may also serve to stabilize active synapses. Thus, I hypothesized that one candidate molecule that may serve as a *'stabilization'* signal is SIRPα. This is due to several reasons: 1) SIRPα is expressed during synaptic refinement; 2) SIRPα signals only in the presence of neural activity; 3) SIRPα has a positive, strengthening effect on presynaptic terminals; and 4) The loss of CD47, a SIRPα receptor, results in fewer functional and structural synapses (Toth et al., 2013; Nagappan-Chettiar et al., 2018; Lehrman et al., 2018).

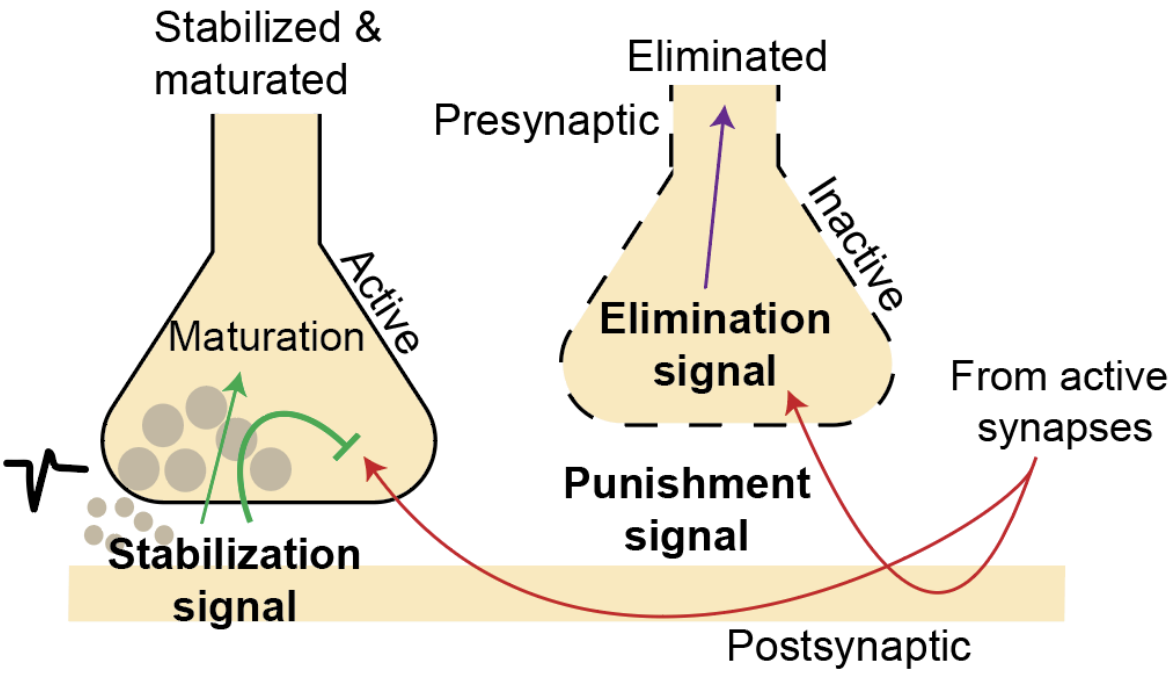

FIGURE 1.5. Proposed model of the signals that govern activity-dependent synaptic refinement.

At inactive synapses: *'Punishment'* signals (red arrows) sent by active connections activate *'elimination'* signals (purple arrow) within inactive connections driving the removal of these inactive inputs.

At active synapses: This *'punishment'* signal (red arrows) likely targets other active inputs as well. Therefore, there must be a local *'stabilization'* signal (green bar) that signals at active synapses to protect active synapses from elimination. The *'stabilization'* signal may counteract the effect of the *'punishment'* signal and prevent *'elimination'* signaling at active synapses.

Signals that regulate synapse maturation (green arrow; discussed in section 1.3) may also serve as a *'stabilization'* signal.

In chapter 4, I ask whether SIRPα is a 'stabilization' signal and if so, how does SIRPα prevent the elimination of active synapses.

1.6 Goals for this dissertation

The major goal of my dissertation is to establish how neurons decide whether to keep or eliminate a synapse during development. Towards this, I determined the molecular signals and mechanisms that detect and translate different levels of neuronal activity to appropriately stabilize and strengthen active synapses and destabilize inactive ones. I did so by addressing these key questions:

1) How is neuronal activity detected and converted into a molecular signal that strengthens and stabilizes synapses? How does neuronal activity drive SIRPα ectodomain cleavage such that SIRPα preferentially strengthens active synapses? These questions are addressed in chapter 2.
2) What are the *"elimination"* signals that direct the elimination of inactive synapses in an activity and competition-dependent manner? How does neuronal activity regulate these signals? These questions are addressed in chapter 3.
3) How are active synapses protected from elimination? How do *'elimination'* signals and signals that strengthen and stabilize synapses interact to ensure the preferential elimination of inactive synapses? Emerging data addressing these questions are discussed in chapter 4.

Chapter 2.

Tyrosine phosphorylation of the Ig superfamily protein SIRPα: Sensing synaptic activity and regulating ectodomain cleavage for synapse maturation

I performed and analyzed the data for all experiments except that in Figures 2.4, G-I and 2.5, C, which were done by Erin M. Johnson-Venkatesh. I wrote the first draft of the manuscript that this chapter is based on, which was later edited by Erin M. Johnson-Venkatesh and Hisashi Umemori. The work in this chapter has been published. Nagappan-Chettiar, S., Johnson-Venkatesh, E. M., Umemori, H. (2018). J Biol Chem. ***293****, 12026-42.*

2. 1 Abstract

Synapse maturation is an activity-dependent process during brain development, where active synapses preferentially undergo maturation to establish efficient synaptic circuits in the brain. Defects in this process are implicated in various neuropsychiatric disorders. We have previously identified that a postsynaptic transmembrane protein, SIRPα (Signal Regulatory Protein-α), plays an important role in directing synapse maturation in an activity-dependent manner. In the presence of synaptic activity, the ectodomain of SIRPα is cleaved and released; then acts as a retrograde signal to induce presynaptic maturation. However, how SIRPα detects synaptic activity to promote its ectodomain cleavage and, ultimately, synapse maturation is not known. Here I show that activity-dependent tyrosine phosphorylation of SIRPα is critical for SIRPα cleavage and synapse maturation. I find that SIRPα is highly phosphorylated on its tyrosine residues in the hippocampus, a structure critical for learning and memory, during synapse maturation. SIRPα is phosphorylated in response to neural activity. Tyrosine phosphorylation of SIRPα is necessary for SIRPα cleavage and presynaptic maturation: the phosphorylation-deficient mutant of SIRPα undergoes much less cleavage and is unable to drive presynaptic maturation. In contrast, phosphorylation of SIRPα does not affect its synaptic localization. Finally, I show that inhibitors of Src and JAK family, and not CaMK, kinases suppress neural activity-dependent phosphorylation and cleavage of SIRPα. Together, our results demonstrate that

SIRPα phosphorylation serves as a method of detecting synaptic activity and linking it to the ectodomain cleavage of SIRPα, which in turn, drives synapse maturation in an activity-dependent manner.

2.2 Introduction

The precise development of synapses, the site of information transfer between neurons in the brain, is critical for proper information processing and brain function. The impaired formation of synapses leads to numerous neurological and psychiatric disorders such as autism and schizophrenia (Kasai et al. 2010; Santini et al., 2013; Tang et al., 2014; Penzes et al., 2013; Sekar et al., 2016). Synapses develop through a series of highly regulated stages: axon elongation and targeting, initial synapse differentiation and synapse maturation stages (Waites et al., 2005; Fox and Umemori, 2006; Shen and Scheiffele, 2010). These stages of synapse development are orchestrated by a number of bidirectional, trans-synaptic signals that organize and coordinate the development of both pre and postsynaptic terminals (Waites et al., 2005; Fox and Umemori, 2006; Shen and Scheiffele, 2010; Siddiqui and Craig, 2011; Chia et al., 2013, Johnson-Venkatesh and Umemori, 2010).

While the initial synapse differentiation stage, during which immature synapses are formed, is considered to be synaptic activity-independent, the synapse maturation stage is regulated by synaptic activity (Katz and Shatz, 1996; Yasuda et al., 2011; Hashimoto and Kano, 2013; Sanes and Lichtman, 1999). During synapse maturation, only the active and functional synapses are strengthened and stabilized to form effective synaptic networks in the brain. However, the molecules and mechanisms by which synapses mature in an activity-dependent manner are largely unknown. Defects in synapse maturation have been implicated in various neurological and psychiatric disorders (Kasai et al. 2010; Santini et al., 2013; Tang et al., 2014; Penzes et al., 2013; Sekar et al., 2016; Lipska et al., 2002; Meyer et al., 2012). Thus, understanding the molecular mechanisms underlying activity-dependent synapse maturation

should further our understanding of, and provide novel therapeutic strategies for neurological and psychiatric disorders.

To identify the molecular mechanisms by which synapses mature, we have purified synaptogenic molecules from developing mouse brains using a synapse formation assay in cultured neurons (Umemori and Sanes, 2008). One of the synaptogenic molecules we identified was SIRPα. SIRPα is highly expressed in the brain and concentrated at the postsynaptic terminals of excitatory synapses (Toth et al., 2013). Using *in vitro* culture systems and *in vivo* mouse mutants, we showed that in the hippocampus, the region central to learning, memory and emotional processing, SIRPα serves as a retrograde, trans-synaptic signal that promotes presynaptic maturation (Toth et al., 2013). Importantly, synaptic activity is necessary for SIRPα to drive presynaptic maturation. When synapses are active, the ectodomain of SIRPα is cleaved and shed, and drives maturation of the presynaptic terminal. Clearly, there are two important questions to address: 1) How does SIRPα detect synaptic activity? 2) How does synaptic activity regulate the cleavage of the SIRPα ectodomain? Addressing these questions will advance our understanding of the mechanisms underlying activity dependent synapse maturation, a process fundamental to the proper wiring of the brain, and shed light on the pathophysiology of neuropsychiatric disorders caused by impaired synapse maturation.

In non-neural systems, an important way in which SIRPα signaling is transduced is via SIRPα tyrosine phosphorylation. The SIRPα intracellular domain contains immunoreceptor tyrosine-based inhibitory motifs (ITIMs). The tyrosine phosphorylation of these ITIMs in response to various stimuli, such as growth factors and ligand binding, recruits and subsequently activates the SH2-domain containing tyrosine phosphatases (SHPs). These phosphatases regulate intracellular signaling pathways, specifically the MAPK and the NFκB pathways, to moderate various cellular functions (Takada et al., 1998; Neznanov et al., 2003). In cultured cells, the tyrosine phosphorylation of SIRPα regulates cell migration and cell proliferation (Motegi et al., 2003; Galbaugh et al., 2010). The expression of wild-type SIRPα, but not a phosphorylation-

deficient SIRPα mutant, positively regulated CHO cell migration in response to insulin (Motegi et al., 2003) and breast cancer cell proliferation (Galbaugh et al, 2010). In the immune system, the tyrosine phosphorylation-dependent signaling of SIRPα regulates inflammatory responses including monocyte adhesion, macrophage migration, phagocytosis, and cytokine release (Smith et al., 2003; Liu et al., 2005; Bian et al., 2016; Alblas et al., 2005; Barclay and Van den Berg, 2014). SIRPα tyrosine phosphorylation has also been implicated in osteoblast differentiation (Holm et al., 2016). In the brain, SIRPα is known to be tyrosine phosphorylated in response to stress, hypothermia or light exposure (Nakahata, et al., 2000; Hamada, et al., 2004; Ohnishi et al., 2010; Maruyama et al., 2012). However, the role of SIRPα tyrosine phosphorylation in the brain is not known.

Here we identify a critical role for the tyrosine phosphorylation of SIRPα in activity-dependent synapse maturation. We show that i) SIRPα is highly phosphorylated on its tyrosine residues during synapse maturation, ii) neural activity induces tyrosine phosphorylation of SIRPα, iii) SIRPα phosphorylation is critical for its synaptogenic activity, iv) SIRPα phosphorylation is necessary for its ectodomain cleavage, and v) inhibitors of Src and JAK family tyrosine kinases suppress the activity-dependent tyrosine phosphorylation and cleavage of SIRPα. These results demonstrate a critical role of SIRPα tyrosine-phosphorylation in sensing synaptic activity, regulating SIRPα ectodomain cleavage, and ultimately, driving synapse maturation in an activity-dependent manner. Our results reveal a novel molecular mechanism by which synaptic activity is converted to synaptogenic activity in order to establish functional synaptic networks.

2.3 Results

Characterization of SIRPα mutant constructs and antibodies

To determine the role of SIRPα tyrosine phosphorylation during synaptic development, I created a tyrosine-phosphorylation deficient SIRPα mutant (SIRPα4YF). In this construct, all four intracellular tyrosine residues in SIRPα were mutated to phenylalanine residues, preventing

tyrosine phosphorylation (Fig. 2.1, A). I confirmed that SIRPα4YF is indeed tyrosine-phosphorylation deficient by examining its JAK2-dependent tyrosine phosphorylation (Stofega et al., 1998; Stofega et al., 2000; Kralovics et al., 2005). In transfected COS cells, SIRPαWT was tyrosine phosphorylated by an active form of JAK2 (JAK2VF) (Kralovics et al., 2005), while SIRPα4YF was not (Fig. 2.1, B, top left panel). I further verified the phosphorylation deficiency of SIRPα4YF by examining its phosphorylation-dependent SHP2 interaction; the adaptor protein SHP2 is known to bind SIRPα following the tyrosine phosphorylation of SIRPα (Kharitonenkov et al., 1997; Fujioka et al., 1996; Timms et al., 1998). I co-transfected COS cells with SIRPα4YF or SIRPαWT, SHP2, with or without JAK2VF. I then immunoprecipitated SIRPα and determined its SHP2 interaction. I found that in the presence of JAK2VF, SHP2 was physically associated with SIRPαWT but not with SIRPα4YF (Fig. 2.1, B, second panel from top left). These results verify that the SIRPα4YF mutant is tyrosine-phosphorylation deficient.

I then characterized the two SIRPα antibodies I used to examine the role of SIRPα tyrosine phosphorylation: an antibody recognizing the extracellular domain of SIRPα (SIRPα N-Term) and an antibody recognizing the intracellular domain of SIRPα (SIRPα C-Term) (Fig. 2.1, C). I have verified that both antibodies i) similarly recognize SIRPαWT and SIRPα4YF by Western blotting and ii) effectively immunoprecipitate both SIRPαWT and SIRPα4YF (83–96% efficiency; Fig. 2.1, D and E). The C-Term antibody recognized both the SIRPα full length and intracellular C-terminal fragment, which is produced after ectodomain cleavage, by Western blotting (Fig. 2.1, E). Both antibodies specifically recognize SIRPα by immunostaining, as confirmed by lack of staining in SIRPα knockout brains (Fig. 2.1, F). These results confirm that the antibodies are suitable for examining the role of SIRPα tyrosine phosphorylation by Western blotting, immunoprecipitation, and immunostaining.

FIGURE 2.1. Characterization of SIRPα mutant constructs and antibodies *(next page)*.
(A) Illustration of the structures of SIRPαWT and SIRPα4YF. Four intracellular tyrosine residues in SIRPαWT were replaced with phenylalanine to generate SIRPα4YF. TM: transmembrane domain. (B) Verification of the tyrosine phosphorylation-deficient mutant of SIRPα (SIRPα4YF). COS cells were transfected with a SIRPα construct (WT or 4YF) and SHP2, together with or without an active form of JAK2 (JAK2VF). Cells were immunoprecipitated for SIRPα protein (with SIRPα N-Term antibody – described below), and the immunoprecipitates were blotted for phosphotyrosine (pY), SHP2, and SIRPα (SIRPα N-Term) (left panel). SIRPαWT is phosphorylated by JAK2VF and binds SHP2; however, SIRPα4YF is not phosphorylated by JAK2VF and does not bind SHP2. Expression levels of transfected proteins in the lysates are shown in the right panel. (C) Illustration showing the recognition sites of the anti-SIRPα antibodies used: SIRPα (N-Term) recognizes the SIRPα ectodomain, and SIRPα (C-Term) recognizes the SIRPα intracellular domain. (D) Immunoprecipitation efficiency of the SIRPα (N-Term) antibody. The same amount of lysates was used for direct blotting (Lysates) and immunoprecipitation followed by blotting (IP). IP efficiency (%) was calculated by quantifying the ratio of SIRPα (IP) to SIRPα (Lysates). The IP efficiency of the SIRPα (N-Term) antibody in detecting SIRPαWT and SIRPα4YF were 83.88% and 86.66%, respectively. (E) Immunoprecipitation efficiency of the SIRPα (C-Term) antibody. The C-Term antibody recognizes both the full length and the intracellular/TM (lacking the ectodomain) SIRPα. IP efficiency was calculated as in (D). The SIRPα (C-Term) effectively immunoprecipitated SIRPαWT (full length: 95.93%; intracellular fragment: 87.89%) and SIRPα4YF (full length: 94.58%; intracellular fragment: 93.78%). (F) Verification of the specificity of SIRPα antibodies by immunostaining. SIRPα KO brains were stained with either SIRPα (N-Term) or SIRPα (C-Term). SIRPα KO brains showed a lack of staining with both antibodies.

Figure 2.1 (Continued)

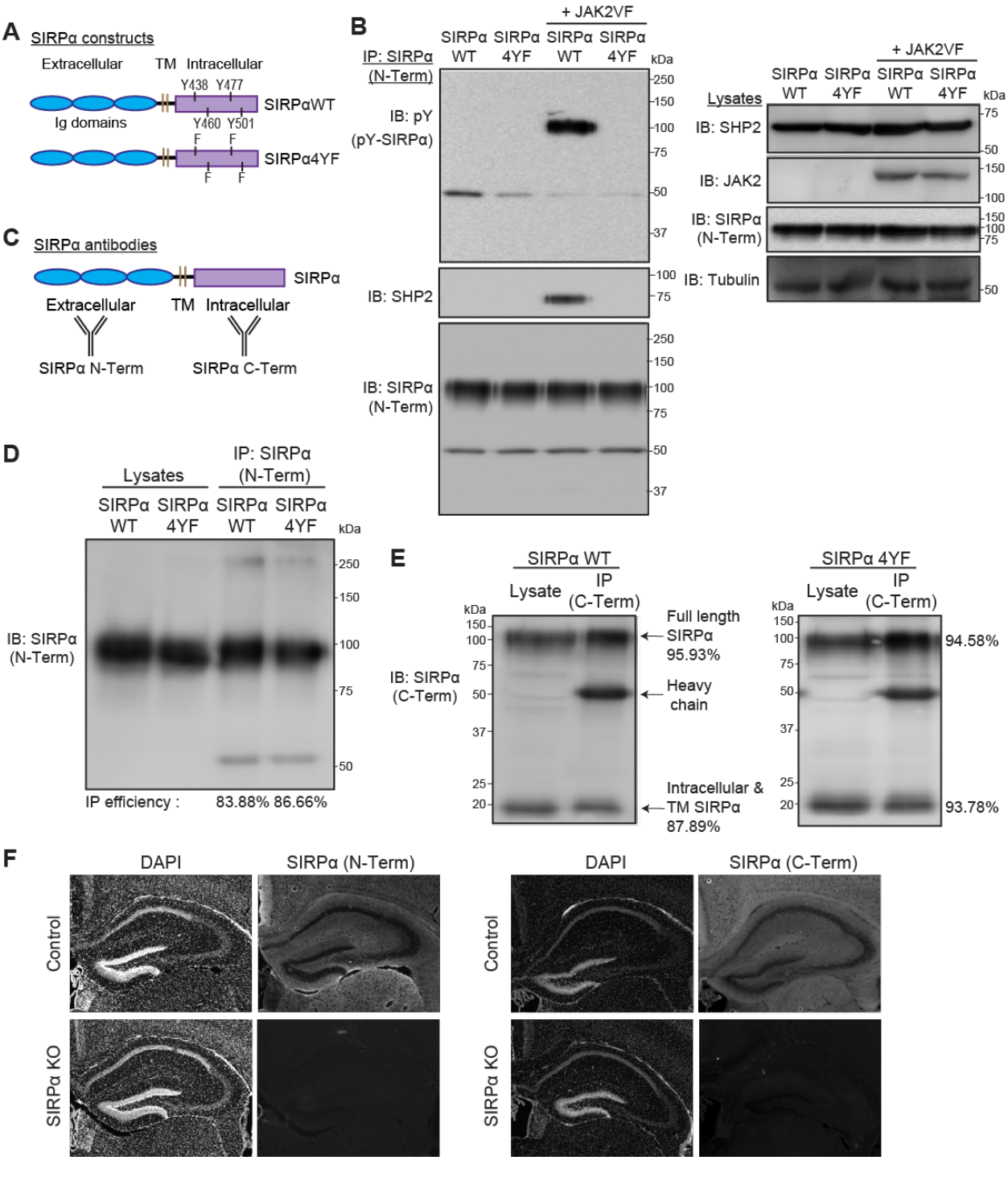

SIRPα is highly phosphorylated on tyrosine residues during synapse maturation in the hippocampus *in vivo*

The synaptic Ig superfamily molecule SIRPα is a critical activity-dependent regulator of excitatory synapse maturation in the hippocampus (Toth et al., 2013). My aim here was to understand how SIRPα detects synaptic activity, and how in turn, this regulates SIRPα's synaptogenic activity. For this, I focused on tyrosine phosphorylation of SIRPα. SIRPα has four tyrosine residues in its intracellular domain (Kharitonenkov et al., 1997). Since tyrosine phosphorylation is a rapid and localized mechanism that moderates the function of a protein (Browning et al., 1985), I hypothesized that SIRPα is tyrosine-phosphorylated in response to synaptic activity during synapse maturation, and that this phosphorylation is necessary for SIRPα's role in driving activity-dependent synapse maturation. To test this idea, I first examined whether SIRPα is tyrosine-phosphorylated during synapse maturation in the mouse hippocampus *in vivo*.

In the mouse hippocampus, initial synapse differentiation occurs during the first two postnatal weeks, between postnatal day 0 (P0) and P14 (Toth et al., 2013; Terauchi et al., 2010). This differentiation stage is followed by an activity-dependent synapse maturation stage that occurs between P15 and P30 (Yasuda et al., 2011; Toth et al., 2013). Afterwards, synapses are maintained throughout life. Hence, I evaluated tyrosine phosphorylation of SIRPα at P6 (during synapse differentiation), P15 (the start of synapse maturation), P20 (during synapse maturation) and in adults (during synapse maintenance). I immunoprecipitated SIRPα from hippocampal lysates and assessed the amount of total and tyrosine-phosphorylated SIRPα present (Fig. 2.2, A). The total amount of SIRPα continuously increased from P6 to adulthood (Fig. 2.2, C; the same results were obtained by directly blotting the lysates for SIRPα. Note that the levels of N-Cadherin and alpha-tubulin were similar across all ages tested, suggesting that the lysis buffer is equally capable of solubilizing synaptic proteins). In contrast, the amount of tyrosine-phosphorylated SIRPα robustly increased from P6 to P15, when synapse maturation starts, and then decreased

afterwards (Fig. 2.2, A and B). The percentage of phosphorylated SIRPα to total SIRPα also peaked around P15 (Fig. 2.2, D). These results demonstrate that both the absolute amount of tyrosine-phosphorylated SIRPα and the relative percentage of SIRPα that is phosphorylated are highest at the beginning of the synapse maturation stage. This suggests that tyrosine phosphorylation of SIRPα may play important roles in regulating synapse maturation in the hippocampus.

Neural activity induces tyrosine phosphorylation of SIRPα

The synapse maturation stage is an activity-dependent stage where active synapses are the ones that undergo maturation (Katz and Shatz, 1996; Yasuda et al., 2011; Hashimoto and Kano, 2013; Sanes and Lichtman, 1999; Toth et al., 2013). Since SIRPα phosphorylation peaks during the synapse maturation stage in the hippocampus (Fig. 2.2), I next asked whether SIRPα phosphorylation is regulated by neural activity. For this, I cultured hippocampal neurons, and at DIV (days in vitro) 12, which is during synapse maturation in cultured hippocampal neurons (Toth et al., 2013), I treated cultures for 20 minutes either with a neurotransmitter receptor inhibitor cocktail (50 μM picrotoxin, 10 μM CNQX and 50 μM AP5) to silence all synaptic activity, or with 55 mM potassium chloride (KCl) to depolarize neurons. This treatment length was chosen because the KCl treatment for 20 minutes showed the most robust and consistent response with regards to SIRPα phosphorylation relative to that of 3 minutes and 1 hour (data not shown). After treatment, I immunoprecipitated SIRPα and examined the amount of total and tyrosine-phosphorylated SIRPα.

I found that the activation of neurons by KCl treatment induced a more than twofold increase in SIRPα phosphorylation relative to untreated and inhibitor treated cultures (Fig. 2.3, A and B), indicating that neural activity induces the tyrosine phosphorylation of SIRPα. The total level of SIRPα was not significantly different in all conditions (Fig. 2.3, C and D). These results support the idea that tyrosine phosphorylation of SIRPα contributes to activity-dependent synapse

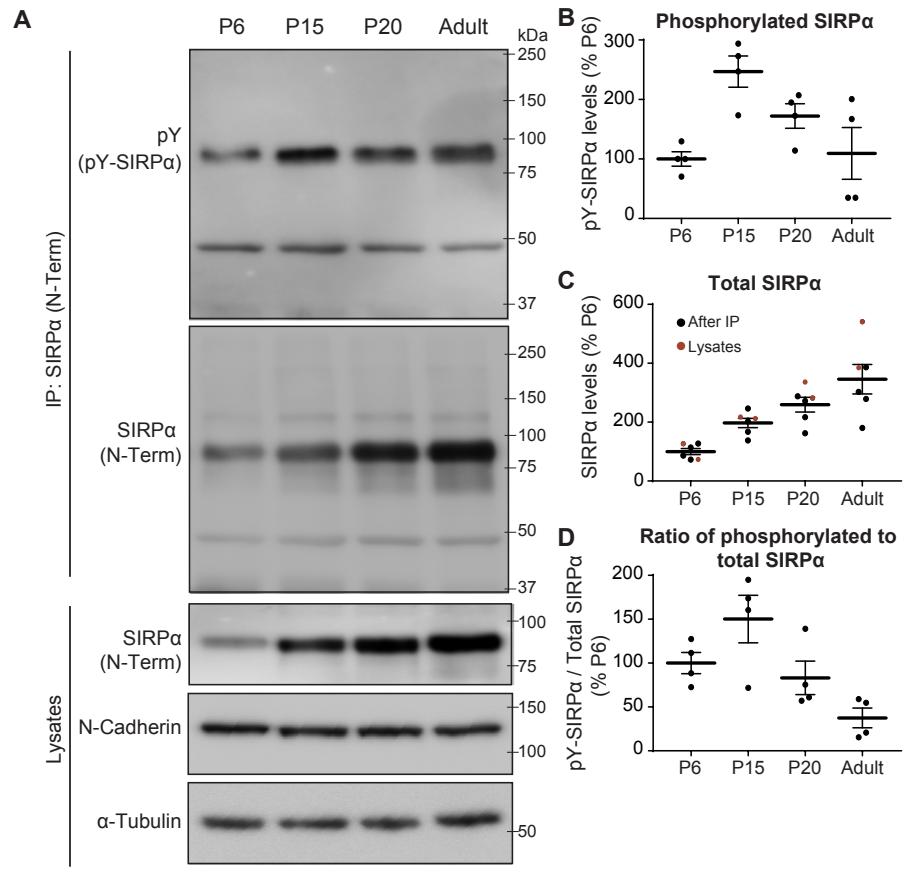

FIGURE 2.2. SIRPα tyrosine-phosphorylation peaks during synapse maturation in the mouse hippocampus.

(A) SIRPα protein was immunoprecipitated (with SIRPα N-Term antibody) from the mouse hippocampal lysates prepared at postnatal day (P) 6, P15, P20 and adult. Immunoprecipitates were subjected to Western blotting using antibodies against phosphotyrosine (pY) and SIRPα (N-Term). Lysates were also directly blotted for SIRPα (N-Term), N-Cadherin, and α-Tubulin. The levels of N-Cadherin and α-tubulin were similar across all ages tested, suggesting that the lysis buffer is equally capable of solubilizing synaptic proteins at different ages. (B) Quantification of the absolute amount of tyrosine-phosphorylated SIRPα (pY-SIRPα) normalized to that at P6. (C) Quantification of total SIRPα (Black dots: After IP; Red dots: Lysates) normalized to that at P6. (D) Quantification of the percentage of tyrosine-phosphorylated SIRPα in total SIRPα (pY-SIRPα/total SIRPα; normalized to P6). Both the absolute amount of phosphorylated SIRPα and the percentage of phosphorylated SIRPα are highest at P15, which corresponds to the beginning of the synapse maturation period in the mouse hippocampus. Equal amounts of total protein were used for immunoprecipitation and blotting. n = 4 mice for each age group.

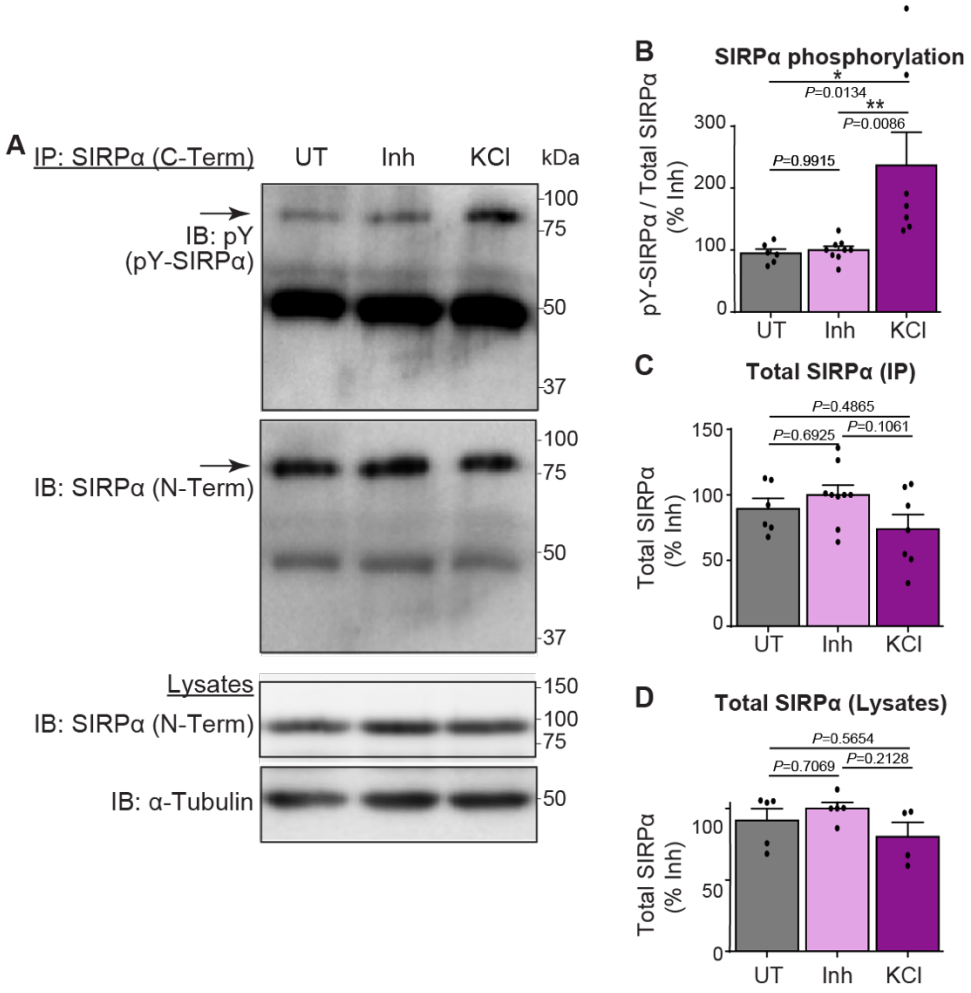

FIGURE 2.3. Activation of neurons induces tyrosine phosphorylation of SIRPα.

(A) Hippocampal neurons were cultured and treated at DIV12 with inhibitor cocktail (50 μM picrotoxin, 10 μM CNQX and 50 μM AP5) for 7 hours. Cultures were washed with new media and left untreated (UT), or treated with either inhibitor cocktail (Inh) or 55 mM KCl for 20 minutes. Cultured neurons were lysed, immunoprecipitated for SIRPα (C-term) and blotted for phosphotyrosine (pY) and SIRPα (N-Term). Lysates were also directly blotted for SIRPα (N-Term) and α-Tubulin. (B) Quantification of the amount of tyrosine-phosphorylated SIRPα (pY-SIRPα / Total SIRPα (IP); normalized to inhibitor group). Amount of phosphorylated SIRPα is significantly increased by KCl-driven neural activation. (C) Quantification of total SIRPα levels (IP) under each condition (normalized to inhibitor group). (D) Quantification of total SIRPα levels (Lysates) under each condition (normalized to inhibitor group). Equal amounts of total protein were used for immunoprecipitation and blotting. n = 6 (untreated), n = 9 (inhibitor) or 7 (KCl) dishes from five independent experiments. Data are mean ± s.e.m. One-way ANOVA followed by Tukey's test.

maturation. The addition of inhibitors showed similar levels of SIRPα phosphorylation as untreated cultures. This may be due to the relatively low level of basal synaptic activity in neuronal cultures in the 20-minute period (Fig. 2.3, B).

Tyrosine phosphorylation of SIRPα is necessary for synapse maturation

Using the SIRPα4YF mutant (Fig. 2.1, A), I next investigated whether tyrosine phosphorylation of SIRPα is necessary for its synaptogenic activity. For this, I utilized SIRPα-deficient neurons (Toth et al., 2013). SIRPα-deficient neurons show defects in presynaptic maturation of excitatory (glutamatergic) synapses. I asked if SIRPα4YF could rescue the impaired presynaptic maturation of SIRPα-deficient neurons. To create the SIRPα-deficient background, I prepared hippocampal cultures from mice bearing the loxP-flanked Sirpa alleles (*Sirpa*$^{fl/fl}$) (Toth et al., 2013) and transfected with the Cre-expression plasmid (=SIRPα KO). For the rescue experiments, I also co-transfected SIRPαWT (=SIRPαWT Rescue) or SIRPα4YF (=SIRPα4YF Rescue) together with Cre (Fig. 2.4, A). Both SIRPαWT and SIRPα4YF expressed equally in neurons (Fig. 2.4, B and C). Additionally, to label transfected neurons, I co-transfected StopYFP, which expresses YFP only when Cre is co-expressed (Dabrowski et al., 2015). This system allows us to temporally control SIRPα inactivation and rescue during synapse development. I transfected neurons sparsely in order to evaluate the effects of SIRPα KO and rescues in a neuron-specific and cell autonomous manner (Fig. 2.4, D).

To evaluate glutamatergic presynaptic maturation, I analyzed the clustering of glutamatergic synaptic vesicles by staining for vesicular glutamate transporter 1 (VGluT1) (Terauchi et al., 2010; Toth et al., 2013) (Fig. 2.4, E). I quantified the number of VGluT1 puncta on the dendrites of transfected neurons (Fig. 2.4, F). The inactivation of endogenous SIRPα (SIRPα KO) significantly decreased the density of VGluT1 puncta on transfected dendrites relative to Control (GFP, instead of Cre, was transfected), consistent with our previous report showing

that SIRPα is necessary for glutamatergic presynaptic maturation (Toth et al., 2013). This decrease was completely rescued by the expression of SIRPαWT. In contrast, SIRPα4YF failed to rescue the decrease in VGluT1 density. These results suggest that tyrosine-phosphorylation of SIRPα is necessary for presynaptic maturation.

To confirm the necessity of SIRPα tyrosine-phosphorylation in synapse maturation, we performed electrophysiological experiments. We recorded miniature excitatory postsynaptic currents (mEPSCs) from transfected hippocampal neurons (Fig. 2.4, G). In agreement with my histological data, we found a marked decrease in mEPSC frequency (reflecting the number of presynaptic inputs) in SIRPα KO neurons relative to control neurons. This decrease in frequency was completely rescued by the expression of SIRPαWT, but not by SIRPα4YF (Fig. 2.4, H). Together, our data demonstrate that SIRPα tyrosine-phosphorylation is critical for SIRPα's synaptogenic function in increasing the number of functional presynaptic inputs.

Interestingly, we noticed that the mEPSC amplitude (reflecting postsynaptic response) was increased in SIRPα4YF-rescue neurons (Fig. 2.4, I), while there was no difference among Control, SIRPα KO, and SIRPαWT-rescue neurons. This suggests that SIRPα phosphorylation may also influence postsynaptic maturation. SIRPα4YF may be interfering with signals that control postsynaptic development.

To rule out the possibility that the inability of SIRPα4YF in driving presynaptic development is due to its inability to localize to synapses, I examined the synaptic localization of SIRPαWT and SIRPα4YF. In neurons, endogenous SIRPα localizes predominantly to excitatory postsynaptic terminals (Toth et al., 2013). To visualize excitatory postsynaptic terminals in cultured hippocampal neurons, I co-transfected EGFP-tagged postsynaptic density 95 (PSD95-EGFP), which accumulates at excitatory postsynaptic terminals and effectively labels them (Terauchi et al., 2015). In control neurons, SIRPα accumulated at PSD95-EGFP positive synapses. This expression of SIRPα on PSD95-EGFP positive puncta was diminished in SIRPα KO neurons (Fig. 2.4, J). Importantly, both SIRPαWT and SIRPα4YF localized to PSD95-EGFP positive puncta

(Fig. 2.4, J and K). Additionally, the intensity of SIRPα staining at synapses was not significantly different between SIRPαWT and SIRPα4YF (Fig. 2.4, L). These results indicate that the tyrosine phosphorylation of SIRPα does not regulate the synaptic targeting of SIRPα.

Tyrosine phosphorylation of SIRPα regulates SIRPα ectodomain cleavage

SIRPα regulates synapse maturation via activity-dependent ectodomain cleavage (Toth et al., 2013). Since we found that tyrosine phosphorylation of SIRPα is critical for synapse maturation (Fig. 2.4), I hypothesized that SIRPα tyrosine-phosphorylation regulates the cleavage of SIRPα. To test this idea, I transfected COS cells with SIRPαWT only, SIRPα4YF only, SIRPαWT+JAK2VF (to drive SIRPα phosphorylation), or SIRPα4YF+JAK2VF. Two days after transfection, I collected the culture media and immunoprecipitated the secreted SIRPα ectodomain. Without tyrosine kinases, the levels of secreted SIRPα were similar between SIRPαWT and SIRPα4YF (Fig. 2.5, A). In contrast, in the presence of JAK2VF, SIRPαWT had significantly more ectodomain released than SIRPα4YF (Fig. 2.5, B). Similar results were obtained using sodium orthovanadate, which inhibits protein tyrosine phosphatases and activates tyrosine kinases (Umemori et al., 1999), to drive SIRPα phosphorylation (Fig. 2.5, C). Significantly more ectodomain was released from SIRPαWT than SIRPα4YF following vanadate treatment. This difference in ectodomain cleavage is not due to lack of surface expression of SIRPα4YF, because both forms of SIRPα were detected on the cell surface when cells were stained for SIRPα without permeabilizing the cell membrane (Fig. 2.5, D). These results indicate that tyrosine phosphorylation of SIRPα plays a critical role in regulating SIRPα ectodomain cleavage in COS cells. Interestingly, after the cleavage of the SIRPα ectodomain, the C-terminal fragment of SIRPα was dephosphorylated (Fig. 2.5, E).

FIGURE 2.4. Tyrosine phosphorylation of SIRPα is necessary for its synaptogenic effects *(next page)*.

(A) Experimental scheme to determine the role of SIRPα tyrosine phosphorylation in synapse development. Cultured hippocampal neurons from *Sirpa*$^{fl/fl}$ mice were transfected with GFP and StopYFP plasmids (Control), Cre and StopYFP plasmids (SIRPα KO), Cre, StopYFP and SIRPαWT plasmids (SIRPαWT Rescue) or Cre, StopYFP and SIRPα4YF plasmids (SIRPα4YF Rescue) at DIV3-4, and stained for VGluT1 or subjected to electrophysiology at DIV16-19. (B) Representative images of SIRPαWT Rescue and SIRPα4YF Rescue neurons stained with SIRPα C-Term antibody. (C) Quantification of SIRPα staining intensity in SIRPαWT Rescue and SIRPα4YF Rescue neurons. The SIRPα staining intensity was similar in both rescue conditions. P = 0.6958 by Student's t-test. (D) Image of transfected neuron showing sparse transfection. (E) Representative images of VGluT1 puncta (red) on transfected dendrites (green). (F) Graph showing quantification of VGluT1 puncta density (number of puncta/dendrite length). The density of VGluT1 puncta is decreased in SIRPα KO cultures than in Control. SIRPαWT rescued these defects, while SIRPα4YF did not. (G) mEPSCs were recorded at DIV18-19 from cultured hippocampal neurons. (H and I) Graphs show quantification of mEPSC frequency and amplitude. mEPSC frequency was decreased in SIRPα KO neurons relative to Control neurons. SIRPαWT rescued these defects, while SIRPα4YF did not. (J - L) Cultured hippocampal neurons from *Sirpa*$^{fl/fl}$ mice were transfected with PSD95-EGFP plasmid (Control), Cre and PSD95-EGFP plasmids (SIRPα KO), Cre, PSD95-EGFP, and SIRPαWT plasmids (SIRPαWT-rescue), or Cre, PSD95-EGFP, and SIRPα4YF plasmids (SIRPα4YF-rescue) at DIV3 and stained for SIRPα (C-Term) at DIV12. (K) Percent of PSD95 puncta that colocalizes with SIRPα. Both SIRPαWT and SIRPα4YF localize to PSD95-positive synapses, P = 0.7063 by Student's t-test. (L) Quantification of SIRPα staining intensity at PSD95-EGFP-positive synapses. Both SIRPαWT and SIRPα4YF express equally at synapses, P = 0.5634 by Student's t-test. n = (F) 18 (Control), 22 (KO), 25 (WT rescue), or 19 (4YF rescue) neurons from 3 independent cultures; (H and I) (frequency, amplitude, group) = (50,31,control), (30,30,KO), (36,32,WT Rescue), and (26,23,4YF Rescue) neurons from 8 independent cultures. Data are mean ± s.e.m. n.s. not significant ($P > 0.05$), *$P < 0.05$, ** $P < 0.01$, ***$P < 0.001$ by Student's t-test or one-way ANOVA followed by Tukey's test. Scale bar = 100 μm (B); 5 μm (E and J); 250 ms, 10 pA (G).

Figure 2.4 (Continued)

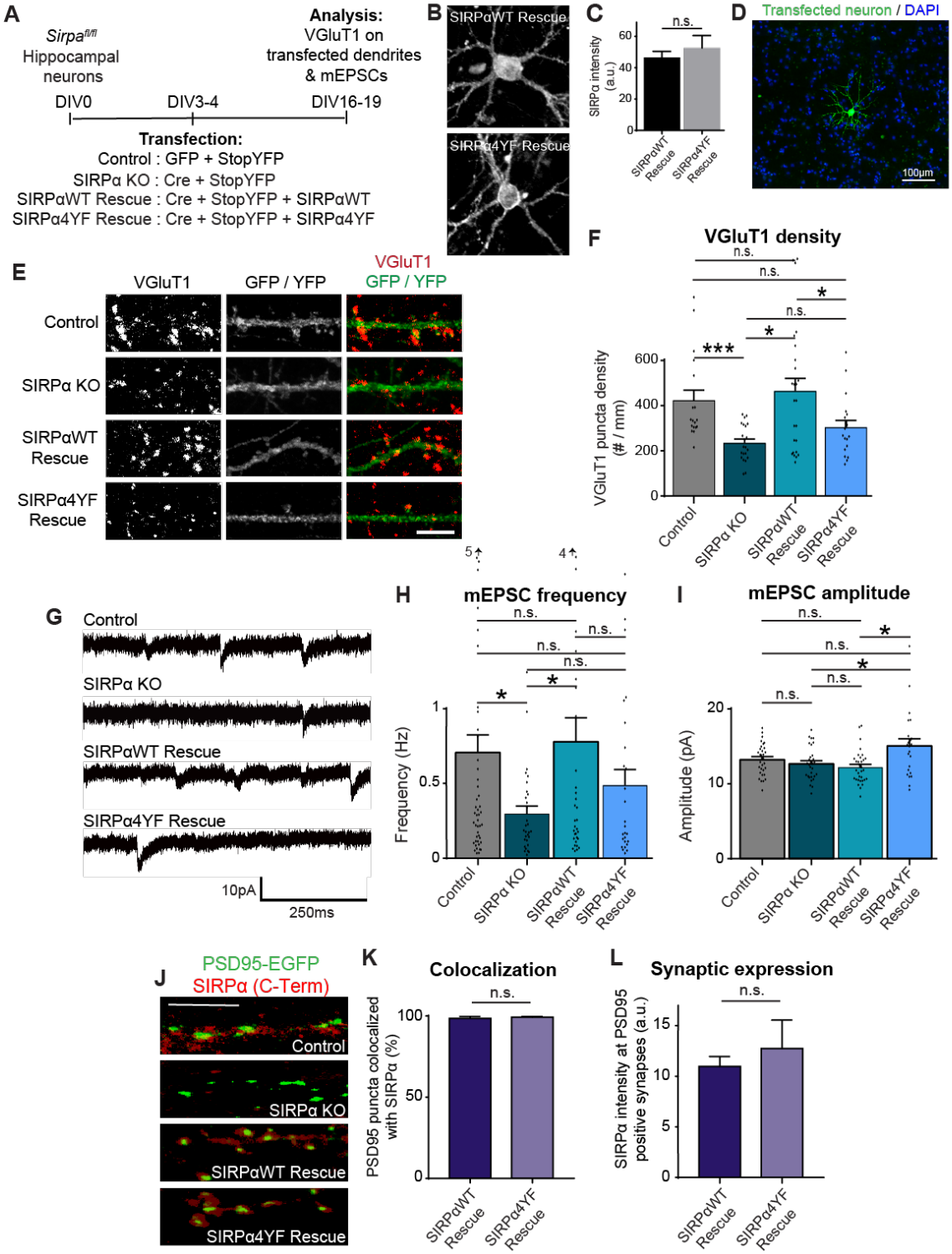

FIGURE 2.5. Tyrosine phosphorylation of SIRPα regulates SIRPα ectodomain cleavage in COS cells *(next page)*.

(A and B) COS cells were transfected with SIRPαWT or SIRPα4YF (A), or SIRPαWT + JAK2VF or SIRPα4YF + JAK2VF (B). Two days after transfection, culture media and cell lysates were collected. Culture media was subjected to immunoprecipitation for secreted SIRPα protein (with SIRPα N-term antibody) and blotted for SIRPα (N-Term). Cell lysates were subjected to Western blotting for SIRPα (N-Term) and JAK2. Graphs show the quantification of the amount of secreted SIRPα ectodomain. (A) When SIRPα was not tyrosine-phosphorylated (without JAK2VF; see Fig. 3B), a similar amount of SIRPα ectodomain was released in the media from SIRPαWT and SIRPα4YF. (B) In the presence of tyrosine kinase (JAK2VF), significantly more SIRPα ectodomain was released in the media from SIRPαWT compared to SIRPα4YF. (C) COS cells were transfected with SIRPαWT or SIRPα4YF. Two days after transfection, cultures were treated with 1 mM sodium orthovanadate for 7-17 hours to promote tyrosine phosphorylation of SIRPα (SIRPαWT, but not SIRPα4YF, is tyrosine-phosphorylated [pY-SIRPα; right bottom panel]). Culture media and cell lysates were collected and subjected to Western blotting: the membranes were first blotted with the SIRPα N-Term antibody, stripped, and then with the SIRPα C-Term antibody. The following SIRPα band intensities were quantified: Media (IB: N-Term, Media), Full-N (N-Term, Lysates), Full-C (C-Term, Lysates, upper band), and C-Fragment (C-Term, Lysates, lower band). The rate of SIRPα ectodomain cleavage was calculated using the formula: Media / ((Full-C + C-Fragment)*(Full-N / Full-C)) / hours (see methods). Experiments were done as a pair (WT and 4YF), and the pairs are connected with lines in the graph. Significantly more SIRPα ectodomain was released in the media from SIRPαWT than SIRPα4YF following vanadate treatment. (D) COS cells were transfected with mCherry only, mCherry and SIRPαWT, or mCherry and SIRPα4YF. Cells were fixed and stained for SIRPα (N-Term) without permeabilization to detect surface expression of SIRPα. Both SIRPαWT and SIRPα4YF are expressed on the surface. (E) Tyrosine phosphorylation of the SIRPα full length and C terminal fragment (arrows) after vanadate treatment. n = 5 (A and B); 7 (C) independent experiments; (E) reproduced 4 times. Data are mean ± s.e.m. Student's t-test (A and B) or two-way ANOVA (C). Scale bar = 20 μm.

Figure 2.5 (Continued)

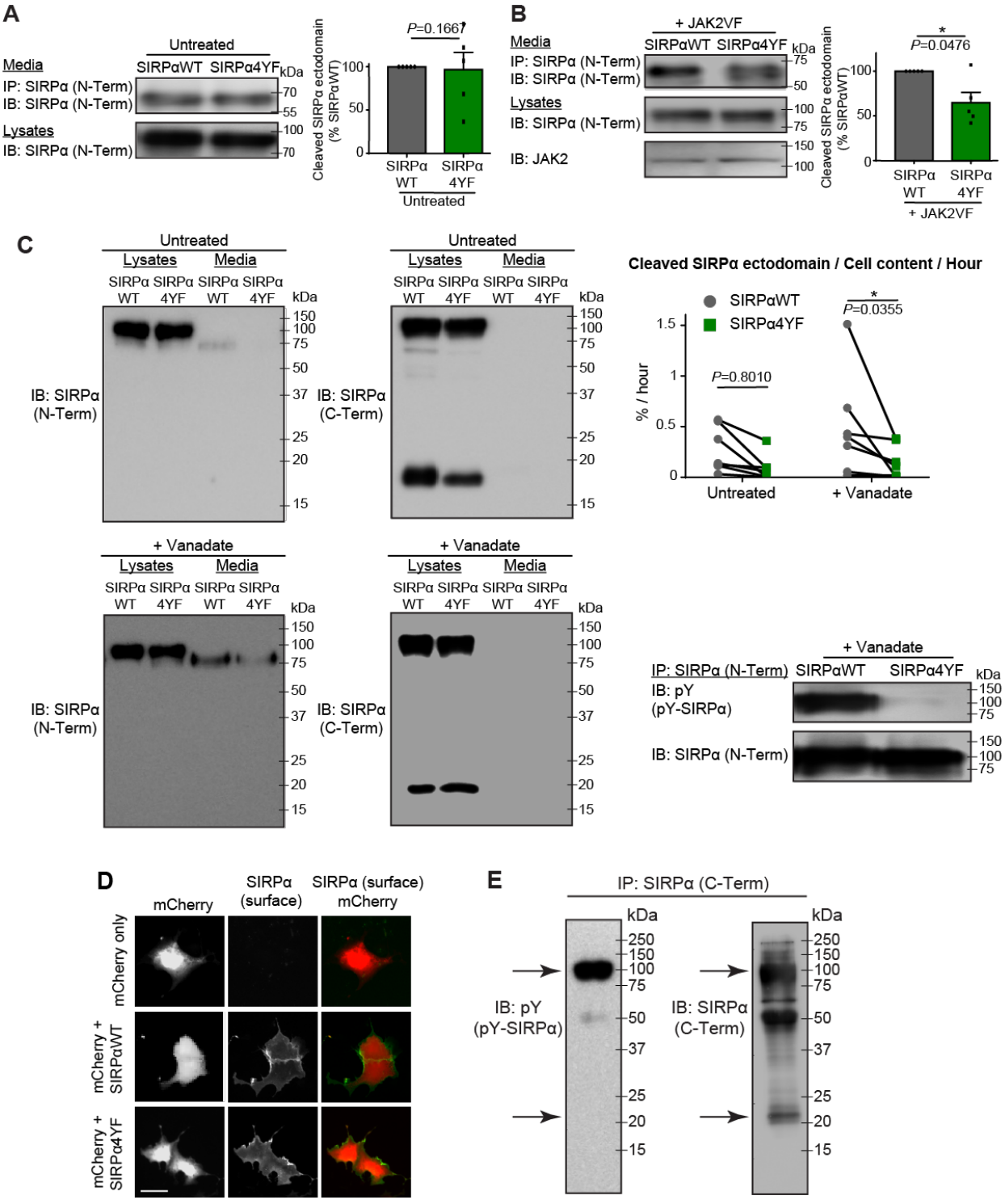

To determine if SIRPα tyrosine phosphorylation regulates ectodomain cleavage in neurons as well, I prepared hippocampal cultures from *Sirpa*$^{fl/fl}$ mice (Toth et al., 2013) and transfected the cultures to create the SIRPαWT-rescue or SIRPα4YF-rescue conditions as described above (Fig. 2.4, A). To identify synapses, I co-transfected PSD95-EGFP. I then left cultures untreated or treated these cultures with KCl for 2 hours at DIV12. After the treatment, I stained the cultures using the SIRPα N-terminal antibody without permeabilization to detect the surface SIRPα ectodomain ("Ectodomain SIRPα"), followed by the SIRPα C-terminal antibody with permeabilization to evaluate total SIRPα ("Total SIRPα"). I imaged these cultures and calculated the ratio of the SIRPα ectodomain to total SIRPα. At the basal level (no KCl conditions), the Ectodomain/Total SIRPα ratio was significantly smaller in SIRPα4WT-rescue neurons relative to SIRPαYF-rescue neurons, suggesting that the basal level of neuronal activity induced more cleavage of SIRPα4WT than SIRPαYF. In SIRPαWT-rescue neurons, KCl treatment significantly decreased the Ectodomain/Total SIRPα ratio relative to control, suggesting that the SIRPαWT ectodomain is further cleaved upon neuronal activation. In contrast, in SIRPα4YF neurons, KCl treatment did not significantly change the Ectodomain/Total SIRPα ratio (Fig. 2.6, A and B). The total level of SIRPα is not significantly different in all conditions (Fig. 2.6, C). These results suggest that neural activity-dependent SIRPα cleavage requires SIRPα tyrosine phosphorylation. To ascertain that the change in the Ectodomain/Total SIRPα ratio is indeed due to SIRPα ectodomain cleavage, I treated SIRPαWT-rescue cultures with the proteinase inhibitors, TIMPs, which inhibit SIRPα ectodomain cleavage (Toth et al., 2013). The treatment of cultures with TIMPs blocked the KCl-driven decrease in the Ectodomain/Total SIRPα ratio, suggesting that the change in the ratio is due to SIRPα ectodomain cleavage (Fig. 2.6, D and E).

FIGURE 2.6. Tyrosine phosphorylation of SIRPα regulates activity-driven SIRPα ectodomain cleavage in neurons *(next page)*.

(A-C) Cultured hippocampal neurons from *Sirpa*$^{fl/fl}$ mice were transfected with Cre, PSD95-EGFP, and SIRPαWT plasmids (SIRPαWT), or Cre, PSD95-EGFP, and SIRPα4YF plasmids (SIRPα4YF) at DIV3 and treated with 55mM KCl for 2 hours at DIV12. Cultures were immunostained with the SIRPα N-Term antibody without permeabilization to detect surface "Ectodomain"-containing SIRPα, followed by the SIRPα C-Term antibody with permeabilization to detect "Total" SIRPα. "Ectodomain" and "Total" SIRPα staining intensity at synapses (identified by PSD95-EGFP) were quantified. (B) The ratio of Ectodomain/Total SIRPα (normalized to SIRPαWT without KCl). KCl-driven neuronal activation decreased the Ectodomain/Total SIRPα ratio in SIRPαWT expressing neurons but not in SIRPα4YF expressing neurons. (C) Total SIRPα was not significantly different in all groups. (D-F) Cultured hippocampal neurons expressing SIRPαWT were prepared as described above. At DIV12 cultures were treated with 55mM KCl or KCl + TIMPs and immunostained as described above. (E) The ratio of Ectodomain/Total SIRPα. TIMPs block the KCl-induced decrease in the Ectodomain/Total SIRPα ratio. (F) Total SIRPα was not significantly different in all groups. n = (A-C) 43 (SIRPαWT, - KCl), 36 (SIRPαWT, + KCl), 30 (SIRPα4YF, - KCl) and 31 (SIRPα4YF, + KCl) neurons from 3 independent cultures; (E) 20 (SIRPαWT, + KCl), and 15 (SIRPαWT, + KCl, + TIMPs) neurons. Data are mean ± s.e.m. n.s. not significant ($P > 0.05$), *$P < 0.05$, **$P < 0.01$, ****$P < 0.001$ by one-way ANOVA followed by Tukey's test.

Figure 2.6 (Continued)

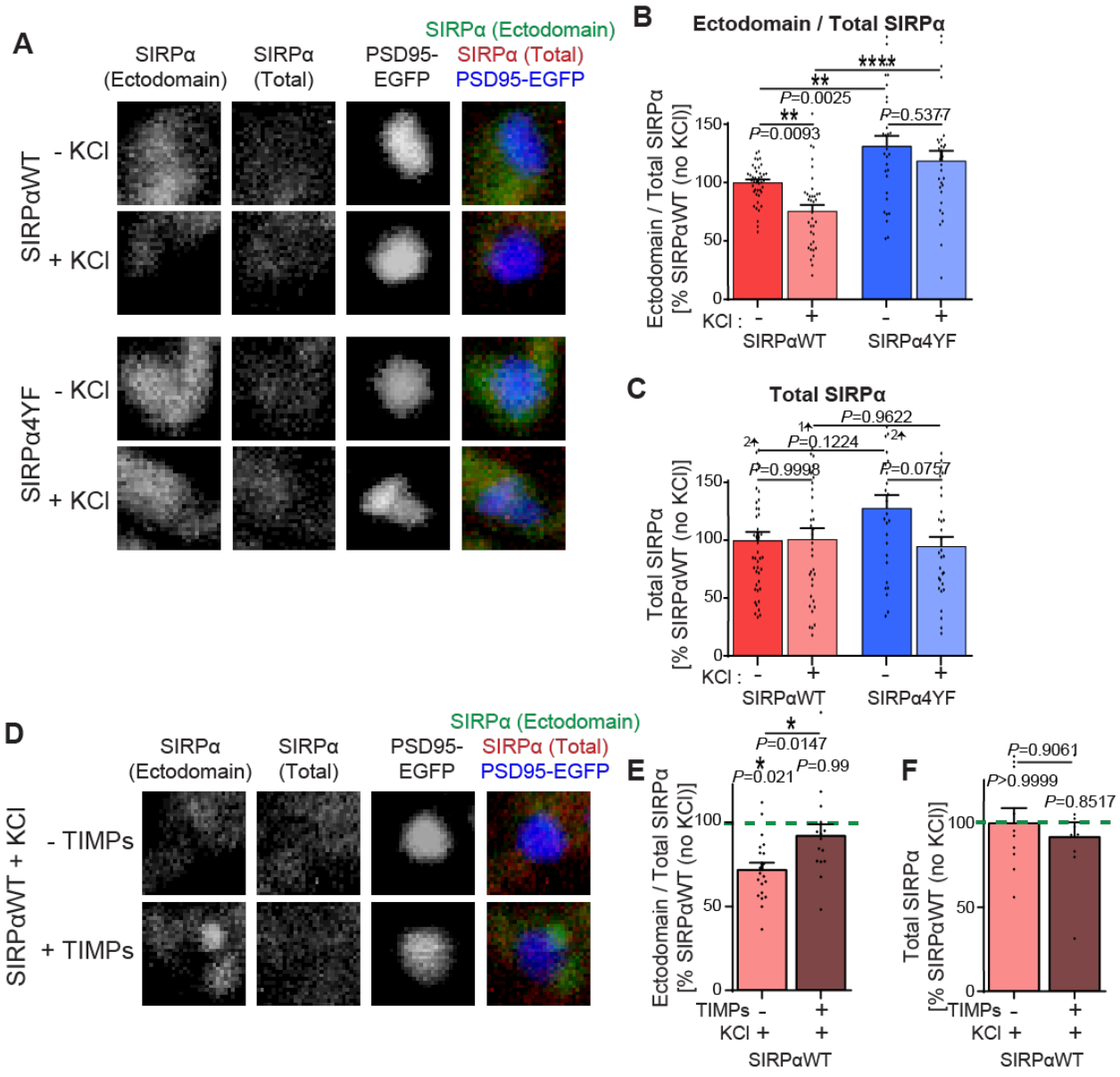

Inhibitors of Src and JAK family kinases suppress neural activity-driven SIRPα tyrosine-phosphorylation

I next wanted to identify the signaling molecules that regulate the tyrosine-phosphorylation of SIRPα in response to neural activity. For this, I focused on two families of tyrosine kinases, Src and JAK families, because they are highly expressed in hippocampal neurons and can be activated by neural activity (Lu et al., 1998; Niimura et al., 2005; Nicolas et al., 2012). Additionally, I showed that in COS cells, JAK2 can phosphorylate SIRPα (Fig. 2.1, B).

To test whether Src and JAK kinase activity contributes to activity-dependent tyrosine-phosphorylation of SIRPα in neurons, I treated hippocampal cultures prepared from WT mice at DIV12 with either 10 μM PP2 (an inhibitor of Src family kinases) (Bain et al., 2007) or 10 μM AG490 (an inhibitor of JAK family kinases) (Nicolas et al., 2012; Chiba et al., 2009) for one hour. Control cultures were treated with DMSO only (PP2 and AG490 were dissolved in DMSO). These cultures were then treated with or without 55 mM KCl for 20 minutes to activate neurons. I then subjected these cultures to immunoprecipitation for SIRPα and immunoblotted for phosphotyrosine and SIRPα. I found that treatment of neurons with either PP2 or AG490 blocked the increase in SIRPα tyrosine-phosphorylation in response to neuronal activation (Fig. 2.7, A and B). These results indicate that the inhibitors, likely through the inhibition of either Src or JAK family kinases, blocked the activity-dependent tyrosine phosphorylation of SIRPα. Interestingly, the treatment of cultures with PP2, but not AG490, diminished the basal level of SIRPα phosphorylation (Fig. 2.7, C and D), suggesting that Src family kinases, but not JAK kinases, also contribute to the basal level of SIRPα phosphorylation in neurons.

CaMK activity is not involved in SIRPα tyrosine-phosphorylation

Work in the lab has previously shown that the cleavage of SIRPα requires CaMK activity (Toth et al., 2013). The inhibition of CaMK activity resulted in a substantial decrease in the amount of cleaved SIRPα. Since SIRPα cleavage is regulated by its tyrosine-phosphorylation (Fig. 2.5

and 2.6), I asked whether CaMK signaling influences tyrosine phosphorylation of SIRPα. To test this, I treated cultured hippocampal neurons at DIV12 with 5 μM KN62 (a CaMK inhibitor) and activated neurons with KCl for 20 minutes. Treatment of KN62 effectively suppressed CaMK activation at synapses (Fig. 2.7, E). Cultures treated with KN62 still showed a marked increase in the level of SIRPα tyrosine-phosphorylation in response to neuronal activation (Fig. 2.7, F and G), suggesting that CaMK activity is not involved in activity-dependent tyrosine-phosphorylation of SIRPα. This implies that SIRPα tyrosine-phosphorylation and CaMK signaling regulate SIRPα ectodomain cleavage via distinct pathways.

Inhibitors of Src and JAK family kinases suppress neural activity-driven SIRPα ectodomain cleavage

Based on my data that inhibitors of Src and JAK family kinases suppress SIRPα tyrosine phosphorylation in response to neural activity (Fig. 2.7), I next wanted to determine if these kinase inhibitors also suppress activity-dependent SIRPα ectodomain cleavage in neurons. I first determined that KCl-dependent neuronal activation affects the SIRPα cleavage by sequential immunostaining (see Fig. 2.6). After KCl treatment, I stained the neurons with the SIRPα N-terminal antibody without permeabilization (to detect surface "ectodomain-containing SIRPα"), and then with the SIRPα C-terminal antibody (to detect "total SIRPα") and VGluT1 antibody (to mark synapses) with permeabilization. I quantified the Ectodomain/Total SIRPα ratio at synapses. I found that KCl treatment resulted in a decrease in this ratio: the intensity of surface ectodomain-containing SIRPα at the synapse significantly decreased following KCl treatment, while the level of total SIRPα stayed constant (Fig. 2.8, A-C). TIMPs, the proteinase inhibitors that inhibit SIRPα ectodomain cleavage, blocked the KCl-driven decrease in the amount of ectodomain SIRPα and the Ectodomain/Total SIRPα ratio (Fig. 2.8, A and B). These results support my conclusion that neuronal activation induces the cleavage of SIRPα ectodomain.

FIGURE 2.7. Inhibition of Src and JAK family kinases, but not CaM kinases, block activity-dependent SIRPα tyrosine-phosphorylation in neurons *(next page)*.

(A and B) Hippocampal neurons were cultured to DIV12 and treated with inhibitor cocktail (50 μM picrotoxin, 10 μM CNQX and 50 μM AP5) for 7 hours. In the last hour, 10 μM PP2, 10 μM AG490, or DMSO was added to these cultures. Cultures were then washed and treated with either inhibitor cocktail or 55 mM KCl, with either PP2, AG490, or DMSO for 20 minutes. SIRPα was immunoprecipitated (with SIRPα C-Term antibody) from the cell lysate and blotted for phosphotyrosine and SIRPα (N-Term). (B) Graph shows fold increase in SIRPα phosphorylation by KCl treatment in the presence of PP2, AG490, or DMSO. KCl treatment significantly increased SIRPα tyrosine-phosphorylation in DMSO-treated neurons, but not in the presence of PP2 or AG490. (C and D) Basal levels of SIRPα tyrosine-phosphorylation in the presence of PP2, AG490, or DMSO. Basal-level SIRPα phosphorylation was decreased by PP2 but not by AG490 application. (E–G) Hippocampal cultures were treated at DIV12, with inhibitor cocktail + 5 μM KN62 for 7 hours. Cultures were washed and treated with DMSO, DMSO + 55 mM KCl, 5 μM KN62, or KCl + KN62 for 20 minutes. (E) Cultures were immunostained for CaMK-pT286 antibody to detect levels of CaMK activation. Treatment of cultures with KN62 effectively suppressed CaMK activation. (F and G) SIRPα was immunoprecipitated from the cell lysates and blotted for phosphotyrosine and SIRPα. Graph (G) shows the amount of tyrosine-phosphorylated SIRPα (normalized to DMSO). KCl-driven tyrosine phosphorylation of SIRPα was not inhibited by KN62. n = (B) 12 (DMSO), 5 (PP2), and 5 (AG490) cultures; (D) 6 cultures per group from 6 independent experiments; (E and G) 5 (KCl) and 6 (KCl + KN62) cultures from 4 independent experiments. Data are mean ± s.e.m. n.s. not significant ($P > 0.05$), *$P < 0.05$, **$P < 0.01$, ****$P < 0.001$ by Kolmogorov-Smirnov test (B and G) or one-way ANOVA followed by Tukey's test (D and E).

Figure 2.7 (Continued)

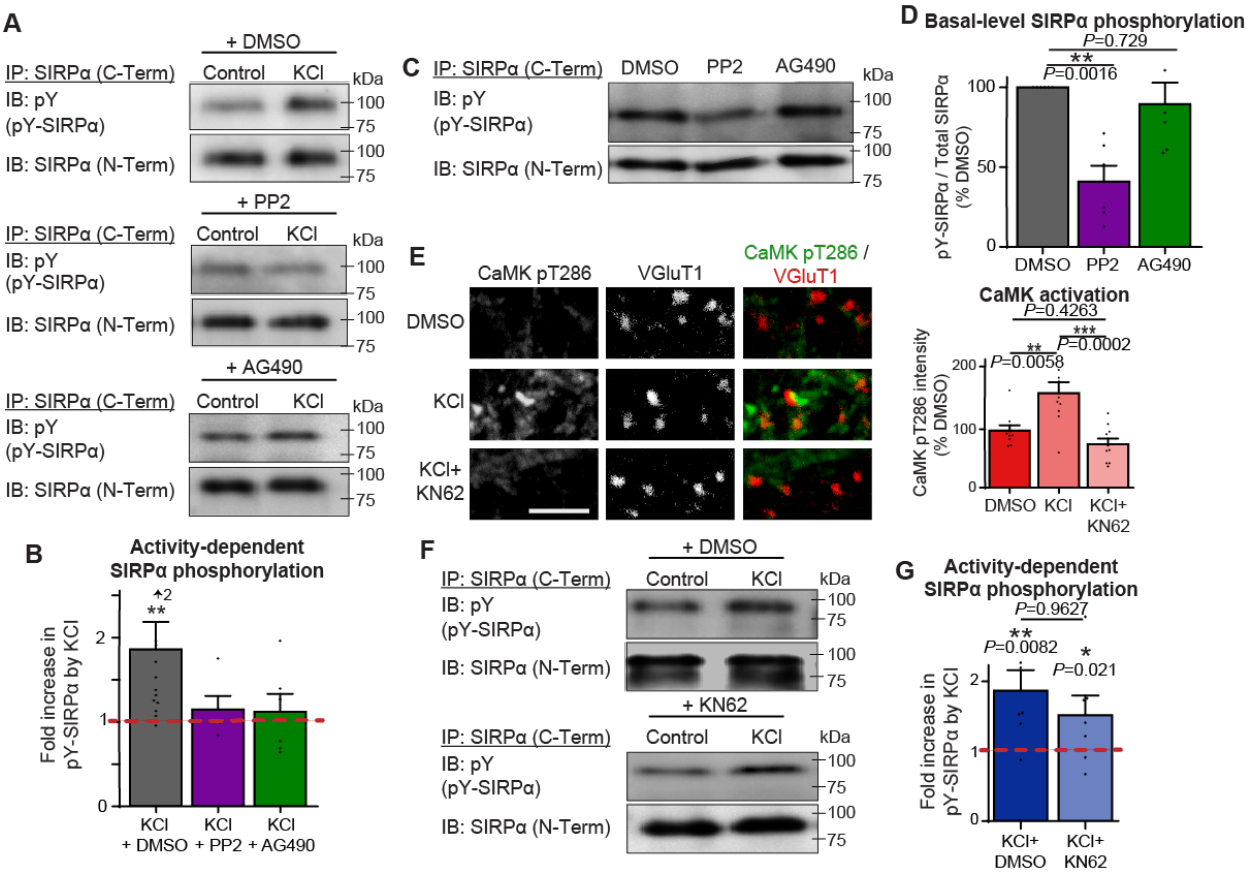

FIGURE 2.8. Inhibition of Src and JAK family kinases prevents activity-dependent SIRPα ectodomain cleavage in neurons *(next page)*.

(A-C) Hippocampal neurons were cultured to DIV12 and left untreated or treated with KCl or KCl + TIMPs for 2 hours. The amount of Ectodomain and Total SIRPα (endogenous) at excitatory synapses (identified by VGluT1 staining) was examined as described in Figure 6. (B) Quantification of the ratio of Ectodomain/Total SIRPα. KCl-driven neuronal activation decreased the ratio of Ectodomain/Total SIRPα. This decrease was blocked by TIMPs. (C) Total levels of SIRPα are not significantly different between all groups. (D-G) Hippocampal neurons were cultured to DIV12 and treated with either 10 μM PP2, 10 μM AG490, or DMSO, with or without 55 mM KCl for 2 hours. The amount of Ectodomain and Total SIRPα at excitatory synapses was examined as described above. (E) Quantification of the ratio of Ectodomain/Total SIRPα. AG490 and PP2 blocked the KCl-induced decrease in the ratio of Ectodomain/Total SIRPα. (F) Quantification of Ectodomain SIRPα. (G) Levels of total SIRPα were not changed in all groups. n = (A-C) 70 (UT), 59 (KCl), 50 (KCl + TIMPs); (D-G) 56 (UT), 55 (KCl), 58 (PP2), 62 (KCl + PP2), 58 (AG490), 62 (KCl + AG490) synapses from 3 independent experiments. Data are mean ± s.e.m. n.s. not significant ($P > 0.05$), *$P < 0.05$, **$P < 0.01$, ***$P < 0.005$, ****$P < 0.001$ by one-way ANOVA followed by Tukey's test.

Figure 2.8 (Continued)

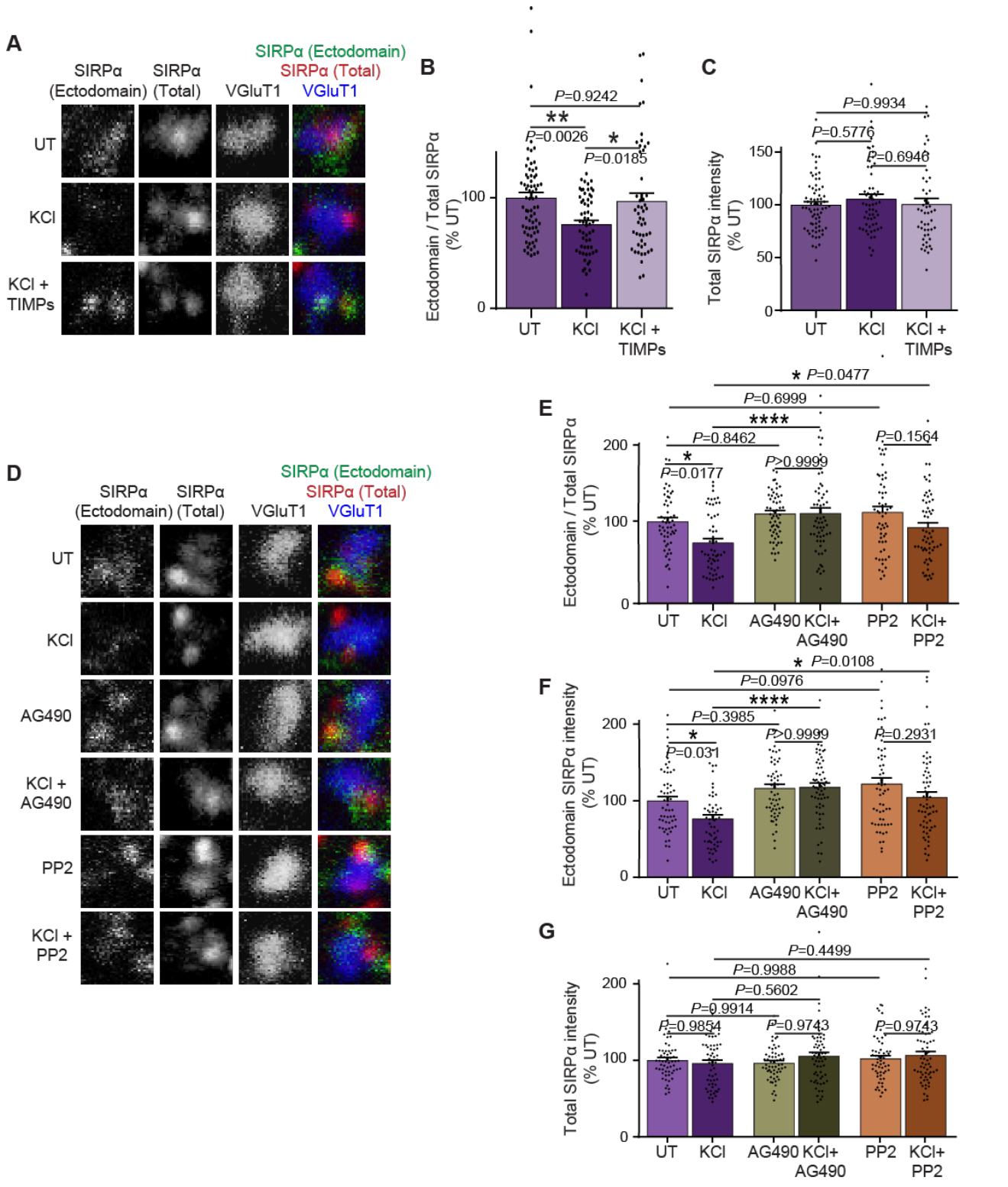

I next performed these experiments with the addition of the kinase inhibitors, PP2 or AG490, which block activity-dependent phosphorylation of SIRPα (Fig. 2.8, D). I found that PP2 or AG490 treatment inhibited the KCl-driven decrease in the amount of ectodomain SIRPα and the Ectodomain/Total SIRPα ratio (Fig. 2.8, E). These results indicate that the inhibition of Src or JAK family kinases inhibits the activity-dependent ectodomain cleavage of SIRPα.

2.4 Discussion

Selective maturation of active synapses is critical for the establishment of functional neural circuits (Katz and Shatz, 1996; Kasai et al., 2010; Yasuda et al., 2011; Santini et al., 2013; Penzes et al., 2013; Tang et al., 2014). While a few molecules have been identified as regulators of synapse maturation (Toth et al., 2013; Bemben et al., 2014; Nagappan-Chettiar et al., 2017; Terauchi et al., 2016), the mechanisms through which these molecules detect synaptic activity and signal synapse maturation selectively at active synapses remain unclear. Here, we identified a critical role for the tyrosine phosphorylation of SIRPα in activity-dependent synapse maturation. We showed that: i) tyrosine phosphorylation of SIRPα peaks in vivo during the synapse maturation period; ii) SIRPα phosphorylation is driven by neural activity; iii) in contrast to wild-type SIRPα,the phosphorylation-deficient SIRPα mutant cannot drive presynaptic maturation; iv) tyrosine phosphorylation of SIRPα controls the ectodomain cleavage of SIRPα, which in turn, signals presynaptic maturation; and v) Inhibitors of Src and JAK family kinases suppress activity-dependent tyrosine-phosphorylation and ectodomain cleavage of SIRPα in neurons. Collectively, our results demonstrate that tyrosine phosphorylation of SIRPα serves as a molecular switch that detects neuronal activity and turns on the maturation of active synapses by promoting the cleavage of SIRPα’s ectodomain.

Tyrosine phosphorylation of SIRPα as a synaptic activity sensor

SIRPα is an activity-dependent regulator of excitatory presynaptic maturation (Toth et al., 2013). The overexpression of wild-type SIRPα in neurons drives presynaptic maturation; however, this only occurs when neuronal activity is present. So, how does SIRPα detect synaptic activity and drive the maturation of active synapses only? Here I showed that tyrosine phosphorylation of SIRPα is driven by neuronal activity (Fig. 2.3) and that this phosphorylation is necessary for SIRPα's ability to drive presynaptic maturation during development (Fig. 2.4). This makes SIRPα tyrosine-phosphorylation a key mechanism through which SIRPα senses neuronal activity and converts it to synaptogenic activity. Tyrosine phosphorylation of SIRPα is a temporally and spatially regulated, activity-dependent mechanism that allows SIRPα to function specifically at active synapses during development.

SIRPα tyrosine-phosphorylation may be a general mechanism for SIRPα to detect various stimulations, not only during development, but also in adulthood. Light stimulation, hypothermia, and stress can affect SIRPα phosphorylation in the adult brain (Nakahata et al., 2000; Hamada et al., 2004; Ohnishi et al., 2010; Maruyama et al., 2012). The precise roles of these phosphorylation events are not known, but tyrosine phosphorylation of SIRPα may serve as a sensor of various brain activities even in adults.

Tyrosine phosphorylation of SIRPα as a 'cleave me' signal

How does SIRPα tyrosine-phosphorylation regulate synapse maturation? Our previous work demonstrated that the ectodomain of SIRPα is cleaved, and this cleavage is essential for presynaptic maturation (Umemori and Sanes, 2008; Toth et al., 2013). Here I showed that SIRPα tyrosine-phosphorylation regulates this cleavage (Fig. 2.5 and 2.6). Thus, I propose that the activity-dependent tyrosine-phosphorylation of SIRPα serves as a mechanism to tag SIRPα for cleavage.

How the tyrosine phosphorylation of SIRPα controls the cleavage of its ectodomain is an important next question. Possible mechanisms include: 1) SIRPα phosphorylation activates downstream signaling that regulates proteinase expression. One possible downstream signaling molecule is SHP2. Upon phosphorylation, SIRPα recruits SHP2 (Fig. 2.1, B). SHP2 has been implicated in the regulation of MMP-2 and 9 expression (Zhao and Agazie, 2015); and 2) SIRPα phosphorylation leads to the recruitment of proteinases. For example, ADAM10, which has an intracellular substrate-binding domain, interacts with Ephrin-family of cell adhesion molecules (Janes et al., 2005; Atapattu et al., 2012). This interaction facilitates Ephrin cleavage. Similar mechanisms might exist for SIRPα.

The cleavage of SIRPα is suggested to be regulated by MMP/ADAM10 proteinases (Toth et al., 2013; Londino et al., 2015). At the synapse, there are several other synaptic proteins including Neuroligins, N-Cadherin and Nectin that are known to undergo MMP/ADAM-mediated proteolytic cleavage (Reiss et al., 2005; Kim et al., 2010; Peixoto et al., 2012; Suzuki et al., 2012). How MMPs and ADAMs recognize these synaptic proteins is unknown, but the phosphorylation of these synaptic proteins may also play a role in tagging them.

Multiple signaling pathways coordinate to regulate SIRPα tyrosine-phosphorylation and cleavage

Src and JAK family kinases are two major tyrosine kinase families in the brain. Furthermore, many members of these kinase families are known to be activated by neuronal activity (Lu et al., 1998; Niimura et al., 2005; Nicolas et al., 2012). Here I identified that the activity of both Src and JAK family kinases regulate tyrosine phosphorylation of SIRPα during synapse maturation. Interestingly, the inhibition of Src family kinases resulted in a decrease in both basal and activity-dependent SIRPα phosphorylation, while the inhibition of JAK family kinases only deterred activity-dependent SIRPα phosphorylation (Fig. 2.7). These results hint at the possibility that these different kinase groups may coordinate to regulate SIRPα phosphorylation during

synapse development, perhaps by phosphorylating different tyrosine residues to send different signals downstream. These data also suggest that Src family kinases may phosphorylate and prime SIRPα to then be phosphorylated by JAK kinases upon stimulation by neuronal activity. Signals from both kinase families need to coincide to drive the activity-dependent tyrosine phosphorylation of SIRPα.

For the ectodomain cleavage of SIRPα, we have previously shown that CaMK signaling is necessary (Toth et al., 2013). Here we showed that tyrosine phosphorylation of SIRPα is also necessary for SIRPα cleavage (Fig. 2.5 and 2.6). However, I found that CaMK signaling is not necessary for the activity-dependent tyrosine phosphorylation of SIRPα (Fig. 2.7). Thus, at least two distinct signaling pathways, CaMK and SIRPα tyrosine-phosphorylation pathways, are necessary for the cleavage of SIRPα. CaMK signaling may be involved in the direct regulation of proteinase activity in response to neuronal activity and act in parallel with Src and JAK family kinase signaling to regulate SIRPα cleavage.

In summary, our work identified a novel molecular mechanism that governs the function of SIRPα in sensing neural activity and driving the maturation of active synapses. SIRPα-driven hippocampal synaptic maturation is a highly regulated process that requires proper signaling of multiple pathways in response to synaptic activity. A comprehensive understanding of the signals that govern synapse development can further our understanding of and expose novel therapeutic strategies to prevent and/or treat various neuropsychiatric disorders associated with abnormal synapse maturation.

2.5 Experimental Procedures

Mouse strains

Sirpa$^{fl/fl}$ and *Actin-CreER* mutant mice were described previously (Toth et al., 2013). Wild-type (WT) mice were ICR/CD-1 (Charles River) (Fig. 2.3, 2.7 and 2.8) or C57/B6 (Jackson) (Fig. 2.2).

All animal care and use were in accordance with the institutional guidelines and approved by the Institutional Animal Care and Use Committee at Boston Children's Hospital.

Primary neuronal cultures, transfection, and treatment

For all neuronal cultures used, hippocampi were dissected from postnatal day (P) 0-1 mice and dissociated with 0.5 % trypsin (Terauchi et al., 2010; Toth et al., 2013; Dabrowski et al., 2015; Terauchi et al., 2015; Terauchi et al., 2016). For immunoprecipitation and western blot experiments, 300,000 cells were plated on poly-D-lysine coated dishes (35 mm). For immunostaining experiments, 75,000-80,000 hippocampal neurons were plated on poly-D-lysine coated glass coverslips (diameter 12 mm) and grown in culture media (B27 (Gibco), 2 mM L-glutamine, 100 U/ml penicillin-streptomycin in Neurobasal medium (Gibco)). For electrophysiology experiments, 80,000 neurons were plated and grown in culture media (GS21 (MTI-GlobalStem, Sigma), 2 mM L-glutamine, 100 U/ml penicillin-streptomycin in NeuralQ medium (Sigma)).

For transfection experiments, 1-2 µg of plasmids per coverslip were transfected using CalPhos transfection kit (Clontech) at DIV3-4 (Terauchi et al., 2010; Toth et al., 2013; Dabrowski et al., 2015; Terauchi et al., 2015; Terauchi et al., 2016). Neurons were cultured for 16-19 days and subjected to biochemical, histological, and electrophysiological experiments.

For the treatment with inhibitors described in Fig. 2.3 and 2.7, neurons were cultured for 12 days, after which culture media was replaced by new media containing inhibitor cocktail (50 µM picrotoxin, 10 µM CNQX and 50 µM AP5) and incubated for 7 hours. Cultures were treated with a kinase inhibitor: 10 µM PP2 or 10 µM AG490 (for the last 1 hour) or 5 µM KN62 (for 7 hours). Since inhibitors were dissolved in DMSO, equal volume of DMSO was added to control cultures. Media was then replaced with new culture media containing inhibitor cocktail or 55 mM KCl, with or without the kinase inhibitor for 20 minutes. For the treatment with inhibitors described in Fig. 2.6 and 2.8, neurons were cultured for 12 days, after which culture media was replaced by new

media. Cultures were then either untreated or treated with 55 mM KCl with or without inhibitors: 10 μM PP2, 10 μM AG490, or 0.5 μg/mL each of TIMP1 and TIMP2 (for 2 hours). Since inhibitors were dissolved in DMSO, equal volume of DMSO was added to control cultures.

COS cell culture and transfection

COS7 cells (ATCC) were cultured in DMEM (Gibco) supplemented with 10% FBS (Corning). Transfections were done via Lipofectamine 3000 (Thermo Fisher) method or via calcium phosphate method. Cells were cultured for 1-3 days following transfection and subjected to biochemical and histological experiments. In the sodium orthovanadate experiments, cultures were treated with 1 mM sodium orthovanadate for 7-17 hours prior to biochemical experiments.

DNA constructs

A cDNA encoding the tyrosine phosphorylation-deficient SIRPα (SIRPα4YF) was generated by PCR using the following primer pairs: Set 1: 5'GCCCACTCGAGTGATCAAGGG 3' and 5'TGTGATATCGTTGATGTCATTTG3'; Set 2: 5'TCAACGATATCACATTTGCAGACCTGAA3' and 5'TTACCGGTCTCAATGCTTGCAAATTCTGTGTGG3'; Set 3:5'TCAACGATATCACAGAA GCAGACCTGAA3' and 5'TTACCGGTCTCAATGCTTGCTTCTTCTGTGTGG3'; Set 4: 5'AGACCGGTAAAGTGCCTAGGCCAGAGGATACCCTCACCTTTGCTGACCTGG3' and 5'CTT CTAGATCACTTCCTCTGGACCTGGACACTAGCAAACTCTGAGAAA3'; and Set 5: 5'AGACC GGTAAAGTGCCTAGGCCAGAGGATACCCTCACCGAAGCTGACCTGG3' and 5'CTTCTAGAT CACTTCCTCTGGACCTGGACACTAGCTTCCTCTGAGAAA3'. The amplified fragments were ligated with SIRPαWT cDNA in the pAP-TAG5 vector (Umemori and Sanes, 2008) (digested with Xho1 and Xba1). This replaces four intracellular tyrosine amino acids with phenylalanine. All PCR products were verified via sequencing. JAK2VF was generated by site-directed mutagenesis of JAK2 cDNA using the following primer pair: 5'TTTTGAATTATGGTGTCTGTTTCTGTGGAGAGG AGAACATT3' and 5'AATGTTCTCCTCTCCACAGAAACAGACACCATAATTCAAAA3'. This

substitutes valine 618 to phenylalanine. PSD95-GFP and StopYFP were described previously (Dabrowski et al., 2015; Terauchi et al., 2015).

Immunoprecipitation and western blotting

For cultured cells, media and cells were collected separately. Cells were lysed in lysis buffer containing: 1% Triton X-100, 50 mM Tris-Cl (pH8), 150 mM NaCl, 1 mM Na3VO4 with a protease inhibitor cocktail tablet (Roche). Dissected hippocampi were lysed by homogenization in 10 volumes of lysis buffer per gram of tissue. Protein concentrations were measured by protein assays (BCA, Pierce). Media or lysates were incubated with 1 µg of anti-SIRPα (p84; BD; BDB552371) or 3 µg of anti-SIRPα C-terminus (QED; 2428) antibodies for 2 hours at 4°C. Equal amounts of lysates and equal volume of media from each experimental condition were used for immunoprecipitation. The immune complexes were precipitated with Protein-L or Protein-A (Pierce). Immunoprecipitates and lysates were subjected to SDS-PAGE. Proteins were transferred to a polyvinylidene difluoride (PVDF) membrane (BioRad), blocked with 3% non-fat milk and blotted using anti-SIRPα (p84; BD; 1:1000), anti-phosphotyrosine (4G10; Millipore; 05-321X; 1:1000), anti-SHP2 (Santa Cruz; SC-7384; 1:1000), anti-αTubulin (DM1A; Invitrogen; 62204; 1:1000), anti-N-Cadherin (BD; 610921; 1:1000) and anti-JAK2 (CST; 3230P; 1:1000). The proteins were visualized by chemiluminescence (BioRad) and imaged with ImageQuant LAS4000. Band intensities were quantified with FIJI software. For this, rectangles of equal length and width were drawn around each protein band within the blot and used as the region of interest. The width of the rectangle was drawn to fit the width of the band, while the length of the rectangle was drawn to include 3 times the length of the band above and below the protein band of interest. An intensity profile plot was created using Image J for each rectangle. The intensity of each peak was measured from this plot, which allows for the background to be subtracted using the intensity of the regions above and below the protein band for each lane. For the quantification of

phosphorylated SIRPα to total SIRPα, the blots were probed first for phosphotyrosine (4G10), stripped, and reprobed for SIRPα.

For the calculation of SIRPα ectodomain secretion (Fig. 2.5C), media and lysates were first blotted with the SIRPα N-Term antibody, stripped, and then with the SIRPα C-Term antibody. Following SIRPα band intensities were quantified: Media (IB: N-Term, Media), Full-N (N-Term, Lysates), Full-C (C-Term, Lysates, upper band), and C-Fragment (C-Term, Lysates, lower band). The rate of SIRPα ectodomain cleavage was calculated using the formula: Media / ((Full-C + C-Fragment) * (Full-N / Full-C)) / hours. (Full-C + C-Fragment), detected by SIRPα C-Term antibody, implies total SIRPα. Since SIRPα in Media was detected with SIRPα N-Term antibody, the ratio of Full-N / Full-C was used to normalize between two blots blotted with N-Term and C-Term antibodies.

Immunocytochemistry

Cultured neurons were fixed with 3% paraformaldehyde (PFA) for 10 min at 37°C and blocked in 2% BSA, 2% normal goat serum and 0.1% Triton X-100 for 1 hour at room temperature. This is followed by incubation with primary antibodies for 3 hours at room temperature or overnight at 4°C. The cultures were then washed with PBS, and secondary antibodies were applied for 1 hour at room temperature. After being washed again with PBS, samples were mounted in glycerol with n-propyl gallate (Sigma). The following antibodies and dilutions were used: anti-VGluT1 (Millipore; AB5905; 1:4000), anti- GFP (Aves Labs; GFP-1020; 1: 5000), anti-SIRPα (clone p84; BD; 1:200). For surface staining, similar protocol as described was used, however, Triton X-100 was omitted to prevent membrane permeabilization.

Image acquisition and analysis

Imaging was done with a confocal microscope (Zeiss LSM 700) using 40x and 63x objectives at a resolution of 1024x1024 pixels. Images were taken as 16-bit, z-stack images with a 0.5 µm step

size. Identical settings for laser power, master gain, digital gain and offset were used for all acquired images within each experiment. For VGluT1 density analysis: transfected pyramidal-like neurons were selected for imaging at random. For analysis, images were stacked and merged using FIJI software, and VGluT1 puncta on transfected dendrites after the primary branch point (identified by GFP or YFP expression) were analyzed using MetaMorph (Molecular Devices). The quantification was done blind. Puncta that were within a region 0.3 μm away from the dendritic shaft and spines were included for analysis. The staining intensity of VGluT1 in the dendritic shaft was subtracted as background. This background intensity was similar between conditions. Puncta smaller than four pixels (~0.04 μm2) were excluded from analysis. Dendritic lengths were measured by manually tracing of analyzed dendritic lengths in FIJI.

For Ectodomain / Total SIRPα analysis, transfected pyramidal-like neurons (Fig. 2.6) or fields of neuronal cultures (Fig. 2.8) were selected for imaging at random. For analysis, images were stacked using FIJI software, and regions of interest (ROI) were selected as follows: 1) For analysis in Fig. 2.6, PSD95-EGFP positive puncta were selected as the ROI; and 2) For analysis in Fig. 2.8, SIRPα (C-Term) positive puncta with >10% overlap with VGluT1 puncta were selected as the ROI. The average intensity of SIRPα (C-Term) and SIRPα (N-Term) staining within the ROI was measured. 5-10 ROIs were selected at random per transfected neuron (Fig. 2.6) or per field of image (Fig. 2.8).

Electrophysiology

mEPSCs were recorded via whole-cell patch-clamp recordings of cultured hippocampal neurons as previously described (Toth et al., 2013; Terauchi et al., 2015). Neurons were placed in HEPES-buffered saline (119 mM NaCl, 5 mM KCl, 2 mM CaCl2, 2 mM MgCl2, 30 mM glucose, 10 mM HEPES) supplemented with 1 μM TTX and 50 μM picrotoxin. Recordings were made with glass pipettes (resistance 4-6 MΩ) filled with internal solution (100 mM gluconic acid, 0.2 mM EGTA, 5

mM MgCl2, 2 mM ATP, 0.3 mM GTP and 40 mM HEPES). Recordings were made with a Multiclamp 700 amplifier (Molecular Devices) and data were collected with Clampex 10.3. (Molecular Devices). mEPSCs were analyzed using Minianalysis 6.0 (Synaptosoft). All recordings and mEPSC analyses were done blind.

Statistical analysis

Statistical analyses were performed using GraphPad Prism software. Statistical tests used were Kolmogorov-Smirnov test, Student's t-test, one-way ANOVA, or two-way ANOVA as indicated in the figure legend. In the case of one-way ANOVA, post hoc analysis was done with Tukey's test. In the case of two-way ANOVA, post hoc analysis was done with Sidak's test. All data are mean ± s.e.m. In all figures, n.s. ($P > 0.05$), * ($P < 0.05$), ** ($P < 0.01$), *** ($P < 0.005$) and **** ($P < 0.001$). Sample sizes were similar to those reported in previous publications (Terauchi et al., 2010; Toth et al., 2013; Dabrowski et al., 2015; Terauchi et al., 2015; Terauchi et al., 2016). Post hoc statistical calculation of sample sizes for imaging and electrophysiology was also done to ensure that sample sizes had sufficient power for subsequent statistical analyses (at least 80% power at the 0.05 level of significance for each set of experiments).

Chapter 3.

Pyk2 and JAK2: Molecular determinants of inactive synapse elimination

I performed experiments and analyzed all data for all figures except Figures 3.1, 3.2, 3.8 and 3.9 C-E which were done by Masahiro Yasuda. Parts of this chapter are from a paper in revision: Yasuda, M., Nagappan-Chettiar, S., Johnson-Venkatesh, E. M., Umemori, H. *Neuron.*

3.1 Abstract

To establish functional neuronal circuits in the brain, synaptic connections are refined by neural activity during development, where active connections are maintained while inactive ones are eliminated. However, the molecular signals that regulate synaptic refinement remain to be elucidated. When we inactivate a subset of neurons in the mouse cingulate cortex, their callosal connections are eliminated through activity-dependent competition. Using this system, we performed an RNAseq screen comparing gene expression in active vs. inactive neurons just prior to the start of synaptic refinement and we identified Pyk2 tyrosine kinase as a key regulator of inactive synaptic elimination. We determined that the transcript encoding Pyk2 is differentially expressed in inactive neurons relative to active neurons prior to the start of elimination. We showed that Pyk2 kinase signaling is necessary for the structural elimination of inactive axons. I showed that: presynaptic Pyk2 is necessary for functional synapse elimination; Pyk2 activation peaks at cortical synapses at the start of elimination; and Pyk2 is activated at inactive synapses in response to signals from other active synapses. Additionally, we determined that JAK2, a Pyk2 interacting kinase, signaling is critical for synaptic elimination. I show that JAK2 signaling drives synaptic elimination and JAK2 is active at inactive synapses. Therefore, we propose that Pyk2 and JAK2 are activity-dependent switches that serve as determinants of inactive synapse refinement.

3.2 Introduction

Formation of appropriate synaptic connections is critical for the proper functioning of the

brain. Early in development, neurons form an excess of immature synapses. To establish efficient and functional neural networks, neurons selectively stabilize active synapses and eliminate inactive synapses. This process is known as activity-dependent synaptic refinement (Balice-Gordon and Lichtman, 1994; Katz and Shatz, 1996; Sanes and Lichtman, 1999; Goda and Davis, 2003; Yasuda et al., 2011). Defects in this fundamental process of wiring the brain have been implicated in various neurological and psychiatric disorders such as schizophrenia and ASD (Innocenti et al., 2003; Paul et al., 2007). Thus, the identification of critical molecular regulators of refinement will lead to the understanding of the fundamental mechanisms underlying appropriate brain wiring and may inform novel therapeutic strategies.

Previous work in the lab elucidated the manner through which neuronal activity regulates refinement in the brain (Yasuda et al., 2011). This work demonstrated that inactive synaptic connections are eliminated only when there are other connections that are active to compete with. When a subset of inputs is inactive, the inactive inputs are eliminated. Contrarily, when all inputs are inactive, elimination does not occur. This suggests that active connections send a *'punishment'* signal to inactive ones and instruct them to leave by triggering *'elimination'* signals within inactive synapses. However, the molecular identities of the *'elimination'* signals, which detect levels of synaptic activity and determine if a synapse should be eliminated during refinement, remain to be elucidated.

At active synapses, connections are strengthened by the presence of *'maturation'* signals. Several molecules including SIRPα-CD47, C1ql1-Bai3 and Fn14, have been implicated in active synapse strengthening (Toth et al., 2013; Nagappan-Chettiar et al., 2018; Kakegawa et al., 2015; Cheadle et al., 2018). In contrast, far less is known about the mechanisms of inactive synapse elimination (summarized in Table 1.1). Some studies have suggested that MHCI-PirB regulates synapse elimination by mediating signaling within the postsynaptic neuron (Datwani et al., 2009; Lee et al., 2014). Other studies have implicated complement proteins as executors of synapse elimination, where complement proteins are thought to recruit microglia to engulf synapses tagged

for elimination (Stevens et al., 2007; Schafer et al., 2012). However, the identity of the *'elimination'* signal, the decision-making molecule *within the presynaptic neuron* that *detects levels of synaptic activity* and determines whether the synapse should be *eliminated*, is unknown.

Here, we established a novel *in vivo* system to study activity-dependent synapse refinement. Using this system in combination with RNAseq, we identify Pyk2 (Fig. 1.4 top), a calcium-dependent protein tyrosine kinase implicated in adult plasticity and degenerative synapse loss, as an activity-dependent determinant of synapse elimination. We show that: 1) inactive connections are not eliminated when Pyk2 kinase activity is suppressed; 2) Presynaptic, and not postsynaptic, Pyk2 regulates physiological refinement of synaptic connections; 3) Pyk2 activation is high at the start of synaptic elimination; 4) Pyk2 is activated at inactive synapses in response to signals from other active connections; 5) JAK2 (Fig. 1.4 bottom), a Pyk2 interacting kinase, signaling is necessary for and can drive synaptic elimination; and 6) JAK2 is active at less active synapses. Together, our findings reveal novel activity-dependent molecular determinants of synapse elimination that can be switched on at inactive synapses to drive their elimination and shape functional neural networks.

3.3 Results

Activity-dependent competition eliminates inactive callosal axons during development

We first developed an *in vivo* system to study activity-dependent synapse refinement (Fig. 3.1 and S1). We focused on the refinement of callosal connections between the cerebral hemispheres (the corpus callosum). The corpus callosum is the largest axon tract in the brain, originating from cortical callosal neurons. It transfers motor, sensory, and cognitive information between the two cerebral hemispheres (Fame et al., 2011). Neural activity plays important roles in the development of callosal axons: neural activity affects both callosal axon refinement (Grigonis and Murphy, 1994) and layer targeting (Mizuno et al., 2007). In our system, we suppressed the neural activity of a subset of cortical callosal neurons by introducing tetanus toxin

light chain (TTLC), which inhibits neurotransmitter release by cleaving the SNARE protein, VAMP2 (Yasuda et al., 2011; Yu et al., 2004). We co-expressed EGFP to label TTLC-expressing neurons (Fig. 3.1 A). As a control, we introduced EGFP alone. We used *in utero* electroporation (Saito and Nakatsuji, 2001; Saito, 2006) to introduce TTLC and/or EGFP into left cingulate cortical neurons: co-electroporation efficiency was 98.7 ± 1.6% (Fig. S1 A and B). Electroporated cells were neurons and not astrocytes or microglia (Fig. S1 C). Of these neurons, 88.9 ± 4.6% were SATB2-positive callosal neurons (Fig. S1 D). We set the condition of electroporation so that ~20% (19 ± 1.1 %) of callosal neurons in layer V of the cingulate cortex were electroporated (Fig. S1 C). Thus, when TTLC is electroporated, there can be a competition between active (~80 %) and inactive (~20 %) callosal neurons.

We performed electroporation at E13.5 and prepared coronal sections at postnatal day (P) 5, P10, and P15 (Fig. 3.1 B). Callosal connections between the cingulate cortices are mostly homotopic, and thus, axon projections and targeting can be readily observed in the same section. At P5, callosal axons from the left hemisphere already project to the right hemisphere in both control (EGFP alone) and TTLC-electroporated brains (Fig. 3.1 C and F). Quantification of the density of EGFP-positive axons in the right hemisphere showed that TTLC did not affect initial axon targeting, as the axon density was similar between controls and TTLC-electroporated brains at P5 (Fig. 3.1 I; see Methods and Fig. S1 E and F for axon density calculation method). However, the axon density from the TTLC-expressing neurons decreased significantly relative to controls from P10 to P15 (Fig. 3.1 D, E, and G–I). These results indicate that inactive callosal axons are eliminated after they project to their target region. We also suppressed neural activity of callosal neurons using the DREADD system (Armbruster et al., 2007), which, like TTLC, led to significantly decreased callosal axon density at P15 (Fig. S1 G and H). Furthermore, TTLC-driven callosal axon elimination is not a result of neuronal death because TTLC-expressing neurons were not TUNEL (transferase–mediated deoxyuridine triphosphate nick end labeling)-positive (Fig. S1 I, TTLC) (Le et al., 2002).

FIGURE 3.1. Activity-dependent competition eliminates inactive callosal axons during development *(next page)*.

(A) *In utero* electroporation of EGFP into the left cingulate cortex (examined at P10). (B) Schematic of experiments. Electroporation of plasmids into the left cingulate cortex at E13.5 followed by analysis of callosal axons at P5, P10 and P15. Callosal axons were analyzed in coronal sections. Pictures were taken from the dotted boxed area. (C–H) Coronal sections of EGFP-only (Control; C–E) and EGFP+TTLC (TTLC; F–H) electroporated brains at P5, P10 and P15. The bottom panels show higher magnification images of callosal axons in the right hemisphere, taken from the boxed areas in the top panels. Scale bars, 200 μm (top), 50 μm (bottom). (I) Quantification of callosal axon densities in TTLC-expressing brains relative to Control brains. To quantify axon density, the EGFP signal intensity of callosal axons was normalized to that of electroporated neurons in the left hemisphere (see Methods and Figures S1E and S1F). Mean ± SEM. n = 9 mice, P5; 7, P10; 16, P15. ***$P < 0.001$ relative to P5, ANOVA followed by Tukey test. (J) Schematic of TTX application experiments. EGFP (Control) or EGFP+TTLC (TTLC) was electroporated at E13.5, Elvax-TTX was implanted at P3 on the cingulate cortex, and callosal axons were examined at P15. (K–M) Callosal axons in Control (K), TTLC without TTX (L), and TTLC with TTX (M) sections. (N) Quantification of callosal axon densities, relative to Control. TTX suppressed the elimination of TTLC-expressing callosal axons. Mean ± SEM. n = 10 mice. ****$P < 0.0001$, ANOVA followed by Tukey test.

FIGURE 3.1. (Continued)

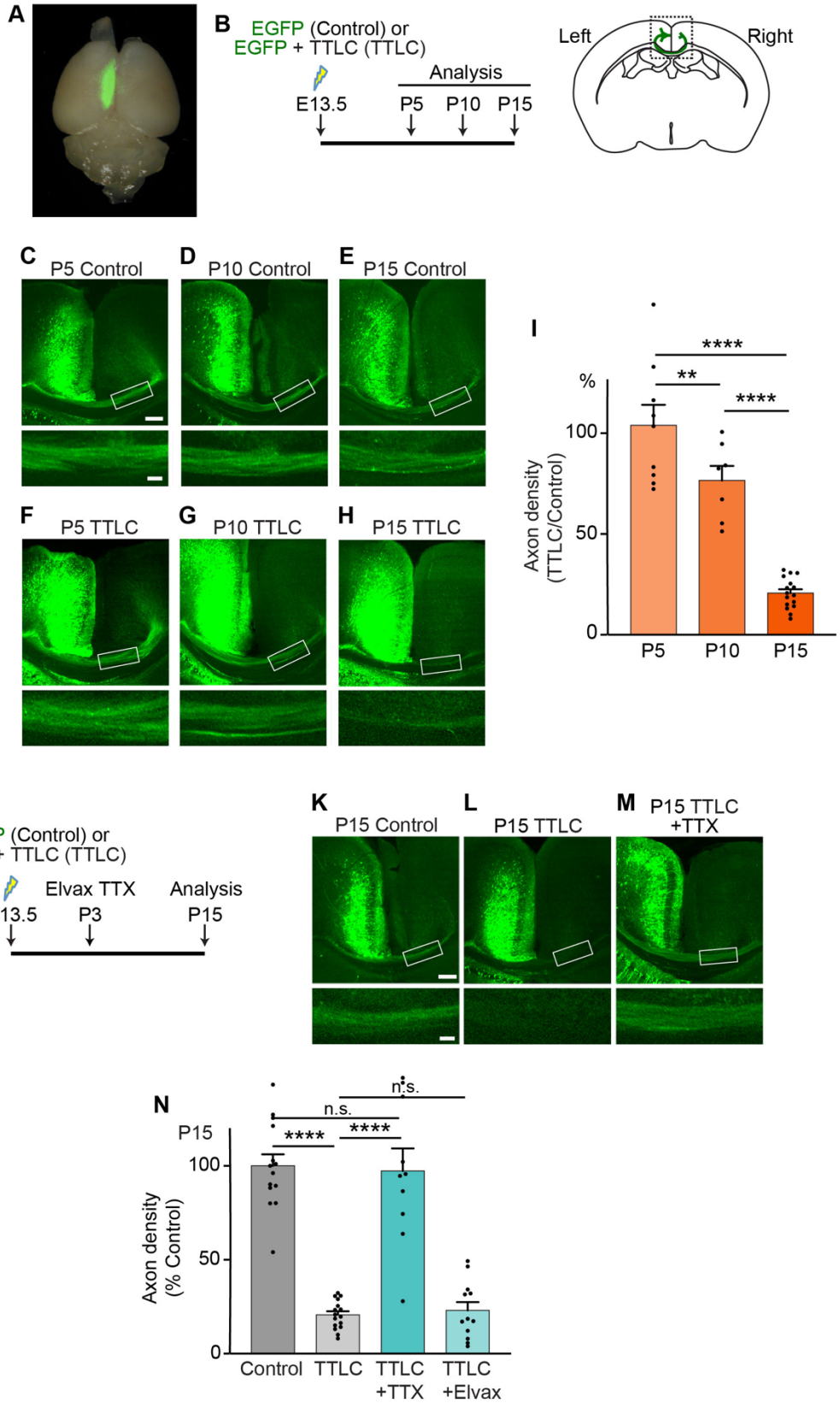

In the experiments described above, both active (~80 %) and inactive (~20 %) cortical callosal neurons were present – so that active callosal connections could compete with inactive connections. We next examined whether active callosal connections are necessary for inactive callosal axon elimination. For this, we globally suppressed the neural activity of callosal connections by applying tetrodotoxin (TTX), which blocks voltage-gated sodium channels and prevents neuronal firing. TTX containing-Elvax (ethylene vinyl acetate copolymer resins) was implanted on the left cortex at P3, and coronal sections were prepared at P15 (Fig. 3.1 J) (Echegoyen et al., 2007; Yasuda et al., 2011). We found that TTX treatment inhibited the elimination of TTLC-expressing callosal axons (Fig. 3.1 K–M), indicating that signals from active connections drive the elimination of inactive connections.

Identification of Pyk2 as a critical regulator of inactive axon elimination

To identify candidate *'elimination'* signals, we hypothesized that molecules that determine the elimination of inactive connections will be differentially expressed by active and inactive neurons just prior to developmental elimination. Therefore, we compared gene expression profiles between active and inactive callosal neurons before the start of elimination. We co-expressed, via *in utero* electroporation, EGFP and TTLC in cingulate cortical neurons (inactive neurons). As control (active neurons), we introduced EGFP alone. At P5, just prior to the start of inactive input elimination (Fig. 3.1 I), we dissected and dissociated the electroporated cingulate cortices, sorted for EGFP-positive neurons and performed whole-transcriptome RNA sequencing.

Our RNAseq data revealed several genes that are differentially expressed by active and inactive callosal neurons (Table 3.1). Of these, we focused on genes encoding kinases because they regulate various aspects of neural network development and function including axon growth, neurite differentiation, synaptic plasticity and axon regeneration (Maness, 1992; Wayman et al., 2008; Liu et al., 2011). These genes include protein tyrosine kinase 2 beta, *Ptk2b*, which encodes for the protein, Pyk2, and calcium/calmodulin dependent protein kinase 2 alpha, *Camk2a*, which

TABLE 3.1. List of genes that are upregulated in inactive callosal neurons relative to active callosal neurons at prior to elimination. Genes with p-value <0.0001 are shown in the table.

Symbol	Definition	Fold change
Cdk5r2	Cyclin dependent kinase 5 regulatory subunit 2	3.55082
Tgfb3	Transforming growth factor beta 3	6.74536
Spock1	Sparc (osteonectin), cwcv and kazal like domains proteoglycan 1	3.05988
Nefl	Neurofilament light	3.97272
Phyhip	Phytanoyl-CoA 2-hydroxylase interacting protein	3.17425
Ptk2b	Protein tyrosine kinase 2 beta	2.93597
Camk2a	Calcium/calmodulin dependent protein kinase 2 alpha	3.11844
Syt13	Synaptotagmin 13	3.31051
Vstm2l	V-set and transmembrane domain containing 2 like	3.19024
Slc17a7	Solute carrier family 17 member 7	3.1791
Cx3cl1	C-X3-C motif chemokine ligand 1	2.9458
Icam5	Intercellular adhesion molecule 5	3.03943

encodes for the protein, CaMKIIα.

To determine if these kinases regulate the elimination of inactive connections, we generated kinase-dead mutants of Pyk2 (Pyk2DN; Huang et al., 2001) and CaMKIIα (CaMKIIαDN; Yamagata et al., 2009), which serve as dominant-negative forms of kinases, and co-expressed them with TTLC and EGFP in a subset of left cortical callosal neurons by *in utero* electroporation. Controls expressed TTLC and EGFP (inactive control) or EGFP alone (active control). TTLC-expressing callosal axons were eliminated by P15. However, when Pyk2DN was co-expressed, TTLC-expressing inactive axons were no longer eliminated (Fig. 3.2 A and B). The co-expression of CaMKIIαDN did not prevent the elimination of TTLC-expressing inactive axons (data not shown). These results suggest that Pyk2 (Fig. 1.4, top), a calcium-dependent, non-receptor tyrosine kinase implicated in plasticity and neurodegenerative synapse loss, regulates the elimination of inactive connections.

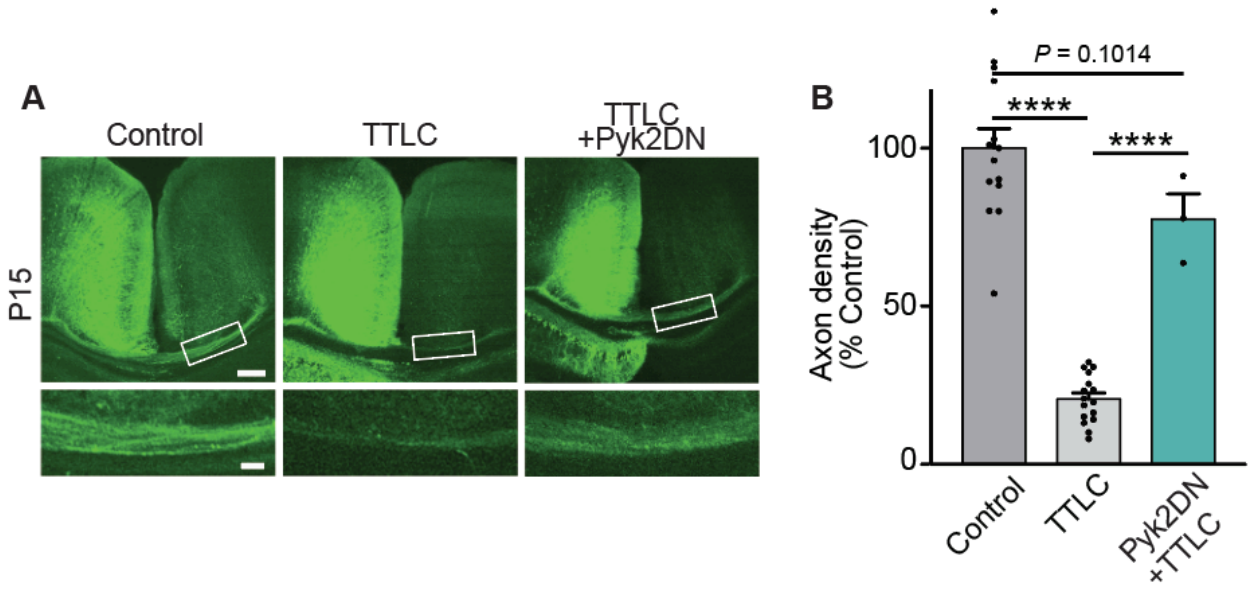

FIGURE 3.2. Pyk2 signaling regulates the elimination of inactive callosal axons during development.

(A-B) A dominant-negative form of Pyk2 (Pyk2DN) was co-electroporated with TTLC into callosal neurons. (A) Callosal axons were examined at P15. Higher magnification images from the boxed areas are shown in the bottom panels. Scale bars, 200 μm (top), 50 μm (bottom). (B) Quantification of callosal axon densities at P15 (n = 14 mice, Control; 16, TTLC; 3, TTLC+Pyk2DN). Mean ± SEM. ****$P < 0.0001$ by ANOVA followed by Tukey test.

Development of tools to determine the role of Pyk2 in synaptic refinement

Pyk2 signaling regulates the elimination of inactive callosal axons (Fig. 3.2). I next asked if Pyk2 is critical to functional synaptic refinement. To address this question, I developed: 1) a method of evaluating functional callosal synaptic refinement (Fig. 3.3) and 2) a conditional Pyk2 knockout mouse line to perform Pyk2 loss-of-function experiments in a cell type-specific manner (Fig. 3.4).

1) Establishment of the callosal fiber fraction method to functionally evaluate callosal synaptic refinement

To physiologically assess how the number of functional callosal inputs converging onto a target neuron changes through development, I developed the callosal fiber fraction (FF) method. For this, I recorded EPSCs (excitatory postsynaptic currents) from layer V pyramidal neurons by the whole-cell patch-clamp technique while electrically stimulating the callosal fiber bundle (Fig. 3.3 A). I recorded two types of EPSC responses: the single fiber response obtained by stimulating the callosal bundle at a minimal intensity at which more than 50 % of trials failed to induce a response (Fig. 3.3 B), and the maximum response obtained by increasing the stimulus intensity until the response amplitude reached a plateau. The FF ratio, calculated as the ratio of the single fiber response to the maximum response (single fiber / maximum), is a measure of the contribution of a single callosal input to the total callosal input received by a cell (Hooks and Chen, 2006, 2008; Noutel et al. 2011; Narushima et al. 2016). The inverse of the FF value provides a rough estimate of the callosal input number received by a cell.

In wildtype C57BL/6 mice, the single fiber response increased from P8-10 to P15-16, indicating that callosal synaptic strengthening occurs during development (Fig. 3.3 C). The maximum response increased significantly between P5-6 and P8-10 and then plateaued between P8-10 and P15-16 (Fig. 3.3 D). The calculated FF ratio decreased between P5-6 and P8-10 (Fig.

FIGURE 3.3. Fiber fraction method to determine functional callosal synapse refinement during development *(next page)*.

(A) Image of a wildtype mouse cortex on a coronal section indicating positions of whole-cell recording and stimulating electrodes. *CC*: corpus callosum.

(B) Representative traces from a cell demonstrating the “failure” method used to identify the single fiber response. Single fiber responses were obtained by stimulating the callosal bundle at a minimal intensity at which more than 50 % of trials failed to induce a response. On the left is a representative image with 10 superimposed trials from one cell. Individual trials are shown on the right. Success trials are in red and failure trials are in black. Arrow indicates stimulus onset.

(C-E) Functional changes in callosal synapses during different developmental ages in C57Bl/6 mice. (C) Representative traces and quantification of single fiber responses at different developmental ages. The single fiber response amplitude increases through development, indicating synaptic strengthening. (D) Representative traces and quantification of the maximum responses at different developmental ages. (E) Quantification of the fiber fraction (FF) ratio (single fiber amplitude / maximal amplitude). The FF ratio decreases from P5–6 to P8–10, indicating that more functional connections are being formed. The FF ratio increases from P8–10 to P15–16, indicating that functional synapse elimination occurs during this time. Data are mean ± SEM. n = 13 cells, P5–6; 48 cells, P8–10; 42 cells, P15–16. ****$P < 0.0001$, Kruskal-Wallis followed by Dunn’s multiple comparison test.

(F-H) In CD1 mice, functional callosal synapse refinement occurs earlier, between P6-7 and P10-11. (F) Representative traces and quantification of single fiber responses. The single fiber response amplitude significantly increased between P6–7 and P10–11 indicating synaptic strengthening. (G) Representative traces and quantification of the maximal response. There is no significant change in the maximum response amplitude suggesting that the total callosal drive to a cortical neuron does not change between P6–7 and P10–11. (H) Quantification of the fiber fraction. The fiber fraction significantly increased between P6–7 and P10–11 suggesting that callosal inputs are eliminated between P6–7 and P10–11. Data are mean ± SEM. n = 29 cells, P6–7; 34 cells, P10–11. ****$P < 0.0001$, Mann Whitney test.

FIGURE 3.3. (Continued)

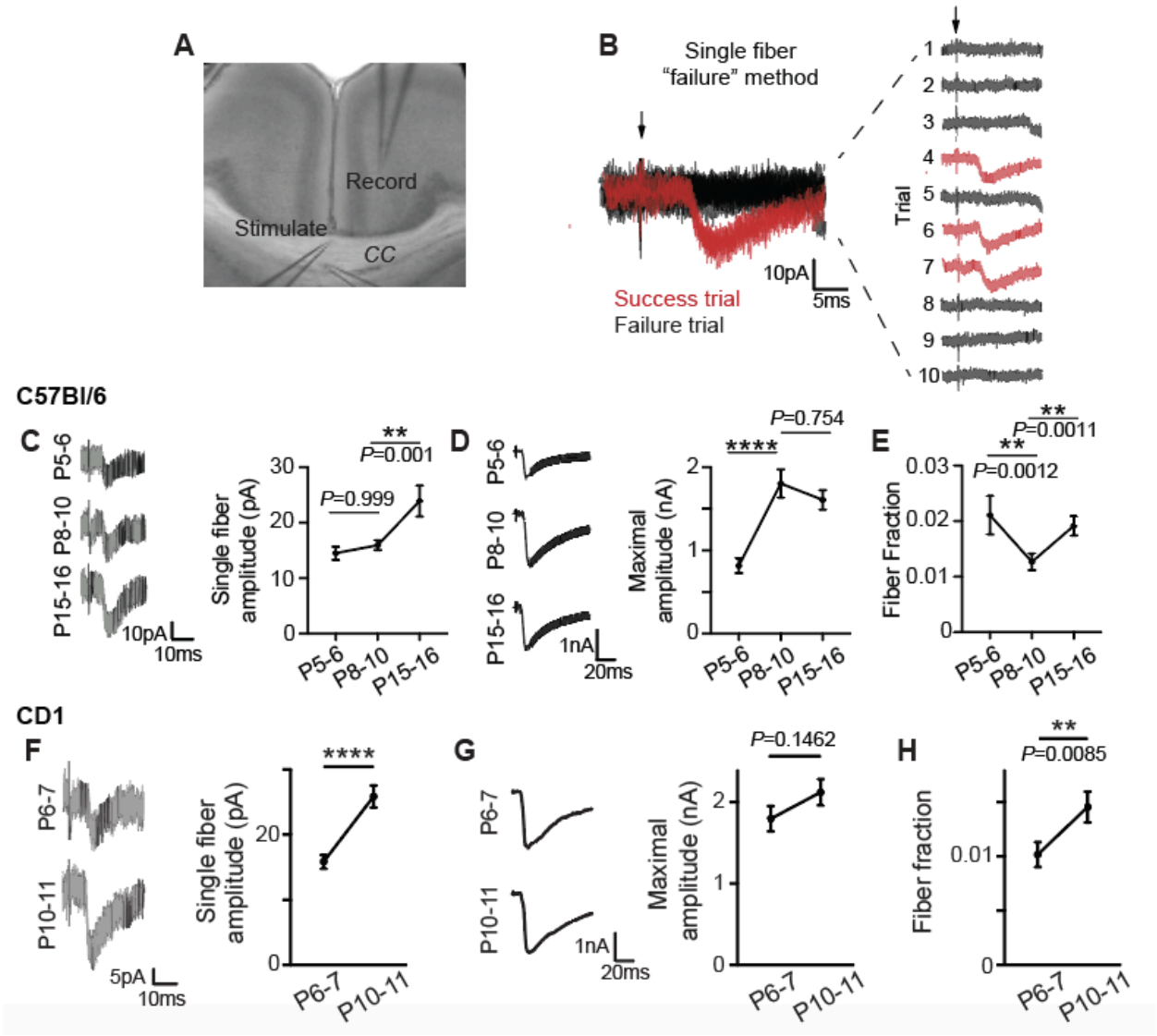

3.3 E), indicating an increase in functional callosal synaptic inputs. The FF then significantly increased between P8-10 and P15-16 (Fig. 3.3 E), suggesting that callosal inputs undergo synapse elimination during this period. The timing of functional synapse elimination is strain dependent: in CD1 mice, the FF ratio increased between P6-7 and P10-11 (Fig. 3.3 F-H), suggesting that synapse elimination occurs earlier in CD1 mice (used in Fig. 3.1, 3.2 and 3.8) than in C57BL/6 mice.

2) Generation of a Pyk2 conditional knockout mouse line

To evaluate the role of Pyk2 loss-of-function in a cell type-specific manner, I created a Pyk2 conditional knockout mouse line ($Pyk2^{fl/fl}$) using the CRISPR (clustered regularly interspaced short palindromic repeat) strategy. To generate $Pyk2^{fl/fl}$, I created a targeting construct composed of floxed full-length mouse *Ptk2b* cDNA with SV40 intron-poly(A), FRT-flanked *EGFP*-poly(A). The Pyk2 cDNA was tagged with FLAG on the 5' end and HA on the 3' end. The targeting construct was introduced into the endogenous *Ptk2b* exon 1, deleting 242 nucleotides containing the start codon (Fig. 3.4 A). This deletion disrupts the expression of the endogenous *Ptk2b* gene but allows the expression of the inserted *Ptk2b* cDNA. Additionally, with this strategy, cells with Pyk2 loss (driven by Cre expression) would express EGFP. The targeting construct was introduced by CRISPR/Cas9-driven homology directed repair. I identified two gRNAs (one targeting the 5' end and another targeting the 3' end of the *Ptk2b* exon 1) with DNA cleavage efficiencies greater than 80% (Fig. 3.4 B). The gRNAs, targeting construct, and Cas9 protein were injected into the cytoplasm of fertilized eggs. $Pyk2^{fl/fl}$ mice were identified by PCR to detect the successful homologous recombination of the targeting construct (Fig. 3.4 C and D). Both the *Ptk2b* mRNA (Fig. 3.4 E) and Pyk2 protein (Fig. 3.4 F) is absent when Cre is present. This suggests that the $Pyk2^{fl/fl}$ mouse line does indeed allow for the conditional (Cre-dependent) disruption of the Pyk2 protein.

FIGURE 3.4. Generation of a Pyk2 conditional knockout mouse (Pyk2$^{fl/fl}$) using CRISPR/Cas9 *(next page)*.

(A) Schematic of the strategy used to generate Pyk2$^{fl/fl}$ mice using the CRISPR/Cas9 method. The targeting vector was constructed by placing the full-length mouse *Ptk2b* cDNA flanked by loxP sites followed by the SV40 intron-poly(A) and *EGFP*-poly(A) flanked by FRT sites. The Pyk2 cDNA was tagged with FLAG on the 5' end and HA on the 3' end. The targeting vector was introduced into the *Ptk2b* genomic sequence, replacing the endogenous *Ptk2b* exon 1, via CRISPR/Cas9-driven homology directed repair. Two guide RNAs (indicated as gRNA1 and gRNA4; stars mark the sites recognized by the gRNAs) were used to cleave the endogenous *Ptk2b* sequence. This cleavage deletes the endogenous start codon, thus, disrupting the expression of the endogenous *Ptk2b*, but allows the expression of the inserted *Ptk2b* cDNA. In the presence of Cre, Pyk2 would be knocked out and EGFP would be expressed.

(B) *In vitro* assay to determine the DNA cleavage efficiency of candidate gRNAs. A ~2kb fragment containing the *Ptk2b* exon 1, and the target sites for all candidate gRNAs tested, was PCR amplified. This fragment was incubated with a candidate gRNA and recombinant Cas9. A negative control lacking a gRNA was included (Uncut). The reactions are separated by agarose gel electrophoresis. Three DNA bands were expected in each lane. The top band indicates remaining uncut DNA. Two smaller bands are the cleaved fragments. Cleavage efficiency = (middle band intensity / middle band size) / [(top band intensity / top band size) + (middle band intensity / middle band size)]. gRNAs 1 and 4 had the highest cleavage efficiencies and were used to generate the Pyk2 conditional knockout mouse.

(C-D) Verification of homologous recombination of the targeting construct. PCR primers were designed to verify correct homologous recombination for both the 5' (A; red arrows) and 3' ends (A; green arrows). Primers were designed such that one primer is located within a unique site on the targeting construct and the other outside on the endogenous genomic sequence. Mouse #40 (Pyk2$^{fl/fl}$) showed positive bands for both the 3' (C) and 5' (D) ends. (C) Positive control: plasmid designed to contain the fragment of genomic DNA, containing both homologous recombination primer detection sites (A, green arrows), expected in the mouse following successful homologous recombination.

(E) Verification of Pyk2 mRNA knockdown. Pyk2$^{fl/fl}$ mice were crossed to Satb2-Cre (Cre is expressed under the Satb2 promoter to drive Cre expression in cortical layers II, III, V and VI as well as in hippocampal neurons). RNA extracted from the CA1 of Pyk2$^{fl/fl}$ (Control) and Satb2-Cre, Pyk2$^{fl/fl}$ (+ Cre) mice were subjected to RT-PCR. Two primer pairs targeting the 5' and 3'

FIGURE 3.4. (Continued)

ends of the Pyk2 mRNA, respectively were used to detect the presence of Pyk2 mRNA. Pyk2 mRNA is not detected in the presence of Cre.

(F) Verification of Pyk2 protein knockdown. $Pyk2^{fl/fl}$ mice were crossed to Satb2-Cre. Protein extracted from the CA1 of $Pyk2^{fl/fl}$ (Control) and Satb2-Cre, $Pyk2^{fl/fl}$ (+ Cre) were subjected to Western blotting using an anti-Pyk2 antibody that detects the C-terminal of Pyk2 protein. Pyk2 protein is not detected in the presence of Cre.

FIGURE 3.4. (Continued)

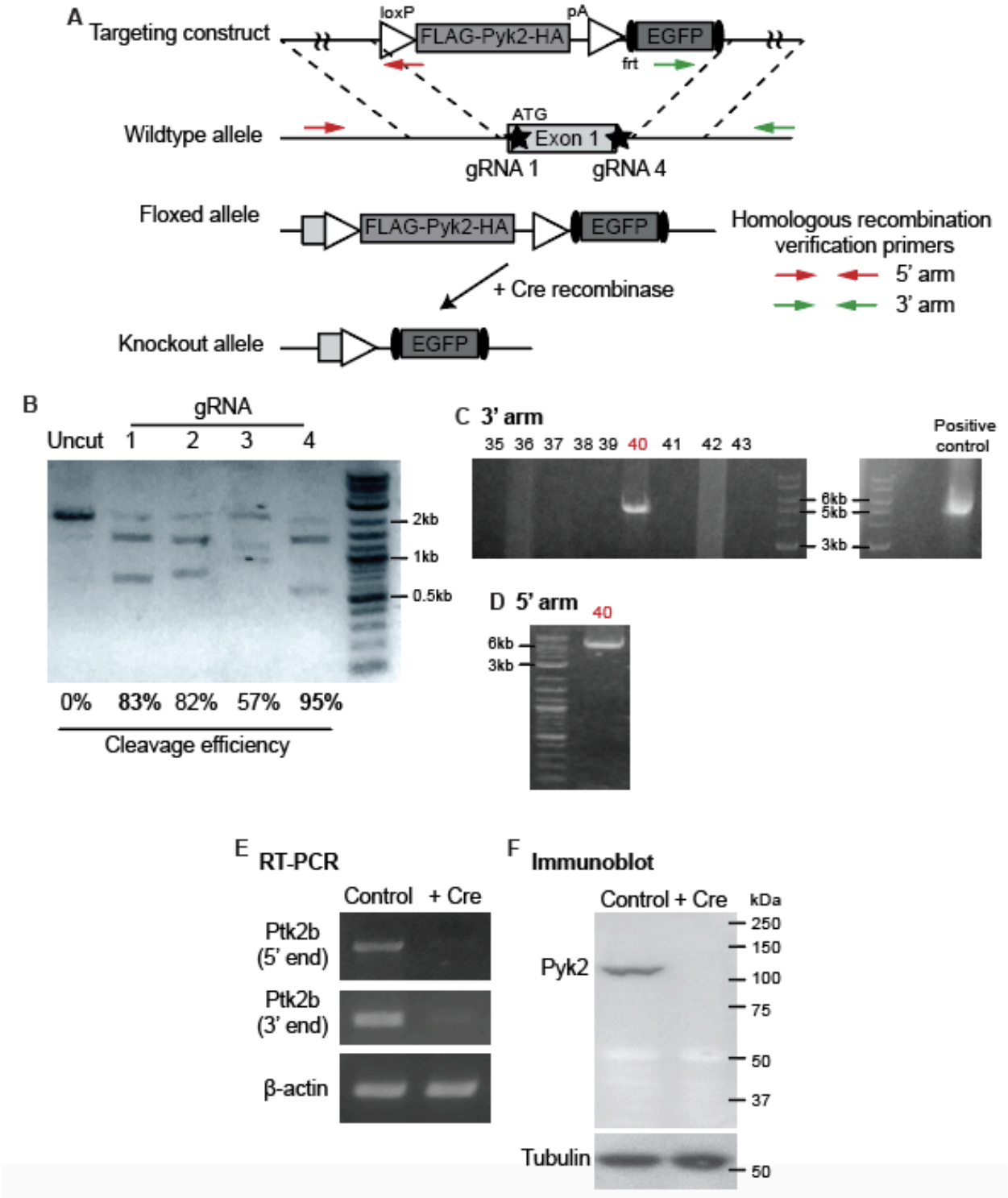

Presynaptic, not postsynaptic Pyk2 is required for functional synapse elimination

Using the fiber fraction method, I examined if neuronal Pyk2 is necessary for the functional elimination of callosal synapses (Fig. 3.5 B). To knockout Pyk2 from cortical neurons, I crossed $Pyk2^{fl/fl}$ with Satb2-Cre mice (Pyk2KO). This results in Pyk2 loss (as detected by GFP expression) from cortical neurons, but not from astrocytes or microglia (Fig. 3.5 A). Further validation of the Satb2-Cre,$Pyk2^{fl/fl}$ line will be done using reporter lines (to evaluate Cre expression) and immunostaining (to evaluate Pyk2 loss). Control mice include both $Pyk2^{fl/fl}$ mice (no cre) and Satb2-Cre, $Pyk2^{WT}$ mice. At P8-11, the single fiber amplitude, maximum amplitude, and FF ratio were not different between controls and Pyk2 KO mice (Fig. 3.5 C-E), suggesting that Pyk2 is not critical to callosal synapse formation. In control mice, there is a significant increase in the fiber fraction ratio between P8-11 and P16-19 which is consistent with synapse elimination occurring during these developmental ages. However, in Pyk2 KO mice, the fiber fraction ratio does not increase between P8-11 and P16-19, suggesting that synapse elimination does not occur in the absence of Pyk2 (Fig. 3.5 E). These results indicate that neuronal Pyk2 is necessary for functional synapse elimination.

Pyk2 is expressed in both pre and postsynaptic terminals (Giralt et al., 2017). To determine whether pre or postsynaptic Pyk2 drives functional refinement, I used an AAV-based strategy to knockout Pyk2 from one cortical hemisphere. I injected AAV expressing Cre, together with AAV-EGFP, into the left cortical hemisphere of $Pyk2^{fl/fl}$ mice at P0-1 (Fig. 3.6 A). As a control, I injected AAV-EGFP only. To evaluate the role of presynaptic Pyk2, I performed fiber fraction experiments while recording from neurons in the right cortical hemisphere (contralateral to site of AAV injection) at P16-19. The single fiber amplitude was not different between controls and presynaptic Pyk2 KO (Pyk2 KO^{Pre}) mice (Fig. 3.6 B). However, the maximum amplitude was significantly greater (Fig. 3.6 C), and the fiber fraction was significantly smaller in Pyk2 KO^{Pre} mice (Fig. 3.6 D). To evaluate the role of postsynaptic Pyk2 (Pyk2 KO^{Post}), I recorded from EGFP-positive cells in the left cortical hemisphere (ipsilateral to site of AAV injection, Fig. 3.6 E). At P16-

FIGURE 3.5. Loss of Pyk2 impairs functional callosal synapse elimination *(next page)*.
(A) Satb2-Cre drives neuronal-specific Pyk2 loss. Coronal sections were prepared from Satb2-Cre, $Pyk2^{fl/fl}$ mice (Pyk2 KO) at P10 and immunostained for EGFP (to identify cells with Pyk2 deleted) and the neuronal marker, NeuN, the astrocytic marker, GFAP, or the microglial marker, Iba1. EGFP-expressing cells were NeuN positive, and GFAP and Iba1 negative, suggesting that Pyk2 KO cells are neurons (not astrocytes or microglia). n = 3 mice.
(B-E) FF analysis in Pyk2 KO mice. (B) Schematic of experiments. The electrically evoked callosal synaptic responses were recorded by whole-cell patch clamp at P8-11 (before refinement) and P16-19 (after refinement). (C) Representative traces and quantification of single fiber responses in Control and Pyk2 KO mice. The single fiber response amplitude increases similarly through development in both Control and Pyk2 KO, indicating synaptic strengthening is not affected by the loss of Pyk2. (D) Representative traces and quantification of the maximal responses. The maximal response is not different in control mice between P8-11 and P16-19. However, the maximal response amplitude is significantly increased in Pyk2 KO mice during development, indicating a higher callosal drive to neurons in Pyk2 KO mice after refinement. (E) Quantification of the FF ratio. The FF ratio significantly increases in Control mice between P8-11 and P16-19, indicating that functional synapse elimination occurs during this time. This increase is absent in Pyk2 KO mice, indicating that functional synapse elimination is not occurring in the absence of Pyk2. In all parameters measured, Pyk2 KO does not affect callosal synapse formation (no significant difference between Control and Pyk2 KO at P8-11). Mean ± SEM. n = 36 cells from 5 mice, P8-11 Control; 26 cells from 3 mice, P8–11 Pyk2 KO; 55 cells from 7 mice, P16-19 Control; 55 cells from 7 mice, P16-19 Pyk2 KO. Kruskal-Wallis followed by Dunn's multiple comparison test.

FIGURE 3.5. (Continued)

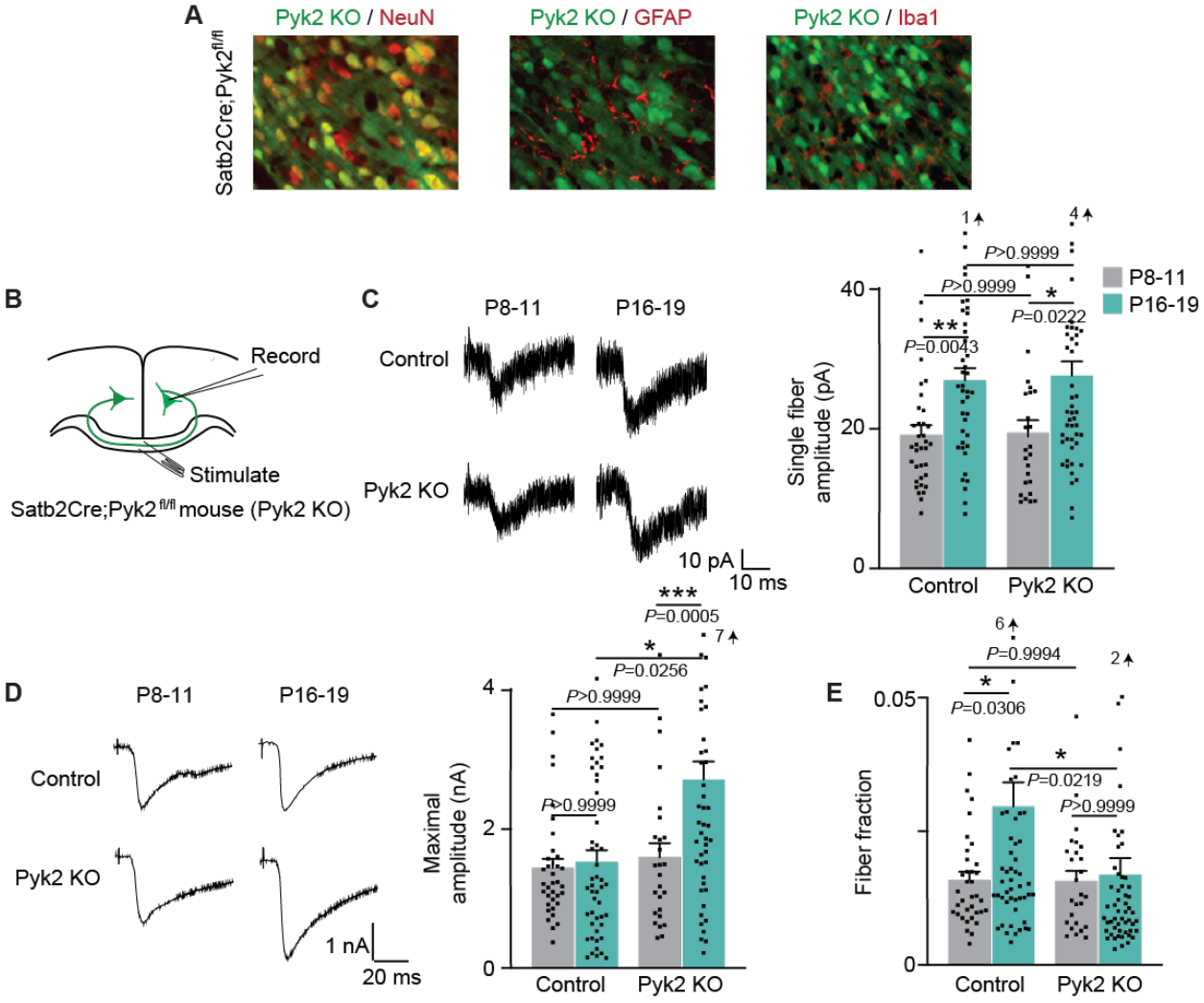

FIGURE 3.6. Presynaptic, not postsynaptic Pyk2, is necessary for functional callosal synapse elimination *(next page)*.

(A-D) The FF analysis in mice in which Pyk2 is inactivated in presynaptic callosal neurons. (A) Schematic of experiments. AAV-EGFP (Control) or AAV-EGFP + AAV-Cre were injected into the left cingulate cortex of $Pyk2^{fl/fl}$ mice. The electrically evoked callosal synaptic responses were recorded by whole-cell patch clamp in the right hemisphere at P16-19 (Pyk2 KO^{Pre}). (B) Representative traces and quantification of single fiber responses. (C) Representative traces and quantification of the maximal responses. (D) Quantification of the FF ratio. The maximal responses are larger in Pyk2 KO^{Pre}. The FF ratio is significantly lower in Pyk2 KO^{Pre} relative to Control. This indicates that presynaptic Pyk2 is critical to synapse elimination. Mean ± SEM. n = 52 cells, Control; 47 cells, Pyk2 KO^{Pre}. Mann Whitney test.

(E-H) The FF analysis in mice in which Pyk2 is inactivated in postsynaptic callosal neurons. (E) Schematic of experiments. AAV-EGFP (Control) or AAV-EGFP + AAV-Cre were injected into the left cingulate cortex of $Pyk2^{fl/fl}$ mice. The electrically evoked callosal synaptic responses were recorded by whole-cell patch clamp from EGFP-positive cells in the left hemisphere at P16-19 (Pyk2 KO^{Post}). (F) Representative traces and quantification of single fiber responses. (G) Representative traces and quantification of the maximal responses. (H) Quantification of the FF ratio. Single fiber responses, maximal responses and the FF ratio is not different between Pyk2 KO^{Post} and Control. This indicates that postsynaptic Pyk2 does not regulate synapse elimination. Mean ± SEM. n = 21 cells, Control; 28 cells, Pyk2 KO^{Post}. Mann Whitney test.

FIGURE 3.6. (Continued)

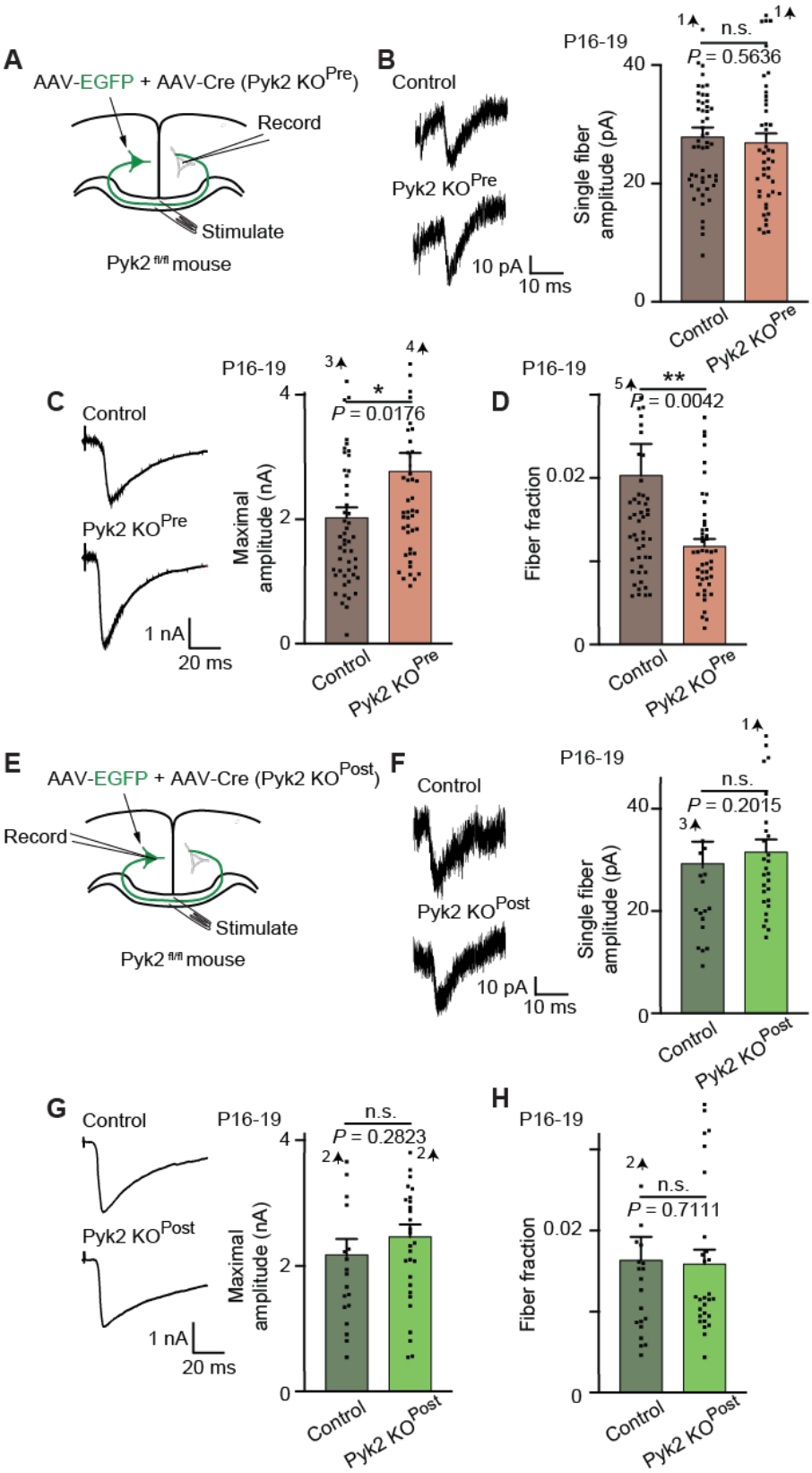

19, the single fiber amplitude, maximum amplitude, and FF ratio were not different between controls and Pyk2 KO^{Post} mice (Fig. 3.6 F-H). These results support the notion that presynaptic, not postsynaptic, Pyk2 kinase is a critical regulator of functional synapse refinement.

Pyk2 is highly activated at cortical synapses *in vivo* during the start of synapse elimination

To be a determinant of synapse elimination, Pyk2 should signal just prior to the elimination of synapses. Thus, I determined when Pyk2 is active at cortical synapses *in vivo*. Based on my FF data, in C57Bl/6 mice, functional callosal synapses are formed between P5-6 and P8-10 and synapse elimination occurs between P8-10 and P15-16. Hence, I evaluated Pyk2 activation at P5 (during synapse formation), P10 (at the start of synapse elimination) and P15. I detected Pyk2 activation using at antibody specific to active Pyk2 (phospho-Pyk2 or pPyk2). Activated Pyk2 is autophosphorylated on tyrosine residue 402 between the FERM and kinase domains (Dikic et al., 1996; Salter and Kalia, 2004). Excitatory presynaptic terminals were labeled by staining for VGluT1 (Fig. 3.7 A). I found that both the intensity of phospho-Pyk2 at VGluT1 synapses and the percent of pPyk2-positive VGluT1 synapses is highest at P10 relative to P5 and P15 (Fig. 3.7 B and C). This suggests that Pyk2 signaling may play important roles synaptic refinement.

Pyk2 is activated at inactive synapses in response to signals from other active synapses

To serve as a synaptic elimination signal under physiological conditions, Pyk2 should be more active at less active synapses. To distinguish between more active and less active synaptic terminals, I used the Synaptotagmin (Syt-1) re-uptake assay. I applied fluorescently labelled-Syt-1 antibody to cultured cortical neurons. This Syt-1 antibody will be taken up into presynaptic terminals as these terminals undergo neurotransmitter vesicle release and endocytosis (Fig. 3.7 D). Thus, synapses that are more active will have a higher intensity of Syt-1 fluorescence. I then immunostained these cultures for phospho-Pyk2 (to identify active Pyk2) and VGluT1 (to label excitatory presynaptic terminals). I found that more active synapses (higher Syt-1 intensity) have

less Pyk2 activation (low phospho-Pyk2 intensity) and that synapses with high Pyk2 activation (high phospho-Pyk2 intensity) have low levels of synaptic activity (low Syt-1 intensity) (Fig. 3.7 E and F). These results suggest that Pyk2 is activated at less active synapses under physiological conditions.

I then examined whether neuronal inactivation can drive the activation of Pyk2 at synapses. To inactivate neurons, I transfected cultured cortical neurons at DIV3-4 with a plasmid expressing the inhibitory DREADD (Designer Receptors Exclusively Activated by Designer Drugs), hM4Di. Neurons were also co-transfected with Synaptophysin-mCherry (Sphy-mCh), which accumulates at presynaptic terminals and effectively labels them (Dabrowski et al., 2015). At DIV14, I treated cultures with 10 μM Clozapine-N-oxide (CNO) to activate hM4Di and hyperpolarize the transfected neuron for 2 hours. Control cultures were treated with equal volumes of water (vehicle). After treatment, I fixed and immunostained for phospho-Pyk2 and analyzed the intensity of phospho-Pyk2 on Sphy-mCh-positive puncta. CNO-treated cultures showed a significant increase in phospho-Pyk2 intensity at synapses relative to vehicle-treated cultures. These results suggest that Pyk2 activation is higher at inactive synapses.

Competition between active and inactive neurons drives synapse refinement. The global inactivation of cortical inputs prevents the elimination of inactive callosal connections. This suggests that active inputs send *'punishment'* signals to drive the elimination of inactive inputs. Therefore, I reasoned that if Pyk2 is the *'elimination'* signal, Pyk2's activation should be higher at inactive synapses only when there are other active ones around. In the DREADD experiment above, the sparse transfection of hM4Di created a condition where only a small subset of neurons was inactivated in the presence of CNO. To determine whether competition between active and inactive neurons are necessary to activate Pyk2 at inactive synapses, I globally suppressed neuronal activity in CNO-treated cultures by bath applying 1 μM TTX (CNO + TTX) or the neurotransmitter receptor inhibitors, 10 μM CNQX and 50 μM APV (CNO + Inh). The global inactivation of these cultures prevented the increased phospho-Pyk2 intensity at Sphy-mCh-

FIGURE 3.7. Pyk2 activation peaks at the start of elimination and localizes to inactive synapses in the presence of other active synapses *(next page)*.

(A-C) Pyk2 activation at synapses peaks *in vivo* at the start of synapse elimination. Scale bar: 20 μm. (A) Brain sections were prepared from mice at P5, P10 and P15. Sections were immunostained for Phospho-Pyk2 and VGluT1. Layer V of the cortex was imaged. (B) Quantification of Phospho-Pyk2 intensity at VGluT1 positive synapses. (C) Quantification of percent VGluT1 synapses that were positive for Phospho-Pyk2. Phospho-Pyk2 intensity at synapses and the percent of synapses that are positive for Pyk2 is highest at P10 relative to P5 and P15. Mean ± SEM. n = 3 mice for each age group. Scale bar: 5 μm

(D-F) Inverse correlation between synaptic activity and Pyk2 activation. Cortical neuronal cultures were subjected to the Synaptotagmin-1 (Syt-1) antibody re-uptake assay at DIV13. Cultures were then immunostained for Phospho-Pyk2 and VGluT1. (D) Syt-1 is taken up at and labels active presynaptic terminals. (E-F) The intensity of Syt-1 and Phospho-Pyk2 at VGluT1-positive puncta was measured. Presynaptic terminals with higher levels of Syt-1 intensity (more synaptic activity) have lower levels of Phospho-Pyk2 intensity (less active Pyk2) while presynaptic terminals with higher levels of Phospho-Pyk2 intensity (more active Pyk2) have lower levels of Syt-1 (less synaptic activity). This data was reproduced in 3 independent experiments. $P < 0.0001$, Spearman correlation. Scale bar: 0.25 μm.

(G-H) Pyk2 is activated at inactive synapses in the presence of neural activity. (G) Cultured cortical neurons were transfected with the inhibitory DREADD, hM4Di and Synaptophysin-mCherry (Sphy-mCherry) at DIV3-4. At DIV14, cultures were treated with vehicle (Control), 10 μM CNO, CNO + 1μM TTX (CNO + TTX) or CNO + inhibitor cocktail (10 μM CNQX and 50 μM APV; CNO + Inh) for 2 hours. Cultures were immunostained with the Phospho-Pyk2 antibody and Sphy-mCherry-positive presynaptic terminals were imaged. (H) Quantification of Phospho-Pyk2 intensity at Sphy-positive synapses. Phospho-Pyk2 is increased with CNO treatment to activate DREADDs. The global suppression of activity by TTX or by the inhibitor cocktail suppresses this increase. Mean ± SEM. n = 39 neurites, 5 cultures, Control; 37, 5, CNO; 14, 3, CNO + TTX; 18, 3, CNO + Inh. ****$P < 0.0001$ by ANOVA followed by Tukey test.

FIGURE 3.7. (Continued)

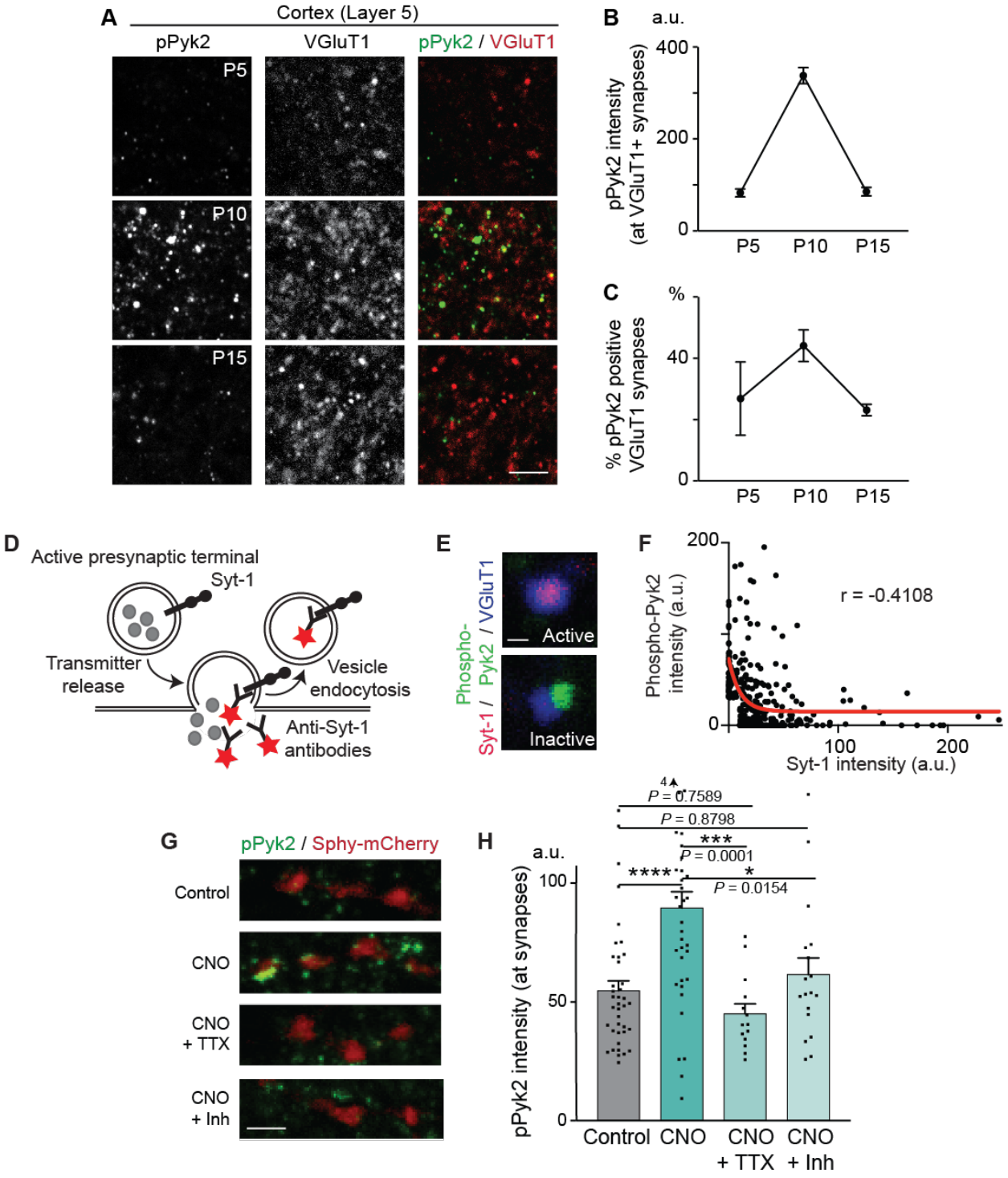

positive synapses, suggesting that signals from active neurons drive Pyk2 activation at inactive synapses. These results suggest that Pyk2 is an activity-dependent candidate *'elimination'* signal that is activated at inactive synapses only in the presence of other active ones.

JAK2, a Pyk2 interacting kinase, is necessary for the elimination of inactive connections

We next asked how Pyk2 drives synaptic elimination. One major form of Pyk2 signaling is via the activation of Pyk2-interacting kinases, a number of which belong to the JAK family and Src family of kinases (Fig. 1.4). Therefore, we tested if members of these kinase families may also regulate the elimination of inactive connections. We generated kinase-dead mutants of kinases belonging to JAK and Src families, which serve as dominant-negative forms of these kinases, and co-expressed them with TTLC in a subset of left cortical callosal neurons. As described above, TTLC-expressing callosal axons were eliminated by P15 (Fig. 3.1 I). However, when a dominant-negative form of JAK2 tyrosine kinase, JAK2DN (Ungureanu et al., 2002), was co-expressed, TTLC-expressing axons were no longer eliminated (Fig. 3.8 F and J). Co-expression of a dominant-negative mutant of JAK1 (JAK1DN) (Shimoda et al., 1997), Fyn (FynDN) (Tezuka et al., 1999), or CSK (CSKDN; data not shown) (Howell and Cooper, 1994) did not inhibit the elimination of inactive axons (Fig. 3.8 G, H and J). None of the dominant-negative mutants affected the initial targeting of callosal axons to the right hemisphere, as assessed at P10 (Fig. 3.8 A–C and E). These results indicate that JAK2 kinase activity specifically is necessary for the elimination of inactive callosal axons.

Overexpression of JAK2DN may not only suppress JAK2 kinase activity, but also disrupt the scaffolding function of JAK2 (Keil et al., 2014). To exclude the possibility that the inhibition of inactive axon elimination with JAK2DN is attributed to the overexpression of JAK2DN itself rather than the suppression of JAK2 kinase activity, we suppressed endogenous JAK2 kinase activity

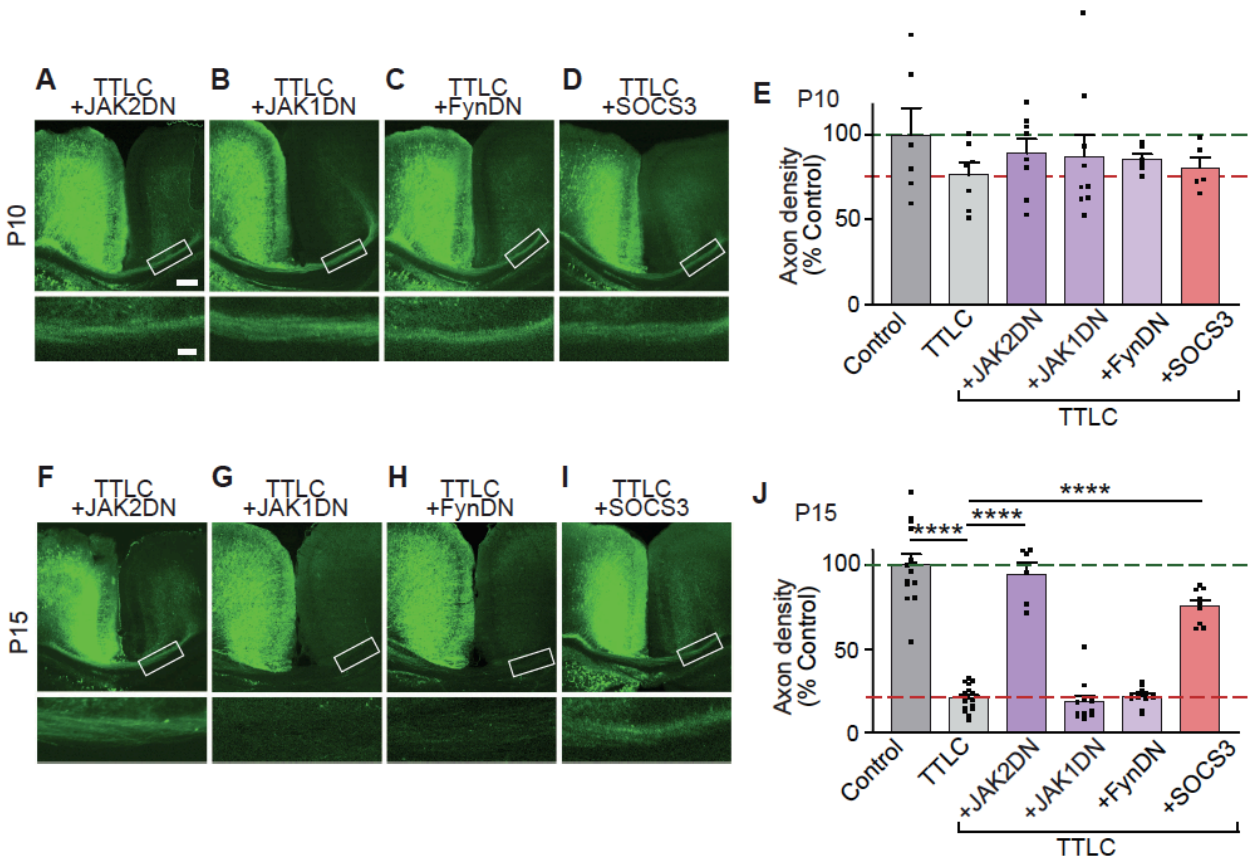

FIGURE 3.8. JAK2, a Pyk2 interacting kinase, signaling mediates developmental inactive callosal axon elimination.

(A–J) Dominant-negative forms of JAK2, JAK1 or Fyn, or wild-type SOCS3 were co-electroporated with TTLC into callosal neurons, and callosal axons were examined at P10 (A–D) and P15 (F–I). Higher magnification images from the boxed areas are shown in the bottom panels. Scale bars, 200 μm (top), 50 μm (bottom). (E and J) Quantification of callosal axon densities at P10 (n = 6 mice, Control; 7, TTLC; 8, JAK2DN; 9, JAK1DN; 6, FynDN; 5, SOCS3) and P15 (n = 14, Control; 16, TTLC; 6, JAK2DN; 12, JAK1DN; 13 FynDN; 9, SOCS3). Mean ± SEM (normalized to Control; Green line: Control; Red line: TTLC). ****$P < 0.0001$, ANOVA followed by Tukey test.

by overexpressing a negative regulator of JAK2, SOCS3 (suppressor of cytokine signaling 3). SOCS3 is expressed in developing neurons (Polizzotto et al., 2000) and efficiently suppresses JAK2 kinase activity by binding to JAK2 (Sasaki et al., 1999; Croker et al., 2003). SOCS3 did not affect initial axon targeting (P10, Fig. 3.8 D and E). We found that at P15, TTLC-expressing axons were still maintained when SOCS3 was co-expressed (Fig. 3.8 I and J). SOCS3 can also regulate JAK1 (Babon et al., 2012), but, since JAK1DN did not affect inactive callosal axon elimination (Fig. 3.8 G and J), SOCS3's effects are likely through the suppression of JAK2 kinase activity. Taken together, these results demonstrate that JAK2 kinase plays a critical role in the elimination of inactive callosal axons.

JAK2 signaling drives functional synaptic refinement

To evaluate the role of JAK2 in functional synapse refinement, I performed electrophysiological experiments. Using the FF method, I evaluated callosal synapse elimination in SOCS3 conditional knockout (KO) mice ($SOCS3^{fl/fl}$) and control C57BL/6 mice. To inactivate SOCS3 (and consequently activate JAK2) from presynaptic neurons, I injected AAV expressing Cre, together with AAV-EGFP, into the left cortical hemisphere of $SOCS3^{fl/fl}$ mice at P0-1 (SOCS3 KO^{Pre}; Fig. 3.9 A). As a control, I injected AAV-EGFP only. Inactivation of SOCS3 was verified by Western blotting (Fig. 3.9 B). Inactivation of SOCS3 did not induce neuronal death (Fig.3.9 C). At P8-10, the single fiber amplitude, maximum amplitude, and FF ratio were not different between controls and SOCS3 KO^{Pre} mice (Fig. 3.9 D-F), suggesting that JAK2 signaling is not critical to callosal synapse formation. In contrast, at P16-19, the FF ratio was significantly larger in SOCS3 KO^{Pre} mice relative to controls (Fig. 3.9 F), indicating that the loss of SOCS3 drives greater functional synapse elimination. These results support the notion that JAK2 kinase is a critical regulator of functional synapse refinement.

FIGURE 3.9. Presynaptic JAK2 signaling drives functional synapse elimination *(next page)*.
(A) Schematic of experiments. AAV-EGFP (Control) or AAV-EGFP + AAV-Cre were injected into the left cingulate cortex of $SOCS3^{fl/fl}$ mice. The electrically evoked callosal synaptic responses were recorded by whole-cell patch clamp in the right hemisphere.
(B) Viral infection of AAV-EGFP and AAV-Cre into $SOCS3^{fl/fl}$ mice (SOCS3 KO^{Pre}) strongly reduced SOCS3 protein levels in EGFP-positive cortical regions relative to controls by P9.
(C) TUNEL staining of Control and SOCS3 KO^{Pre} cortical neurons at P15. Both Control and SOCS3 KO neurons were negative for TUNEL staining suggesting that the loss of SOCS3 does not induce cell death. DNase 1-treated cortical section is used as a positive control for TUNEL staining. Experiment was reproduced using 6 brain sections from 2 mice in each condition.
(D-F) The FF analysis in mice in which SOCS3 is inactivated in presynaptic callosal neurons. (D) Representative traces and quantification of single fiber responses. (E) Representative traces and quantification of the maximal responses. (F) Quantification of the FF ratio. The FF ratio is not different between Control and SOCS3 KO^{Pre} mice at P8–10. However, the FF ratio is significantly higher in SOCS3 KO^{Pre} relative to Control at P16–19. This indicates that JAK2 signaling does not affect early synapse formation, but is critical to synapse elimination. Mean ± SEM. n = 66 cells, P8–10 Control; 40 cells, P8–10 SOCS3 KO^{Pre}; 55 cells, P16–19 Control; 40 cells P16–19 SOCS3 KO^{Pre}. $^{****}P < 0.0001$, Kruskal-Wallis followed by Dunn's multiple comparison test.

FIGURE 3.9. (Continued)

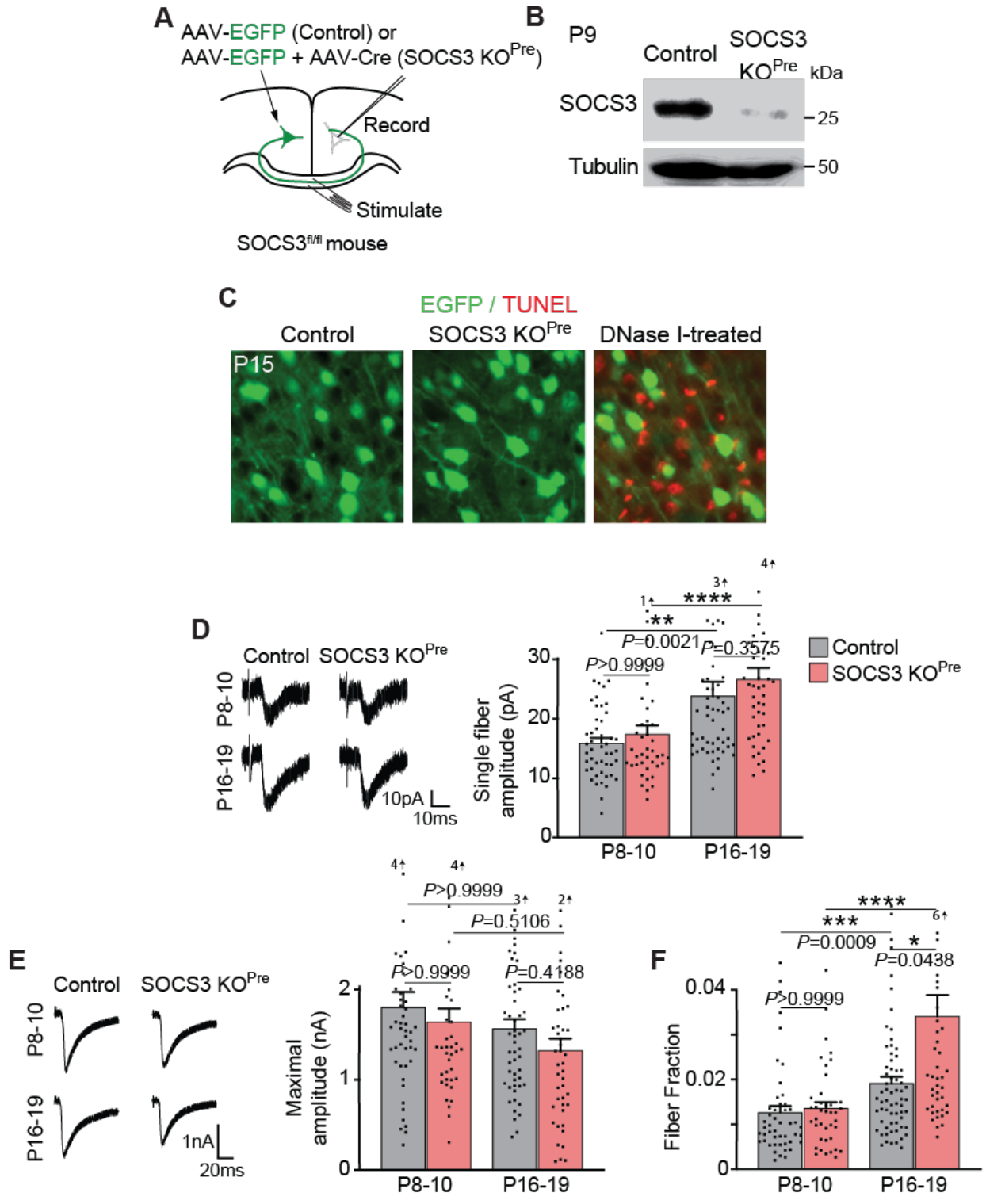

JAK2 signaling is required for structural synaptic refinement

Thus far, I have examined the role of JAK2 signaling in functional synaptic elimination. I next asked if JAK2 signaling regulates the structural refinement of callosal synapses as well. For this, I virally introduced Synaptophysin-mCherry (Sphy-mCherry), which labels presynaptic terminals, and EGFP into the left cortical hemisphere of $SOCS3^{fl/fl}$ (Control) and Emx1-Cre, $SOCS3^{fl/fl}$ (SOCS3 KO) mice (Fig. 3.10 A). I then quantified the density and size of Sphy-mCherry puncta in the right cortical hemisphere at P19, after the completion of synaptic refinement. The Sphy-mCherry density and size were lower in SOCS3KO mice relative to Control mice (Fig. 3.10 B and C). This suggests that the loss of SOCS3 results in fewer and smaller callosal synapses. These results support the notion that JAK2 kinase is a critical regulator of structural synapse refinement.

JAK2 is activated at inactive synapses in response to signals from other active synapses

To serve as a synaptic elimination signal under physiological conditions, JAK2 should be more active at less active synapses. I examined this possibility using an antibody specific to active JAK2 (phospho-JAK2). Activated JAK2 is phosphorylated on two tyrosine residues in the activation loop (Y1007 and Y1008) (Feng et al., 1997). To distinguish between more active and less active synaptic terminals, I used the Synaptotagmin (Syt-1) re-uptake assay (Fig. 3.7 D). I then immunostained the cultures for phospho-JAK2 (to identify active JAK2) and VGluT1. I found that more active synapses (higher Syt-1 intensity) have less JAK2 activation (low phospho-JAK2 intensity) and that synapses with high JAK2 activation (high phospho-JAK2 intensity) have low levels of synaptic activity (low Syt-1 intensity) (Fig. 3.11 A and B). These results suggest that JAK2 is activated at less active synapses under physiological conditions.

We then examined whether JAK2 is localized at synapses *in vivo* and if so, whether its kinase activity at synapses is regulated by neural activity-dependent competition. Immunostaining of cortical sections revealed that phospho-JAK2 was localized at synaptic terminals (Fig. 3.11 C).

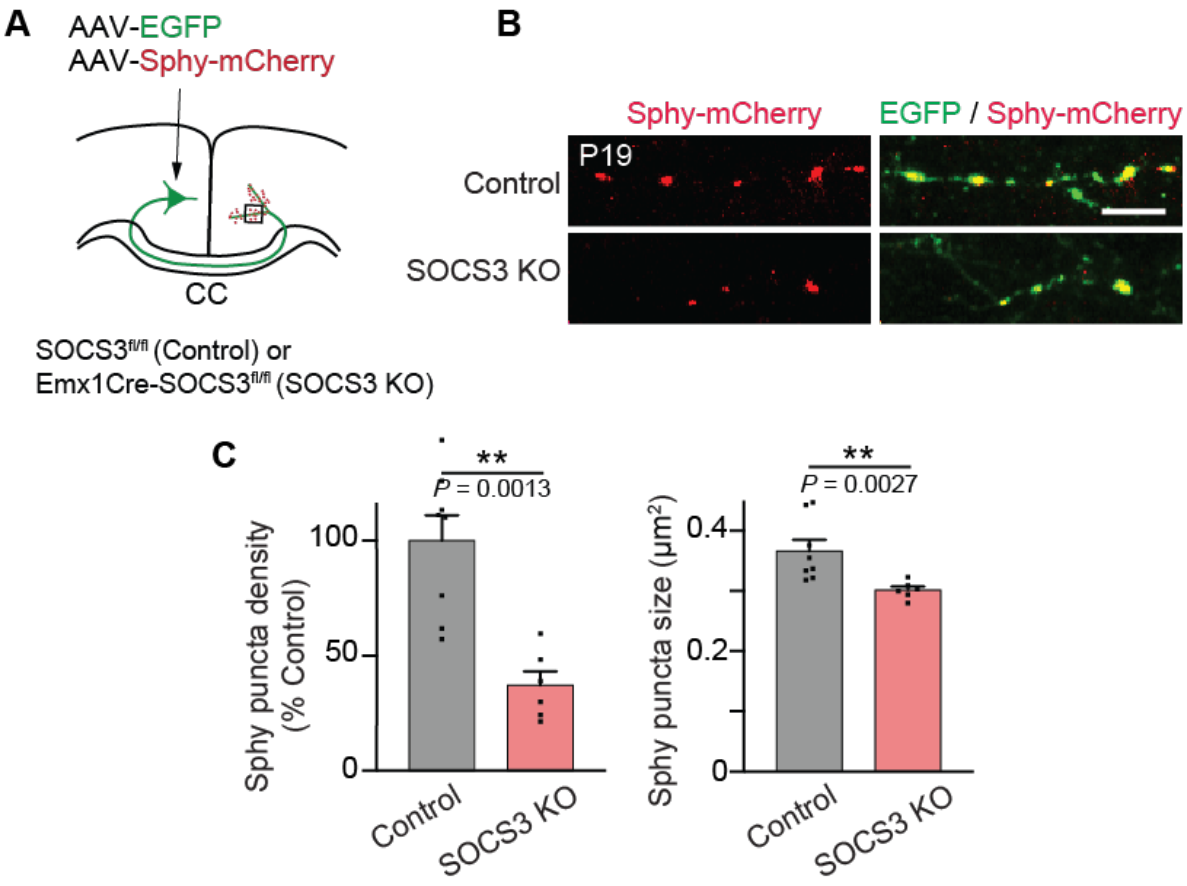

FIGURE 3.10. JAK2 signaling results in fewer structural synapses.

(A) Schematic of experiments. SOCS3$^{fl/fl}$ mice were crossed to Emx1-Cre to knockout SOCS3 in all cortical neurons (SOCS3 KO). AAV-EGFP + AAV-Synaptophysin-mCherry (Sphy-mCherry) were injected into the left cingulate cortex of Control and SOCS3 KO mice at P5. Sphy-mCherry labelled presynaptic terminals were imaged in layer V of the right hemisphere at P19 (boxed area).

(B) Confocal images from EGFP/Synaptophysin-mCherry in Control and SOCS3 KO mice.

(C) Quantification of the density (number per axon area) and size of Synaptophysin-mCherry puncta. Sphy puncta density shown as % relative to that in Control. Mean ± SEM. n = 10 images from 3 mice, Control; 8 images from 3 mice, SOCS3 KO. Mann-Whitney test. Scale bar, 5 µm.

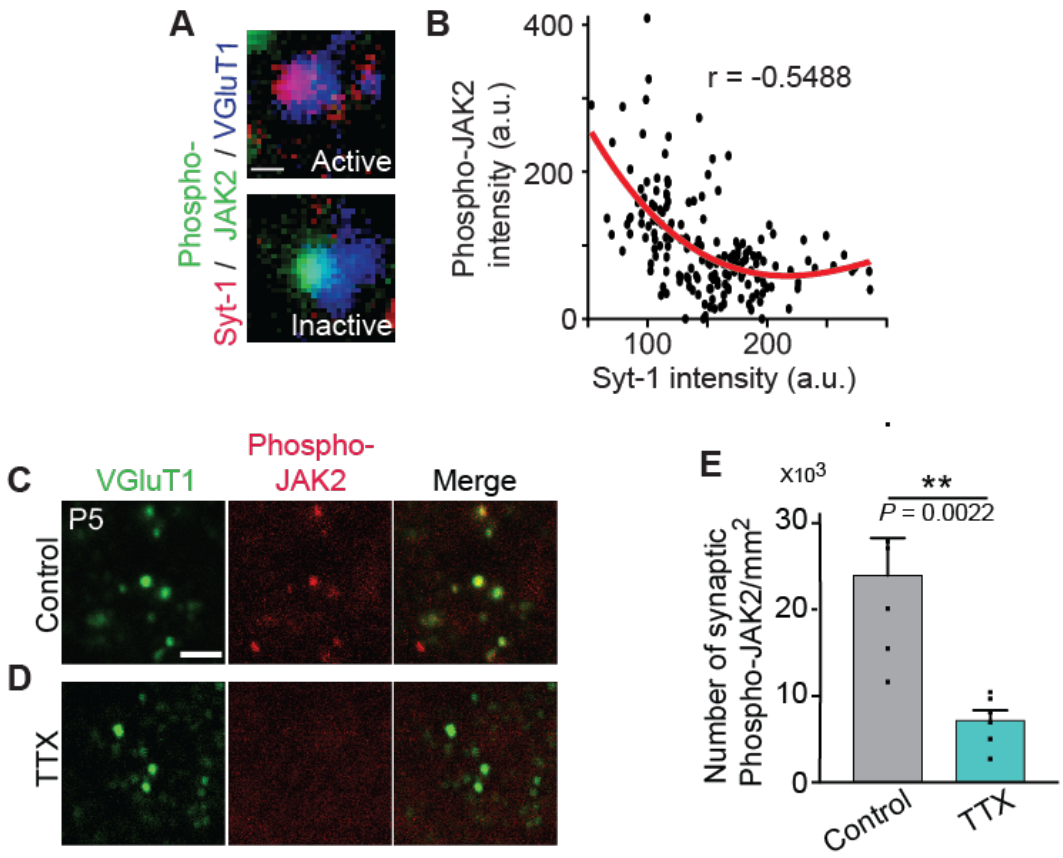

FIGURE 3.11. JAK2 is activated at inactive synapses in the presence of other active synapses.

(A-B) Inverse correlation between synaptic activity and JAK2 activation. Cortical neuronal cultures were subjected to the Synaptotagmin-1 (Syt-1) antibody re-uptake assay at DIV13. Cultures were then immunostained for Phospho-JAK2 and VGluT1. The intensity of Syt-1 and Phospho-JAK2 at VGluT1-positive puncta was measured. Presynaptic terminals with higher levels of Syt-1 intensity (more synaptic activity) have lower levels of Phospho-JAK2 intensity (less active JAK2) while presynaptic terminals with higher levels of Phospho-JAK2 intensity (more active JAK2) have lower levels of Syt-1 (less synaptic activity). This data was reproduced in 3 independent experiments. $P < 0.0001$, Spearman correlation. Scale bar: 0.25 μm.

(C-D) Phosphorylation of JAK2 at synapses by activity-dependent competition. Cortical sections from P5 Control and TTX-treated brains (TTX containing-Elvax was implanted on the left cortex at P3) were stained for VGluT1 and Phospho-JAK2. Synaptic JAK2 is activated only when there are active neurons. Mean ± SEM. n = 6 sections from 3 mice. Mann-Whitney test.

Application of TTX (TTX containing-Elvax was implanted on the left cortex at P3, and coronal sections were prepared at P5) to the mouse brain diminished phospho-JAK2 staining at synapses (Fig. 3.11 D and E), suggesting that JAK2 is activated at synapses only when there are other active synapses *in vivo*. Taken together, these results demonstrate that JAK2 is an *'elimination'* signal that signals at inactive synapses in the presence of other active connections to drive synaptic elimination.

3.4 Discussion

Activity-dependent synapse refinement is a critical step for the development of functional circuits in the brain. Here, we established a novel *in vivo* system to examine activity-dependent synapse refinement in the mammalian brain and identified Pyk2 and JAK2 tyrosine kinases as key determinants of inactive synapse elimination. We showed that: 1) Pyk2 activity is required for the elimination of inactive connections; 2) Presynaptic, and not postsynaptic, neuronal Pyk2 is necessary for functional synaptic refinement; 3) Pyk2 activation peaks at the start of refinement and Pyk2 is activated at inactive synapses only when other neurons are active; 4) Signaling of a Pyk2 interacting kinase, JAK2, is necessary for elimination; 5) JAK2 signaling is sufficient to drive the functional and structural elimination of active connections; and 6) JAK2 is activated at inactive synapses. Collectively, our results demonstrate that Pyk2 and JAK2, localized at presynaptic terminals, senses signals from other active connections and serves as a determinant of activity-dependent synapse refinement. We propose that Pyk2 and JAK2 are neuronal activity-dependent switches, which can be turned on at inactive synapses to drive synapse elimination (Fig. 3.12).

Pyk2 as an activity-dependent *'elimination'* signal in the brain

Synapses are eliminated in an activity and competition-dependent manner (Fig. 3.1; Penn et al., 1998; Buffelli et al., 2003; Kano and Hashimoto, 2009, Yasuda et al., 2011). Here, we established an *in vivo* system to decipher the molecular mechanisms underlying activity-

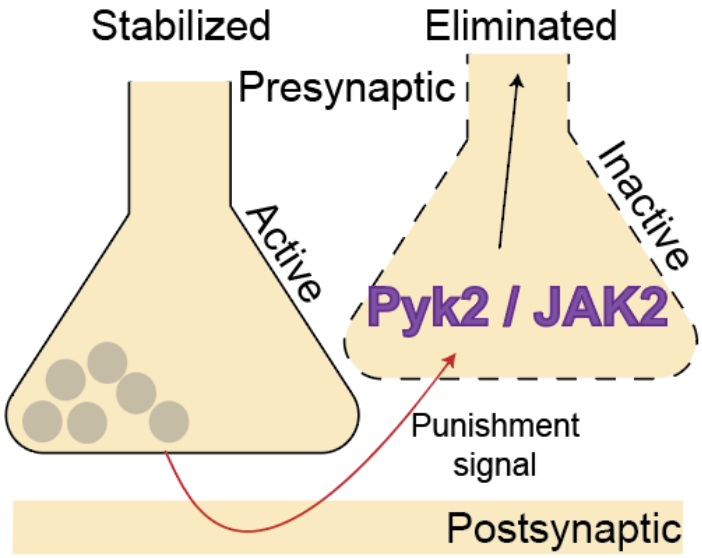

FIGURE 3.12. Proposed model of synaptic elimination.

Pyk2 and JAK2 sense signals from active synapses and are activated at inactive synapses. Thus, Pyk2 and JAK2 are neuronal activity-dependent switches, which serves as a determinant of activity-dependent synapse refinement.

dependent synapse refinement focusing on the cortical callosal connections, whose proper development is critical for language acquisition, social interaction, attention, visual function, and perception (Innocenti et al., 2003; Paul et al., 2007; Pietrasanta et al., 2014). We demonstrated that inactive callosal connections are eliminated after they project to their target region and that other active callosal connections are necessary for the elimination of inactive callosal connections (Fig. 3.1). These results indicate that inactive synapses detect signals from active connections and drive the elimination of the inactive connections; i.e., there are *'elimination'* signals within inactive synapses that are activated in the presence of other active synapses and subsequently drive the removal of that inactive synapse.

To identify activity-dependent *'elimination'* signals, we used this *in vivo* callosal system in combination with RNAseq and determined the differentially expressed genes in active and inactive neurons just prior to synapse elimination (Table 3.1). The results of this screen provide a transcriptional understanding of molecular changes in inactive neurons vs. active neurons just prior to the start of developmental synaptic elimination. The screen identified inactive neuron enrichment of transcripts encoding molecules that can be associated with less active synapses such as ICAM5 (a negative regulator of synapse maturation; Ning et al., 2013) and CX3CL1 (a regulator of microglial engulfment of synapses; Gunner et al., 2019).

Among the top differentially expressed genes, we focused on kinases, a class of molecules implicated in various aspects of neural network development and function (Maness, 1992; Wayman et al., 2008; Liu et al., 2011), and identified Pyk2 kinase as an activity-dependent *'elimination'* signal. Pyk2 is activated in a neuronal activity and competition-dependent manner (Fig. 3.7) and is a critical regulator of inactive synapse elimination (Fig. 3.2, 3.5 and 3.6). Contrary to other known molecular regulators of synapse elimination (Table 1.1), presynaptic, and not postsynaptic, Pyk2 signaling is necessary to drive synapse elimination (Fig. 3.2 and 3.6). These are consistent with the definition of the *'elimination'* signal - the decision-making molecule within the presynaptic neuron that detects levels of synaptic activity and determines whether the

synapse should be eliminated. How Pyk2 interacts with the other known molecular regulators of synaptic elimination is an interesting next question.

JAK2, a Pyk2-interacting kinase, drives synapse elimination

Once activated, Pyk2 can signal via the activation of JAK and Src family kinases (Dikic et al., 1996; Takaoka et al., 1999; Frank et al., 2002). Among the members of the JAK2 and Src family kinases, we determined that JAK2, and not JAK1, Fyn or CSK, is necessary for the elimination of inactive inputs (Fig. 3.8). JAK2 is activated at inactive synapses and JAK2 activation drives functional and structural synapse elimination (Fig. 3.9, 3.10 and 3.11). In non-neuronal cells, Pyk2 and JAK2 are known to interact with and activate one another (Takaoka et al., 1999; Frank et al., 2002). Additionally, our preliminary data shows that the overexpression of Pyk2 in cortical neurons drives JAK2 activation in the same neurons (M. Yasuda; data not shown), suggesting that Pyk2 and JAK2 may signal in the same *'elimination'* signaling pathway.

While it is evident that presynaptic JAK2 signaling drives the elimination of inactive inputs (Fig. 3.8 and 3.9), postsynaptic JAK2 likely regulates synaptic maturation. JAK2 phosphorylates the postsynaptically expressed SIRPα (Fig. 2.1). JAK family kinases drive SIRPα tyrosine phosphorylation in the presence of neuronal activity (Fig. 2.7). This leads to SIRPα ectodomain cleavage, which leads to synaptic maturation (Fig. 2.8). Thus, these findings suggest that JAK2, in response to neuronal activity, activates and signals through different pathways in different subcellular regions. This tight, subcellular regulation of JAK2 signaling pathways allows the differential regulation and appropriate modification of different subcellular regions in an activity-dependent manner. This subcellular regulation of JAK2 is further discussed in Chapter 5.

Mechanisms of synapse elimination

How do Pyk2 and JAK2 drive synaptic elimination? Possible mechanisms through which, Pyk2/JAK2 drive inactive synapse elimination include: 1) Glial engulfment. Once activated, JAK2

activates STAT proteins and regulates transcription (Shuai and Liu, 2003; Nicolas et al., 2012). We have determined that STAT1 signaling is necessary for inactive axon elimination (data not shown, M. Yasuda). STAT1 and Pyk2 have been implicated in the regulation of several pro-inflammatory genes (Di Liberto et al., 2018; Murphy et al., 2019). In neurons, STAT1 can drive chemokine and complement factor expression (Di Liberto et al., 2018). This may then signal to recruit microglia and eliminate synapses via microglial engulfment; and 2) Cytoskeletal rearrangement. Pyk2 has been implicated in cytoskeletal rearrangement. In AD, Pyk2 signals through RhoA, an actin regulator, to drive Aβ-triggered synapse loss (Lee et al., 2019). In smooth muscle cells, JAK2 activation causes actin cytoskeleton reorganization in arteries (Guilluy et al., 2010). These findings suggest that Pyk2 and JAK2 may regulate the cytoskeleton to destabilize inactive synapses.

Signals that drive Pyk2 activation during synaptic refinement are still unknown. Pyk2 is activated in a neuronal activity and competition-dependent manner (Fig. 3.7). Therefore, there must be an intrasynaptic *'punishment'* signal from active connections triggering Pyk2 activation. The identity of the *'punishment'* signal remains unknown (*'punishment'* signals are discussed in Chapter 5). However, it is possible that the *'punishment'* signal acts by regulating intracellular calcium levels or calmodulin signaling. It is suggested that calcium/calmodulin activates Pyk2, a calcium-dependent kinase, by binding and releasing the Pyk2 kinase domain from autoinhibition (Xie et al., 2008; Kohno et al., 2008). Postsynaptic calcium influx and calmodulin signaling have been implicated in synapse elimination (Ko et al., 2011; Kano et al., 2013). The role of presynaptic calcium/calmodulin in Pyk2 regulation and synaptic elimination will be interesting to address.

3.5 Experimental Procedures

Mouse strains

CD1 mice (Charles River), C57Bl/6, Emx1-Cre, Satb2-Cre and SOCS3$^{fl/fl}$ mice (Jackson), and Pyk2$^{fl/fl}$ (Fig. 3.4) were used in this study. Emx1-Cre, Satb2-Cre and Pyk2$^{fl/fl}$ mice were on a

C57Bl/6 background while SOCS3$^{fl/fl}$ mice were on a mixed background. Both male and female mice were used. No differences were observed between male and female mice. Mice were housed in OptiMICE cages (4–5 mice per cage) with a 12-h/12-h light/dark cycle. The housing room temperature was 22 ± 1 °C. Mice were allowed *ad libitum* access to food and water. All animal care and experiments were performed in accordance with the institutional guidelines and approved by the Institutional Animal Care and Use Committees at Boston Children's Hospital.

Plasmid constructs

The pUBC-EGFP vector was built by replacing the CAG promoter of pCAG vector (Matsuda et al., 2007) with the UBC-EGFP fragment from FUGW vector (Lois et al., 2002). pUBC-mCherry vector was built by replacing EGFP coding sequence with the mCherry coding sequence. pUBC-IRES-EGFP and pUBC-IRES-mCherry vectors were built by adding PCR-amplified IRES between the UBC promoter and coding sequences. To build the pUBC-TTLC-IRES-EGFP, PCR-amplified TTLC gene (Yasuda et al., 2011) was inserted into the pUBC-IRES-EGFP vector. For pUBC-JAK2WT-IRES-EGFP, PCR amplified mouse JAK2 coding sequence with primers (gcaacgcgtaccatgggaatggcctgccttaca and ggcgctagctcacgcagctatactgtcccg) was cloned into pUBC-IRES-EGFP. JAK2DN (JAK2K882E) was generated by PCR with site-directed mutagenic primers (JAK2DN: ctggcgaggtggtcgctgtggagaaactccagcacagcact and agtgctgtgctggagtttctccacag cgaccacctcgccag). FynDN (FynK295M; Tezuka et al., 1999) was previously described. JAK1DN (JAK1K907E) was generated by site-directed mutagenesis into JAK1 (previously described; Shimoda et al., 1997) with mutation primers (caggggagcaggtagctgtcgagtccctgaagcctgagagt and actctcaggcttcagggactcgacagctacctgctcccctg). pUBC-SOCS3-IRES-EGFP was built by inserting RT-PCR amplified coding sequence of SOCS3 fragment (with gaacgcgtaccatggtcacccacagcaag ttt and atcgctagcttaaagtggagcatcatactg) into pUBC-IRES-EGFP. pUBC- hM4D(Gi)-mCherry was built by subcloning hM4D(Gi)-mCherry from pAAV-hSyn-DIO-hM4D(Gi)-mCherry (Addgene # 44362) into pUBC vector. pAAV- hM4D(Gi)-mCherry was built by replacing hChR2(H134R)-EYFP

in pAAV-hSyn-hChR2(H134R)-EYFP (Addgene # 26973) with hM4D(Gi)-mCherry

All DNA sequences were verified by DNA sequencing.

Generation of the Pyk2 conditional knockout mouse

Targeting construct generation: DNA fragments were amplified by PCR. FLAG and HA-tagged Pyk2 cDNA was amplified from UBC-Pyk2WT (M. Yasuda). FLAG-tag was introduced to the 5' end and HA-tag to the 3' end via PCR. Point mutations were also introduced to prevent gRNA recognition of target construct sequence. Primers used (5' to 3'): GCTTATCGATACCATGGAC TACAAAGACGATGACGACAAGTCCGGGGTGTCTGA, TCGGGTCGACGTAAAGTGCCCA, TTACGTCGACCCGAGGGCCCCCCAGA, and AGGATTTAAATTCAAGCGTAATCTGGAACA TCGTATGGGTACTCTGCAGGCGGGTGG. The 5' and 3' homologous arms were amplified via PCR from BAC clone RP23-391F5 (BACPAC Resources). All fragments were cloned into the pSV-loxP-sv40-intron-polyA-EGFP-FRT vector.

gRNA identification: Candidate gRNA sequences were identified using online tools (ChopChop, Feng Zhang and IDT). DNA cleavage efficiency was determined using the Guide-it sgRNA screening kit (TaKaRa). gRNAs used were 3'AGTCCGGCCGCAUUUCACGG5' and 5'AGAGAUCCAGGUAAGGGUGG3'.

The targeting construct, gRNAs and Cas9 were injected into fertilized eggs by the Gene Manipulation and Genome Editing Core, Boston Children's Hospital.

In utero electroporation

E13.5 pregnant female mice were anesthetized by isoflurane inhalation. The abdominal skin and wall were cut and the uterus containing embryos was pulled out, and 2 µl of DNA [up to 3 µg/µl; the amounts of DNA electroporated were: EGFP 0.5 µg, TTLC 0.5 µg, JAK2 and JAK1 1.5 µg, Fyn and CSK 1 µg, SOCS3 0.5 µg (the amount of DNA was determined based on the molecular weight), dissolved into mammalian ringer solution] was injected with a glass micropipette into the

left lateral ventricle of embryos. The head of the DNA-injected embryo was placed between tweezer electrodes and five electric pulses (a voltage of 40–50 V was applied so that an 80 mA current flows, 50 ms duration, 950 ms intervals) were delivered using CUY21 electoroporator (NepaGene). After electroporation of embryos, the uterus was returned into the abdominal cavity. The cavity was filled with warm sterile saline, and the abdominal wall and skin were closed with suture (Saito and Nakatsuji, 2001; Saito, 2006).

Axon density analysis (see Fig. S1 E and F)

For the analysis of callosal axon density in the brains expressing EGFP in callosal neurons, 50 μm-thick frozen sections were cut and mounted on glass slides. Images including both cortical hemispheres were taken with a 4x lens on an Olympus BX63 epi-fluorescence microscope using cellSens Dimensions software to obtain unsaturated images. Focus was adjusted to obtain the highest EGFP signal intensity in the electroporated hemisphere. Images were then analyzed with ImageJ software. To quantify the callosal axon density, the total EGFP fluorescence intensity of a 200-μm length of callosal axon bundle in the right hemisphere (adjacent to the midline) was divided by the total value of the EGFP intensity in the cingulate cortex of the electroporated hemisphere.

Elvax-TTX implantation

P3 mice were anesthetized, their scalp was incised, and a rectangular window was made on the left side of the skull by cutting 3 sides (2.5 x 1.5 mm). The cut skull piece was flipped to expose the cortex. A 25 G needle, which was bent 0.5 mm from the tip to a 90° angle, was used to make a 0.5 mm depth cut to the cortex (1.5 mm from the midline) and TTX-Elvax or control Elvax (0.5 x 1 x 0.02 mm) (Yasuda et al., 2011) was inserted into the cut. The wound was closed and sutured. The animals were placed on a heated pad for recovery and returned to their cage.

Brain fixation

Mice were euthanized and perfused transcardially with PBS followed by 4% paraformaldehyde/PBS. Brains were removed and post-fixed with 4% paraformaldehyde/PBS for 16 hours. After cryoprotection in 30% sucrose/PBS, brains were frozen in OCT embedding compound.

Immunohistochemistry

Immunohistochemistry was performed as described (Yasuda et al., 2011). 16-20 μm coronal sections were cut on a cryostat. Sections were blocked in blocking buffer (2% BSA, 2% goat serum, 0.1% Triton X-100 in PBS and 1mM sodium orthovanadate) for 1 hour, followed by incubation with primary antibodies in blocking buffer at 4°C for 16 hours. Sections were washed 3 times in PBS, and secondary antibodies in blocking buffer were applied for 2 hours at RT. Antibodies and dilutions used were: Phospho-Pyk2 (Invitrogen, 1:500), Phospho-JAK2 (Millipore, 1:200), VGluT1 (Millipore, 1:5000), NeuN (Millipore, 1:100), GFAP (Synaptic Systems, 1:500), IbaI (Wako, 1:500). TUNEL staining was carried out using the Roche In Situ Cell Death Kit (TMR red). Images of single focal planes were taken with sequential scanning using a confocal microscope (Zeiss LSM700; 40X or 63X objective).

Primary cortical neuronal cultures

Cortices were dissected from P0 pups. Cortical neurons were dissociated with 0.5% trypsin, plated on poly-D-lysine-coated coverslips (60,000 cells/coverslip; diameter 12 mm), and grown in culture medium (B27 plus (Gibco), 2mM L-glutamine, 100 units/ml penicillin-streptomycin in neurobasal plus medium (Gibco)).

Synaptotagmin re-uptake assay

At DIV13, cultured neurons were treated with Oyster-550-labeled Synaptotagmin-1 antibody

(Synaptic Systems; 1:200) for 10 minutes at 37 °C. Neurons were fixed with 4% paraformaldehyde (PFA) for 10 min at 37 °C and blocked in 2% BSA, 2% normal goat serum and 0.1% Triton X-100 for 1 hour at room temperature. Neurons were then incubated with Alexa-488-labeled phospho-JAK2 (1:100) and VGluT1 (1:5000) antibodies overnight at 4 °C. Neurons were washed with PBS, incubated with the secondary antibody for 1 hour at room temperature, washed with PBS, and mounted in glycerol with *n*-propyl gallate (Sigma). The following antibodies and dilutions were used: anti-VGluT1 (Millipore; AB5905; 1:4000), 488-conjugated anti-pY402 Pyk2 (Invitrogen; 44-618A1; 1:500), 488-conjugated anti-pY1007/1008 JAK2 (Millipore; 04-1098; 1:200). Neurons were imaged with a confocal microscope (Zeiss LSM700; 63X objective, 2.5X zoom). Image stacks consisting of three optical sections (0.5 µm apart) were made by ImageJ and the intensity of Syt-1 and phospho-JAK2 or phospho-Pyk2 at VGluT1-positive puncta were quantified.

In vitro DREADD assay

At DIV3-4, cultured neurons were transfected with 1-2 µg of UbC-Sphy-mCherry only or UbC-Sphy-mCherry and UbC-hM4Di expressing plasmids using CalPhos transfection kit (Clontech). At DIV13-14, 250 µL culture media was replaced by new media containing 50 µM picrotoxin with 10 µM CNO only (CNO), 10 µM CNO + 1 µM TTX (TTX) or 10 µM CNO + 10 µM CNQX and 50 µM AP5 (Inh). Controls received 50 µM picrotoxin with equal volume of water (vehicle). Cultures were incubated for 2 hours and fixed with 4% PFA for 10 min at 37°C and blocked in 2% BSA, 2% normal goat serum and 0.1% Triton X-100 for 1 hour at room temperature. This is followed by incubation with primary antibodies for 3 hours at room temperature or overnight at 4°C. The cultures were then washed with PBS, and secondary antibodies were applied for 1 hour at room temperature. After being washed again with PBS, samples were mounted in glycerol with n-propyl gallate (Sigma). The following antibodies and dilutions were used: anti-pY402 Pyk2 (Invitrogen; 44-618A1; 1:500) and anti-VGluT1 (Millipore; AB5905; 1:4000). Neurons were imaged with a

confocal microscope (Zeiss LSM700; 63X objective). The intensity of phospho-Pyk2 at Synaptophysin-mCherry and VGluT1-positive puncta were quantified.

Stereotaxic viral injection

P0.5–1 $Pyk2^{fl/fl}$ or $SOCS3^{fl/fl}$ pups were anesthetized by hypothermia. 800 nl of viral solution was stereotactically injected (100 nL/min) into the left cortex using the following coordinates: 1.2 mm anterior from lambda, 0.4 mm lateral from midline, 0.4 mm ventral from the skull surface. For FF experiments, viruses injected were 1 x 10^{12} gc/ml AAV-EGFP, or 1 x 10^{12} gc/ml AAV-EGFP and 1 x 10^{12} gc/ml AAV-Cre. For Synaptophysin-mCherry experiments, viruses injected were 1 x 10^{12} gc/ml AAV-EGFP and 1 x 10^{12} gc/ml AAV-Synaptophysin-mCherry.

Slice preparation for electrophysiology

Mice were decapitated and the forebrain was quickly removed. Coronal sections (350 μm) of the cingulate cortex were then cut using a VT1200S (Leica, Germany) vibratome. Sections were cut in ice cold solution containing: 2.8 mM KCl, 1 mM $MgCl_2$, 2 mM $MgSO_4$, 1.25 mM NaH_2PO_4, 1 mM $CaCl_2$, 206 mM sucrose, 10 mM glucose, and 26 mM $NaCO_3$. Slices were then recovered in artificial cerebral spinal fluid (aCSF) at room temperature for at least one hour. aCSF contained 118 mM NaCl, 2.5 mM KCl, 1.3 mM $MgCl_2$, 1.2 mM NaH_2PO_4, 2.5 mM $CaCl_2$, 10 mM glucose, and 26 mM $NaCO_3$. All solutions were bubbled continuously with 95% O_2/5% CO_2.

Fiber fraction analysis

Pyramidal cells in layer V of cingulate cortex, opposite to the virally infected side, were targeted for patch clamping. Pipettes (4-6 MΩ) filled with internal solution (35 mM CsF, 100 mM CsCl, 10 mM EGTA, and 10 mM HEPES, pH adjusted to 7.3 with CsOH) supplemented with the voltage-gated calcium channel blocker, D600 (methoxyverapamil hydrochloride; 0.1 mM; Sigma). A pair of glass electrodes, filled with 1 M NaCl and 25 mM HEPES, were placed dorsoventrally flanking

the callosal tract at the midline of cortical hemispheres (Figures 8D and 8H) in a location that evoked the maximal callosal current and allowed the isolated activation of callosal inputs only (Kumar and Huguenard, 2001). Data were collected with a Multiclamp 700B amplifier (Molecular Devices, San Jose, CA) using Clampex 10.2 (Molecular Devices), and digitized using a Digidata 1440 (Molecular Devices). Cells were held at -70 mV and the callosal bundle was stimulated at an inter-trial interval of 20 seconds.

Single fiber callosal response measurement

The single fiber callosal response was determined using the "failures" method (Kumar and Huguenard, 2001). The callosal bundle was stimulated five times at a fixed stimulus intensity (between 4–6 μA). If the stimulus intensity failed to elicit a response in more than 50% of trials (response detected in at least one but no more than two of the five trials), the cell was stimulated ten more times at the same stimulus intensity. All detected synaptic responses, with fixed latencies (6–8 msec) from stimulus onset, were averaged and recorded as the single fiber response. If no responses were detected, the stimulus intensity was raised by 5 μA and the "failures" method was repeated. The stimulus intensity was decreased by 5 μA if a response was evoked in more than 50 % of trials and the "failures" method was repeated.

Maximal callosal response measurement

The callosal bundle was stimulated at 100 μA and the stimulus strength was gradually increased with 10–50 μA increments until the maximum callosal response was evoked. The maximum evoked response was defined as the biggest response evoked where at least three more increases in stimulus intensity no longer evoked a larger callosal response.

Fiber fraction calculation

The fiber fraction ratio is calculated as the average single fiber response / maximal response. The fiber fraction indicates the contribution of a single callosal fiber to the total callosal input received by a single neuron. The inverse of the fiber fraction is an estimate of the number of callosal inputs received by a neuron (Hooks and Chen, 2006, 2008; Noutel et al. 2011; Narushima et al. 2016).

Statistical analysis

Statistical analyses were performed using GraphPad Prism software. Statistical tests used were Mann-Whitney test, one-way ANOVA, or Kruskal-Wallis test as indicated in the figure legend. In the case of one-way ANOVA, post hoc analysis was done with Tukey's test. In the case of Kruskal-Wallis, post hoc analysis was done with Dunn's test. All data are mean ± s.e.m. In all figures, n.s. ($P > 0.05$), * ($P < 0.05$), ** ($P < 0.01$), *** ($P < 0.005$) and **** ($P < 0.001$). Sample sizes for imaging were similar to those reported in previous publications (Yasuda et al., 2011; Terauchi et al., 2010; Toth et al., 2013; Dabrowski et al., 2015; Terauchi et al., 2015; Terauchi et al., 2016). Sample sizes for electrophysiology was calculated such that sample sizes had sufficient power for subsequent statistical analyses (at least 80% power at the 0.05 level of significance for each set of experiments).

Chapter 4.

To keep or not to keep: The interaction between *'elimination'* signals (Pyk2 and JAK2) and *'stabilization'* signals (SIRPα)

I performed the experiments and analyzed the data for all figures except figure 4.2 (with Akiko Terauchi). I wrote the chapter.

4.1 Abstract

During the critical activity-dependent process of synaptic refinement, active synapses are preferentially strengthened while inactive synapses are eliminated. Our work, and that of others, have shown that active synapses are eliminated in an activity and competition-dependent manner. Inactive synapses are eliminated, but only when there are active ones to compete with. This suggests that active connections send *'punishment'* signals that trigger *'elimination'* signals within inactive synapses and instruct them to leave. A logical extension of this model suggests that the *'punishment'* signals may target other active synapses as well. Thus, to prevent the elimination of active synapses, a *'stabilization'* signal should signal locally at active synapses and protect them. However, the molecular identity of the *'stabilization'* signal and the mechanism through which it protects synapses is unknown. Here, I determine that SIRPα, a molecule that drives synapse maturation, may also serve as a *'stabilization'* signal. We show that: the loss of SIRPα drives aberrant synaptic elimination; SIRPα suppresses the activation of the *'elimination'* signals, Pyk2 and JAK2; and SIRPα can rescue JAK2 signaling-driven synapse elimination. Therefore, we propose that SIRPα is a *'stabilization'* signal that protects active synapses from elimination by preventing the activation of *'elimination'* signals.

4.2 Introduction

Previous work in the lab and the work shown in chapter 3 has elucidated the manner through which neuronal activity regulates refinement in the brain (Yasuda et al., 2011). These

works established that inactive connections in the brain are eliminated only when there are other active connections to compete with. This suggests that active connections send a *'punishment'* signal to inactive ones and instruct them to leave by triggering *'elimination'* signals within inactive synapses. In chapter 3, we identified Pyk2 and JAK2 as determinants of inactive synapse elimination. Signaling of the *'elimination'* signals, Pyk2 and JAK2 are critical regulators of synaptic elimination. We also demonstrated that Pyk2/JAK2 are active at inactive synapses, but only in the presence of other active connections. This further lends credence to the notion that a *'punishment'* signal is sent from active synapses to drive the elimination of inactive ones.

However, in the brain, there are multiple synapses, with different levels of synaptic activity, in close proximity to one another. Therefore, we reason that the *'punishment'* signal may also affect other synapses that are active and need to be maintained. This raises the need for a protective, *'stabilization'* signal that signals locally and preferentially at active synapses to counteract the *'elimination'* signals and prevent these synapses from being eliminated (Fig. 1.5). *However, the identity of the 'stabilization' signal in the brain remains to be elucidated.*

One molecule that may serve as a *'stabilization'* signal is SIRPα. In the developing brain, neuronal activity drives the cleavage and release of the SIRPα extracellular domain. In turn, the cleaved extracellular domain of SIRPα promotes the strengthening of the presynaptic terminals through CD47, a SIRPα receptor (Toth et al., 2013). Fewer retinogeniculate synapses are found in mice lacking CD47 (Lehrman et al., 2018). This suggests that SIRPα-CD47 may signal locally at active synapses and protect them from elimination. However, whether SIRPα stabilizes active synapses and prevents their elimination is unknown. Additionally, whether SIRPα, a signal that strengthens synapses, interacts with the destabilizing *'punishment'* and *'elimination'* signals remains to be elucidated.

In this chapter, I demonstrate that SIRPα plays a critical role in preventing aberrant synapse elimination. SIRPα suppresses the activation of Pyk2 and JAK2, the *'elimination'* signals and SIRPα signaling rescues JAK2-driven synaptic elimination. Together, our findings reveal that

SIRPα is indeed a *'stabilization'* signal that protects synapses from elimination by suppressing the activation of *'elimination'* signals. This interaction between the *'stabilization'* and *'elimination'* signals offer neurons a way to finely balance synapses that are kept and eliminated during synaptic refinement to precisely fine-tune and shape functional neural networks.

4.3 Results

Loss of SIRPα signaling drives functional synaptic elimination

I first reasoned that if SIRPα is indeed a *'stabilization'* signal, then in the absence of SIRPα, more elimination should occur. To test this hypothesis, I performed FF experiments on SIRPα KO mice (Actin-CreER, SIRPα$^{fl/fl}$ mice injected with Tamoxifen at P0; SIRPα is inactivated after Tamoxifen injections, Fig. 2.1 F). Control mice are SIRPα$^{fl/fl}$ mice (no Cre) injected with Tamoxifen (Fig. 4.1 A). At P8-10, the single fiber amplitude, maximum amplitude, and FF ratio were not significantly different between controls and SIRPα KO mice (Fig. 4.1 B-D), suggesting that SIRPα signaling is not critical to callosal synapse formation. In contrast, at P16-19, the FF ratio was significantly larger in SIRPα KO mice relative to controls (Fig. 4.1 D), indicating that the loss of SIRPα drives greater functional synapse elimination. These results support the notion that SIRPα protects synapses from elimination and stabilizes them.

SIRPα suppresses Pyk2 and JAK2 activation

In the absence of SIRPα, more synaptic elimination occurs (Fig. 4.1). To be a *'stabilization'* signal, SIRPα would need to counteract the destabilizing effects driven by the *'elimination'* signals. Thus, I asked if SIRPα may regulate the activation of Pyk2 and/or JAK2, the *'elimination'* signals. To address this question, I prepared the extracellular fragment of SIRPα (soluble SIRPα; sSIRPα) protein and we bath-applied it to cultured primary cortical neurons at DIV11, which is during synapse maturation in cultured neurons (Toth et al., 2013; 2 nM concentration for 1 hour). The bath-application of sSIRPα allows SIRPα to signal in an activity-independent manner (Toth et al.,

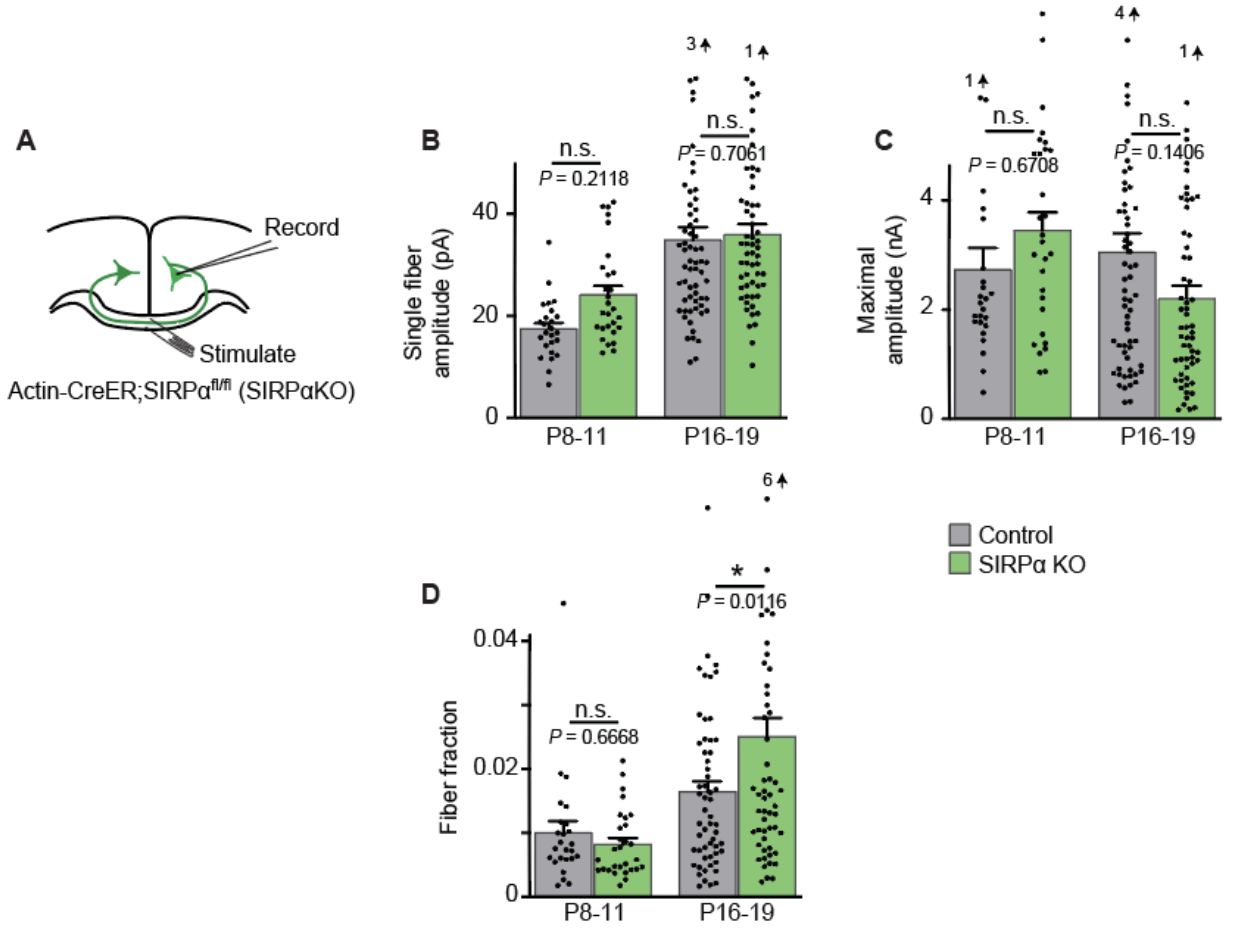

FIGURE 4.1. Loss of SIRPα impairs functional callosal synapse elimination.

(A-D) FF analysis in SIRPα KO mice. (A) Schematic of experiments. Actin-CreER, SIRPα mice (injected with Tamoxifen at P0) were used to drive SIRPα KO from all cells. The electrically evoked callosal synaptic responses were recorded by whole-cell patch clamp at P8-11 (before refinement) and P16-19 (after refinement). (B) Quantification of single fiber responses. (C) Quantification of the maximal responses. (D) Quantification of the FF ratio. The FF ratio is not different between Control and SIRPα KO mice at P8–10. However, the FF ratio is significantly higher in SIRPα KO relative to Control at P16–19. This indicates that SIRPα does not affect early synapse formation, but is critical to prevent synapse elimination. Mean ± SEM. n = 25 cells, P8–10 Control; 29 cells, P8–10 SIRPα KO; 63 cells, P16–19 Control; 58 cells P16–19 SIRPα KO. ANOVA followed by Sidak's test.

2013). We then immunostained these cultures for Phospho-Pyk2 or Phospho-JAK2 to assess Pyk2 and JAK2 activation, respectively (Fig. 4.2 A and C). The bath-application of sSIRPα significantly decreases the density of both Phospho-Pyk2 and Phospho-JAK2 puncta (Fig. 4.2 B and D). This suggests that SIRPα signaling can suppress the activation of Pyk2 and JAK2 kinases. Evaluating the effect of sSIRPα application on the activation of other kinases not involved in synapse elimination (e.g.: Fyn, JAK1 and CSK; Fig. 3.8) will be a necessary control to ensure that SIRPα is not non-specifically inhibiting kinase activation.

The bath application of sSIRPα (for 1-4 days) is known to increase size and function of the presynaptic terminals (Toth et al., 2013). Pyk2 and JAK2 activation is regulated by neuronal activity (Fig. 3.7 and 3.11). To ensure that Pyk2 and JAK2 activation is suppressed by SIRPα, and not merely as a result of changes to synaptic activity, we acutely treated (for 1 hour) cultured neurons with sSIRPα. This acute treatment is likely not altering presynaptic function. Presynaptic terminal size and density (as indicated by immunostaining for VGluT1) is not different between controls and sSIRPα-treated cultures (Size: Controls, 0.1768 ± 0.014 μm^2; sSIRPα-treated, 0.1832 ± 0.009 μm^2; P = 0.5556 by Mann-Whitney test; Density: Controls, 0.06234 ± 0.013 puncta/μm^2; sSIRPα-treated, 0.05973 ± 0.02 puncta/μm^2; P = 0.9048 by Mann-Whitney test). These findings support the notion that SIRPα is a *'stabilization'* signal that functions by suppressing the activation of the *'elimination'* signals.

SIRPα can protect against JAK2-driven synapse elimination

Next, I asked whether SIRPα can prevent synapse elimination driven by the *'elimination'* signals. I have shown that the activation of JAK2 signaling via the suppression of the endogenous JAK2 inhibitor, SOCS3 (SOCS3 KO^{Pre}) results in increased functional and structural synapse elimination (Fig. 3.9 and 3.10). Synapse formation is not affected in SOCS3 KO^{Pre} mice (Fig. 3.9). Using this system, I asked whether SIRPα can rescue the increased, JAK2 signaling-driven

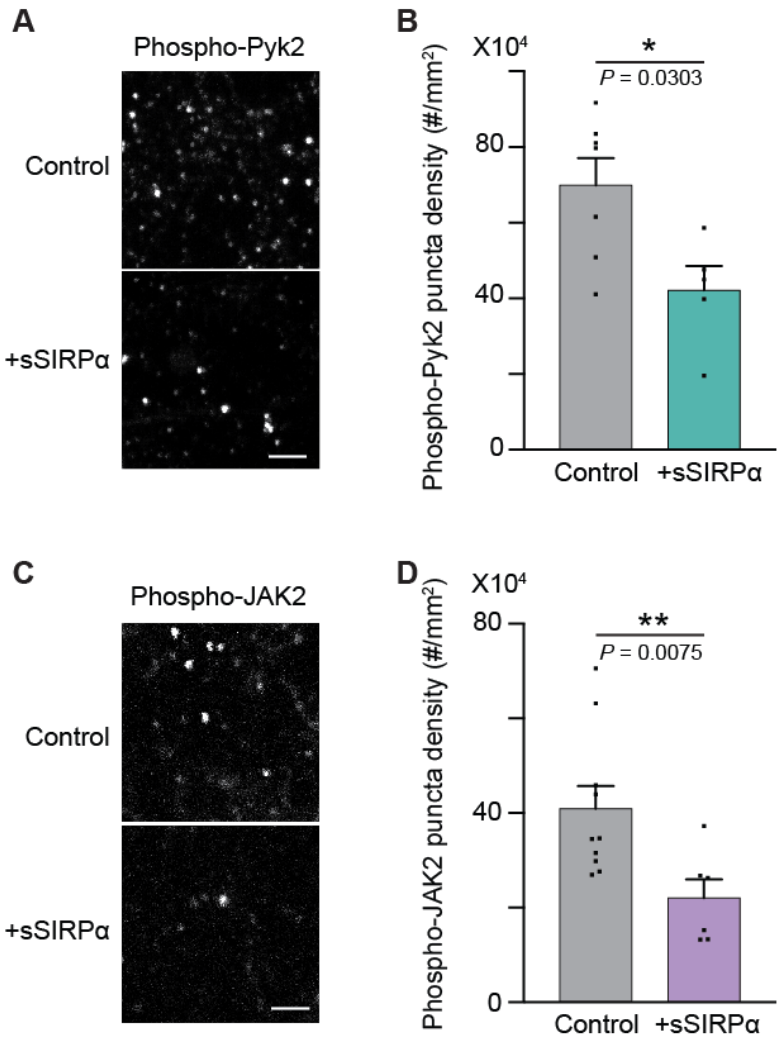

FIGURE 4.2. SIRPα can suppress Pyk2 and JAK2 activation.

(A-B) SIRPα decreases Pyk2 activation *in vitro*. (A) Cortical neuronal cultures were treated with PBS (Control) or 2 nM soluble SIRPα protein (+sSIRPα) for 1 hour at DIV11. Cultures were immunostained for Phospho-Pyk2. (B) Quantification of Phospho-Pyk2 puncta density. Phospho-Pyk2 density decreases with SIRPα treatment. Mean ± SEM. n = 7 images, Control; 5 images, +sSIRPα, reproduced in 2 independent experiments. Mann Whitney test. Scale bar, 2 μm.

(C-D) SIRPα decreases JAK2 activation *in vitro*. Cortical neuronal cultures were treated with PBS (Control) or 2 nM soluble SIRPα protein (+sSIRPα) for 1 hour at DIV11. Cultures were immunostained for Phospho-JAK2. (D) Quantification of Phospho-JAK2 puncta density. Phospho-JAK2 density decreases with SIRPα treatment. Mean ± SEM. n = 10 images, Control; 6 images, +sSIRPα. Mann Whitney test. Scale bar, 1 μm.

elimination. To test this, I developed an AAV strategy to drive SIRPα signaling in a neuronal activity-independent manner. In the presence of neuronal activity, the extracellular domain of the postsynaptically expressed SIRPα is cleaved and released to signal to the presynaptic terminal. The overexpression of the extracellular domain of SIRPα (SIRPαExt) drives synapse maturation even in the absence of neuronal activity *in vitro* (Toth et al., 2013). Thus, by overexpressing SIRPαExt, SIRPα signaling can be activated at all synapses regardless of synaptic activity levels. To overexpress SIRPαExt *in vivo*, I created an AAV expressing SIRPαExt (AAV-SIRPαExt; Fig. 4.3 A). AAV-SIRPαExt also expresses mCherry to allow identification of infected neurons. The secretion of SIRPαExt from cultured cortical neurons infected with AAV-SIRPαExt was verified by Western blotting (Fig. 4.3 B).

To inactivate SOCS3 (and consequently activate JAK2) from presynaptic neurons, I injected AAV expressing Cre, together with AAV-EGFP, into the left cortical hemisphere of $SOCS3^{fl/fl}$ mice at P0-1 (SOCS3 KO^{Pre}). To overexpress SIRPαExt in postsynaptic neurons of the SOCS3 KO^{Pre} mice, I injected AAV-SIRPαExt into the right cortical hemisphere (SOCS3 KO^{Pre}+SIRPαExt; Fig. 4.3 C and D). Electrically evoked callosal responses were recorded from mCherry positive neurons in the right cortical hemisphere at P16-18, after callosal refinement occurs (Fig. 3.9 and 4.3 C). The FF ratio is significantly lower in SOCS3 KO^{Pre} + SIRPα mice than in SOCS3 KO^{Pre} mice (Fig. 4.3 E-G). The postsynaptic overexpression of SIRPαExt rescued fiber fraction levels in SOCS3 KO^{Pre} mice to levels observed in wildtype mice (Fig. 3.9 F and 4.3 G). This suggests that SIRPα is rescuing the increased JAK2 signaling-driven synapse elimination. Further experiments at earlier timepoints will be done to ensure that the overexpression of SIRPαExt are not affecting axon targeting or synapse formation.

4.4 Discussion

Synaptic refinement is a critical process driven by neuronal activity that finely balances the stabilization and destabilization of synapses. Too much synaptic elimination in the brain

FIGURE 4.3. SIRPα signaling rescues functional synapse loss in mice with activated JAK2-signaling *(next page)*.

(A-B) An AAV expressing the SIRPα extracellular domain. (A) Schematic of the AAV construct generated (AAV-SIRPαExt). This construct allowed the expression of the FLAG-tagged, SIRPα extracellular domain (SIRPαExt) under the neuron-specific human Synapsin I promoter (hSyn). mCherry is also expressed to allow detection of infected cells. SS: signal sequence. (B) Verification of AAV-SIRPαExt. Cultured cortical neurons were infected at DIV3 with AAV-SIRPαExt or AAV-EGFP (as a Control). The culture media is collected at DIV10 and immunoprecipitated for FLAG. Immunoprecipitates were blotted for SIRPα. FLAG-tagged SIRPα extracellular domain (the bioactive SIRPα fragment; ~75 kDa) is detected in the media of cultures expressing AAV-SIRPαExt.

(C-G) FF analysis to determine if SIRPα prevents JAK2-driven synaptic elimination. (C) Schematic of experiments. AAV-EGFP + AAV-Cre were injected into the left cingulate cortex of $SOCS3^{fl/fl}$ mice at P1-2 (SOCS3 KO^{Pre}). AAV-SIRPαExt was injected into the right cingulate cortex of $SOCS3^{fl/fl}$ mice (SOCS3 KO^{Pre} + SIRPαExt). The electrically evoked callosal synaptic responses were recorded by whole-cell patch clamp from mCherry-positive cells in the right hemisphere at P16-18. (D) Coronal section of a P16 mouse brain injected with AAV-SIRPα (right cortical hemisphere) and AAV-EGFP + AAV-Cre (left cortical hemisphere). (E) Quantification of single fiber responses. (F) Quantification of the maximal responses. (G) Quantification of the FF ratio. The higher FF ratio in SOCS3 KO^{Pre} mice is decreased when SIRPαExt is expressed. n = 35 cells, 3 mice, SOCS3 KO^{Pre}; 21 cells, 2 mice, SOCS3 KO^{Pre} + SIRPαExt. Mann-Whitney's test.

FIGURE 4.3. (Continued)

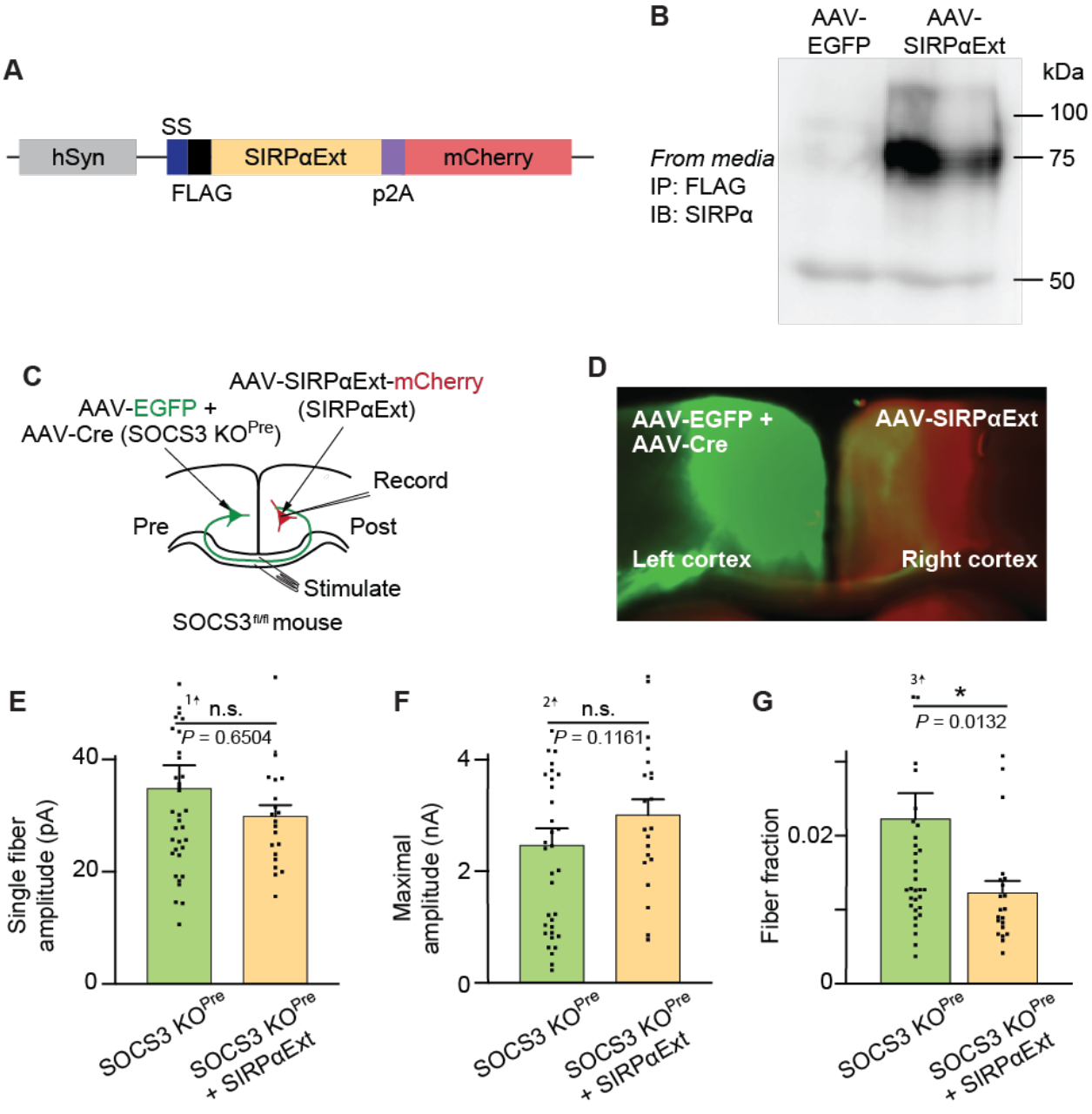

underlies disorders like schizophrenia (Sekar et al., 2016; Sellgren et al., 2019). Insufficient synaptic elimination is linked to disorders like Rett's syndrome and ASD (Noutel et al., 2011; Tang et al., 2014). However, the mechanisms by which signals that eliminate synapses and signals that strengthen synapses coordinate to ensure the preferential stabilization and strengthening of active synapses and elimination of inactive ones are unknown. Here, we identified SIRPα as a *'stabilization'* signal. We showed that: 1) SIRPα signaling is necessary to prevent aberrant synaptic elimination; 2) SIRPα suppresses Pyk2 and JAK2 activation; and 3) SIRPα rescues JAK2-driven synaptic elimination. Taken together, the results in this chapter demonstrates that SIRPα is a *'stabilization'* signal that prevents synaptic elimination by suppressing the activation of *'elimination'* signals (Fig. 4.4).

SIRPα as a *'stabilization'* and *'maturation'* signal

It is clear that synaptic refinement is an activity and competition-dependent process. Inactive synapses are eliminated only when there are other active connections (Fig. 3.1). This suggests that active connections are sending a *'punishment'* signal that switches on *'elimination'* signals at inactive synapses to drive their elimination (Fig. 1.2). Here, I have logically extended this model and reasoned that the *'punishment'* signal from active synapses may target other active ones as well. Therefore, to prevent the elimination of functional synapses, a local feedback signal at active synapses, a *'stabilization'* signal, is necessary. I demonstrated that in the absence of SIRPα, an excess of synapses is eliminated (Fig. 4.1). This supports the notion that a protective signal is necessary to prevent the aberrant elimination of synapses that should be maintained.

Prior to the work in this chapter, SIRPα was regarded to be a *'maturation'* signal (Chapter 2; Toth et al., 2013). SIRPα signaling increases the size of presynaptic terminals, accumulation of synaptic vesicles, number of functional synapses and neurotransmitter release probability, all markers of synaptic strengthening (Fig. 2.4; Toth et al., 2013). However, here we do not detect SIRPα-driven changes in single fiber responses, a marker of synaptic strengthening (Fig 4.1 and

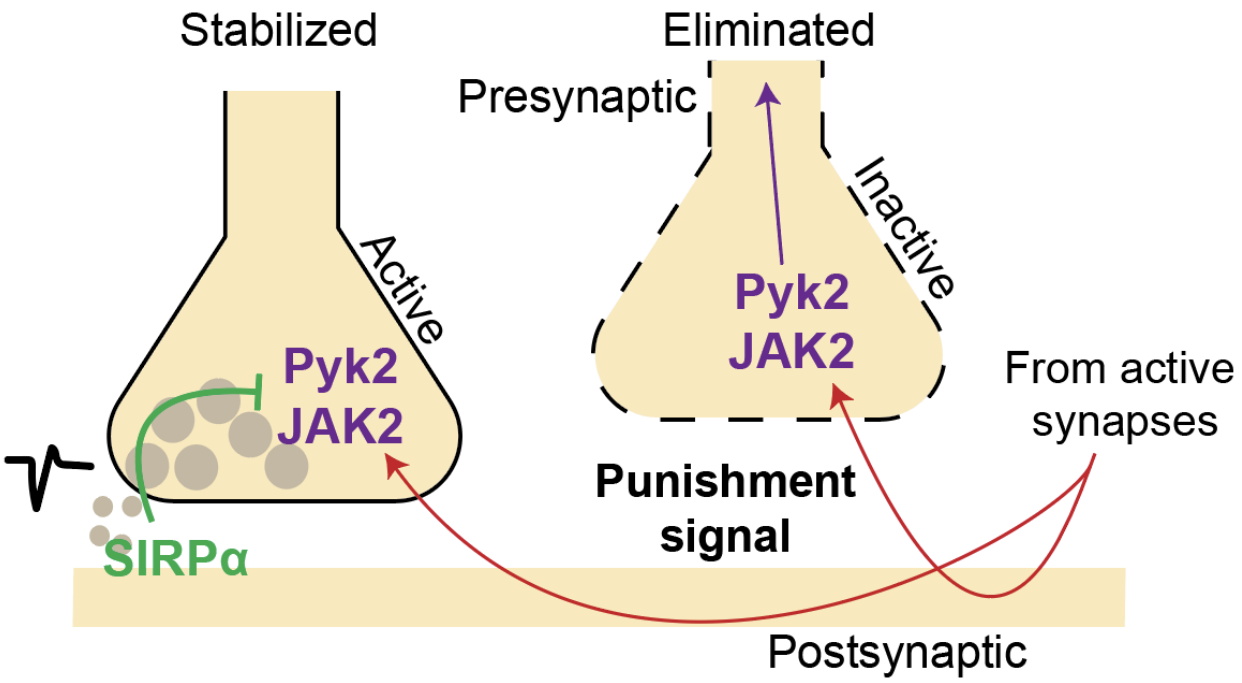

FIGURE 4.4. Proposed model of synapse stabilization

'Punishment' signals (red arrows) sent by active connections activate Pyk2 and JAK2 (*'elimination'* signals) to drive synapse elimination. At active synapses, SIRPα (*'stabilization'* signal) signals to protect active synapses from elimination by suppressing the activation of Pyk2 and JAK2. SIRPα does not signal at inactive synapses. Therefore, Pyk2 and JAK2 are active and the inactive synapse is eliminated.

4.3). In contrast, impaired C1ql1-Bai3 and Fn14 signaling, other known *'maturation'* signals, result in decreased single fiber strength (Kakegawa et al., 2015; Cheadle et al., 2018). It is possible that SIRPα first stabilizes synapses and then induces maturation. Indeed, in the prior study, SIRPα demonstrated impaired maturation at P30, a later age than that examined in this chapter (Toth et al., 2013). Additionally, SIRPα is known to regulate presynaptic, but not postsynaptic, maturation. Loss of SIRPα signaling show no defects in PSD95 immunostaining and mEPSC amplitude, markers of postsynaptic strength (Toth et al., 2013). Therefore, single fiber amplitude (often a marker of postsynaptic strength) may not reflect SIRPα-driven presynaptic strengthening.

Here, I showed that SIRPα is also a *'stabilization'* signal. SIRPα signaling stabilizes synapses and protects synapses from the destabilizing JAK2 signaling (Fig. 4.1 and 4.3). This is in contrast to the other molecules implicated in active synapse maturation, Fn14 and C1ql1-Bai3. C1ql1 and Fn14 signaling promote the elimination of *'losing'* synapses (Kakegawa et al., 2015; Cheadle et al., 2018). Thus, SIRPα may be regulating both the stabilization and maturation of active synapses. It is also possible that SIRPα may serve only as a *'stabilization'* signal and synapses protected by SIRPα are strengthened by other *'maturation'* signals like C1ql1 and Fn14.

Mechanisms of synapse stabilization

Mechanistically, our data suggest that SIRPα protects synapses by suppressing Pyk2 and JAK2 signaling. Bath application of SIRPα suppresses Pyk2 and JAK2 activation (Fig. 4.2). Overexpression of the bioactive fragment of SIRPα, the SIRPα extracellular domain, rescues JAK2-signaling driven functional synaptic elimination (Fig. 4.3). How SIRPα signals to regulate Pyk2 and JAK2 remains to be addressed. It is likely that the presynaptic SIRPα receptor, CD47 is involved. The loss of CD47 impairs synaptic refinement in the retinogeniculate system. CD47 KO mice have fewer functional and structural synapses (Lehrman et al., 2018). Of note, Lehrman et al. suggest that microglial SIRPα is the critical player in synaptic protection. Microglia from SIRPα KO mice engulf more synaptic material than microglia from wild-type mice in an *in vitro*

engulfment assay (Lehrman et al., 2018). Our work suggests that neuronal SIRPα is the critical *'stabilization'* signal. The neuron-specific manipulation of SIRPα *in vitro* alters synaptic strength (Fig. 2.4; Toth et al., 2013). Additionally, neuronal SIRPα is cleaved and released in an activity-dependent manner (Fig. 2.6). It is likely that neuronal SIRPα and microglial SIRPα regulate different stages of synaptic elimination; i.e., neuronal SIRPα detects synaptic activity and determines which synapses to protect and subsequently, microglial SIRPα prevents microglial engulfment and removal of these synapses. Further cell type-specific experiments will be necessary to distinguish the roles of neuronal and microglial SIRPα in synaptic refinement.

How SIRPα-CD47 signaling suppresses Pyk2/JAK2 activation is an interesting next question. CD47 can regulate intracellular calcium levels (Rogers et al., 2014). This change in calcium levels may suppress Pyk2, a calcium-dependent kinase, activation. An additional possibility is that SIRPα prevents active synapses from receiving the *'punishment'* signal (*'punishment'* signals are discussed in Chapter 5), which in turn, suppresses the activation of the *'elimination'* signals.

Developmental signals in neuropsychiatric diseases

Diseases such as schizophrenia, ASD, and AD are characterized by aberrant synaptic connectivity that occurs as a result of improper synaptic elimination (Tang et al., 2014; Sekar et al., 2016; Sellgren et al., 2019; Salazar et al., 2019). Both Pyk2 and JAK2 pathways are implicated in schizophrenia and AD, diseases characterized by excessive synapse loss (Chiba et al., 2009; Costain et al., 2013; Lambert et al., 2013; Hsu et al., 2014; Dourlen et al., 2017; Salazar et al., 2019). Whether SIRPα can protect synapses and prevent this disease-driven synapse loss is an interesting question that may lead to novel approaches in treating these diseases.

4.5 Experimental procedures

Mouse strains

Sirpa$^{fl/fl}$ and *Actin-CreER* mutant mice were described previously (Toth et al., 2013). Tamoxifen (100 μg) was injected at P0-P1 to induce the Cre recombinase-mediated excision of the *Sirpa* gene. C57Bl/6 and SOCS3$^{fl/fl}$ mice (Jackson) were used in this study. All mice, except C57Bl/6 mice, were on mixed backgrounds. Both male and female mice were used. No differences were observed between male and female mice. Mice were housed in OptiMICE cages (4–5 mice per cage) with a 12-h/12-h light/dark cycle. The housing room temperature was 22 ± 1 °C. Mice were allowed ad libitum access to food and water. All animal care and experiments were performed in accordance with the institutional guidelines and approved by the Institutional Animal Care and Use Committees at Boston Children's Hospital.

Primary cortical neuronal cultures

For all neuronal cultures used, cortices were dissected from postnatal day (P) 0-1 mice and dissociated with 0.5 % trypsin (Terauchi et al., 2010; Toth et al., 2013; Dabrowski et al., 2015; Terauchi et al., 2015; Terauchi et al., 2016). 60,000 hippocampal neurons were plated on poly-D-lysine coated glass coverslips (diameter 12 mm) and grown in culture media (GS21 (MTI-GlobalStem, Sigma), 2 mM L-glutamine, 100 U/ml penicillin-streptomycin in NeuralQ medium (Sigma)).

sSIRPα treatment assay

Soluble SIRPα proteins (sSIRPα) were produced by transfecting HEK293TT cells with plasmid expressing the FLAG-tagged SIRPα extracellular domain (Toth et al., 2013). Secreted proteins (sSIRPα) were purified from the culture media by affinity chromatography on anti-FLAG-agarose (Umemori and Sanes, 2008).

Primary neurons were cultured for 11 days after which 2 nM sSIRPα was bath applied. Since sSIRPα was in PBS, an equal volume of PBS was added to control cultures. Cultures were incubated for 1 hour at 37 °C. Neurons were fixed with 4% paraformaldehyde (PFA) for 10 min at 37 °C and blocked in 2% BSA, 2% normal goat serum, 0.1% Triton X-100 and 1mM sodium orthovanadate for 1 hour at room temperature. Neurons were then incubated with phospho-JAK2 (1:100) or phospho-Pyk2 (1:500), Neurofilament (1:500) and VGluT1 (1:5000) antibodies overnight at 4 °C. Neurons were washed with PBS, incubated with the secondary antibody for 1 hour at room temperature, washed with PBS, and mounted in glycerol with *n*-propyl gallate (Sigma). The following antibodies and dilutions were used: anti-VGluT1 (Millipore; AB5905; 1:4000), Phospho-Pyk2 (Invitrogen; 44-618A1; 1:500), Phospho-JAK2 (Millipore; 04-1098; 1:100) and Neurofilament (BioLegend; 837904; 1:500). Neurons were imaged with a confocal microscope (Zeiss LSM700; 63X objective). Image stacks consisting of three optical sections (0.5 µm apart) were made by ImageJ and the density phospho-JAK2 or phospho-Pyk2 puncta were quantified.

Stereotaxic viral injection

P0.5–1 *SOCS3*$^{fl/fl}$ pups were anesthetized by hypothermia. 800 nl of AAV-SIRPαExt or PBS was stereotactically injected (100 nL/min) into the right cortex using the following coordinates: 1.2 mm anterior from lambda, 0.4 mm lateral from midline, 0.4 mm ventral from the skull surface. 24 hours later, same pups were anesthetized by hypothermia. 800 nl of AAV-Cre and AAV-EGFP was stereotactically injected (100 nL/min) into the left cortex using the following coordinates: 1.2 mm anterior from lambda, 0.4 mm lateral from midline, 0.4 mm ventral from the skull surface. Viruses injected were 1 x 10^{12} gc/ml AAV-SIRPαExt, or 1 x 10^{12} gc/ml AAV-EGFP, or 1 x 10^{12} gc/ml AAV-EGFP and 1 x 10^{12} gc/ml AAV-Cre.

Fiber fraction analysis (See section 3.5 for additional details)

Mice were decapitated and the forebrain was quickly removed. Coronal sections (350 μm) of the cingulate cortex were then cut using a VT1200S (Leica, Germany) vibratome. Sections were cut in ice cold solution containing: 2.8 mM KCl, 1 mM $MgCl_2$, 2 mM $MgSO_4$, 1.25 mM NaH_2PO_4, 1 mM $CaCl_2$, 206 mM sucrose, 10 mM glucose, and 26 mM $NaCO_3$. Slices were then recovered in artificial cerebral spinal fluid (aCSF) at room temperature for at least one hour. aCSF contained 118 mM NaCl, 2.5 mM KCl, 1.3 mM $MgCl_2$, 1.2 mM NaH_2PO_4, 2.5 mM $CaCl_2$, 10 mM glucose, and 26 mM $NaCO_3$. All solutions were bubbled continuously with 95% O_2/5% CO_2.

Pyramidal cells in layer V of cingulate cortex were targeted for patch clamping. For Fig. 4.3; cells infected with AAV-SIRPαExt (identified by mCherry expression) were targeted for patch clamping. Pipettes (4-6 MΩ) filled with internal solution (35 mM CsF, 100 mM CsCl, 10 mM EGTA, and 10 mM HEPES, pH adjusted to 7.3 with CsOH) supplemented with the voltage-gated calcium channel blocker, D600 (methoxyverapamil hydrochloride; 0.1 mM; Sigma). A pair of glass electrodes, filled with 1 M NaCl and 25 mM HEPES, were placed dorsoventrally flanking the callosal tract at the midline of cortical hemispheres (Figures 8D and 8H) in a location that evoked the maximal callosal current and allowed the isolated activation of callosal inputs only (Kumar and Huguenard, 2001). Data were collected with a Multiclamp 700B amplifier (Molecular Devices, San Jose, CA) using Clampex 10.2 (Molecular Devices), and digitized using a Digidata 1440 (Molecular Devices). Cells were held at -70 mV and the callosal bundle was stimulated at an inter-trial interval of 20 seconds.

Statistical analysis

Statistical analyses were performed using GraphPad Prism software. Statistical tests used were Mann-Whitney test and one-way ANOVA as indicated in the figure legend. In the case of one-way ANOVA, post hoc analysis was done with Sidak's test. All data are mean ± s.e.m. In all figures,

n.s. ($P > 0.05$), * ($P < 0.05$), ** ($P < 0.01$), *** ($P < 0.005$) and **** ($P < 0.001$). Sample sizes for imaging (Fig. 4.2) were similar to those reported in previous publications (Terauchi et al., 2010; Toth et al., 2013; Dabrowski et al., 2015; Terauchi et al., 2015; Terauchi et al., 2016). Statistical calculation of sample sizes for electrophysiology was done to ensure that sample sizes had sufficient power for subsequent statistical analyses (at least 80% power at the 0.05 level of significance for each set of experiments).

Chapter 5.

Extended discussion and additional observations

I performed the experiments and analyzed the data for all figures except figure 5.1 (Masahiro Yasuda). I wrote the chapter.

5.1 Abstract

The work presented in this thesis focuses on the activity-dependent molecular mechanisms underlying the two critical steps of synaptic refinement: the stabilization and strengthening of active synapses, and the elimination of inactive ones. Chapter 2 established the mechanism through which neuronal activity regulates SIRPα function to drive synapse maturation. We demonstrated that the tyrosine phosphorylation of SIRPα in response to neuronal activity drives SIRPα extracellular domain cleavage and release, subsequently, promoting presynaptic strengthening. Chapter 3 determined that Pyk2 and JAK2 tyrosine kinases are neuronal activity and competition-dependent *'elimination'* signals that determine the elimination of inactive synapses. Chapter 4 presented emerging evidence showing that SIRPα is a *'stabilization'* signal that protects active synapses from elimination by suppressing the *'elimination'* signals, Pyk2 and JAK2. Together, I propose that Pyk2 and JAK2 are *'elimination'* signals that are activated at and drive the elimination of inactive synapses, in response to *'punishment'* signals from other active synapses. Active synapses are protected from elimination and strengthened by SIRPα, a *'stabilization'* signal that suppresses Pyk2/JAK2 activation (Fig. 4.4). However, to develop a complete understanding of synaptic refinement, there are several key questions that remain to be addressed. 1) Are the *'elimination'* signals, Pyk2 and JAK2 specific to callosal synapses or do they regulate the elimination of non-callosal synapses as well? 2) How do *'elimination'* signals drive the removal of synapses? 3) What are likely *'punishment'* signals from active synapses? 4) How does synaptic refinement affect brain function? What happens to brain

function when refinement goes wrong? In this chapter, I address these questions and present additional data that furthers our understanding of activity-dependent synaptic refinement.

5.2 The specificity of the *'elimination'* signals

In this thesis, we used callosal synapses as an *in vivo* system to study the molecular mechanisms of activity-dependent synaptic refinement. We developed novel assays to assess the refinement of callosal synapses, both structurally and functionally (Fig. 3.1 and 3.3). Using these assays, we determined that Pyk2 and JAK2 are determinants of inactive synapse elimination (Chapter 3). *A question that arises is whether Pyk2 and JAK2 are specific signals for callosal synapse elimination, or if they regulate the elimination of non-callosal synapses as well*. Here, we consider the projection-specificity and region-specificity of these *'elimination'* signals.

5.2.1 JAK2 kinase is a projection-specific *'elimination'* signal

Inactive corticostriatal projections are not eliminated

To manipulate callosal projecting neurons, we targeted neurons in layer V of the cortex (Fig. 3.1 and S1). A notable feature of many layer V callosal projecting neurons is that these cells are known to send axon collaterals to the striatum as well (Cowan and Wilson,1994; Kim et al., 2015). Therefore, we asked if the corticostriatal projecting axons are also eliminated in an activity-dependent manner during development. We used *in utero* electroporation to introduce TTLC and EGFP into left layer V cingulate cortical neurons at E13.5 as described (Fig. 3.1 B and 5.1 A). While inactive callosal axons were developmentally eliminated (Fig. 3.1 I), inactive corticostriatal axons were not (Fig. 5.1 B). Quantification of the density of EGFP-positive corticostriatal axons showed that TTLC did not affect corticostriatal projections (Fig. 5.1 B). Contrary to callosal axons, the inactive corticostriatal axons persisted into adulthood (Fig. 5.1 C). These results show that corticostriatal axons, unlike callosal axons, do not undergo activity-dependent elimination. These findings

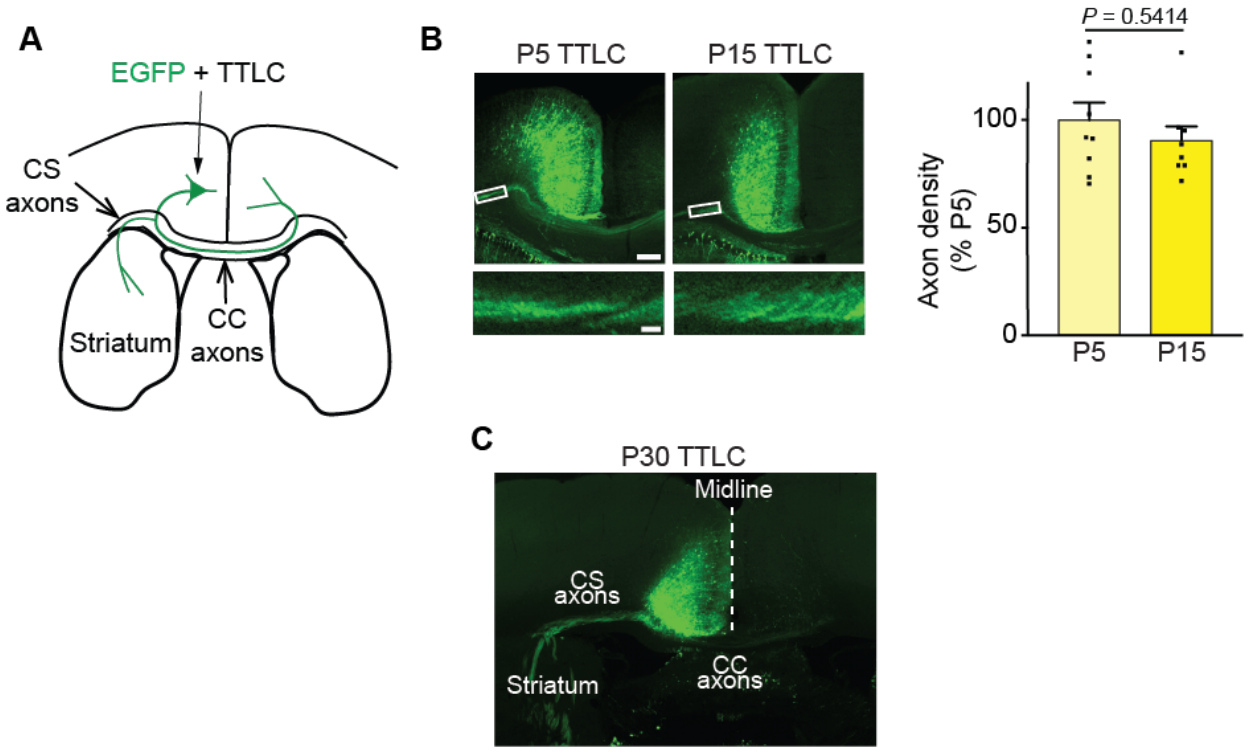

FIGURE 5.1. Inactive corticostriatal connections are not eliminated during development. (A) Schematic of experiments. EGFP and TTLC (TTLC) were electroporated into the left cingulate cortex of CD1 mice. Electroporated neurons send axons to the contralateral cortical hemisphere (callosal axons, CC axons) and to the striatum (corticostriatal axons, CS axons).

(B) Coronal sections of EGFP+TTLC electroporated brains at P5 (left) and P15 (right). The bottom panel show higher magnification images of corticostriatal axons taken from the boxed areas in the top panels. Scale bars, 200 μm (top), 50 μm (bottom). Graph shows quantification of corticostriatal axon densities in TTLC-expressing brains. The EGFP signal intensity of corticostriatal axons was normalized to that of electroporated neurons in the ipsilateral hemisphere. Mean ± SEM. n = 9 mice, P5 TTLC; 8 mice, P15 TTLC. Mann Whitney test.

(C) Example image from a P30 TTLC electroporated brain. Corticostriatal axons were still maintained, while callosal axons were eliminated.

suggest that there are likely projection-specific mechanisms underlying activity-dependent refinement.

JAK2 is activated at callosal projections but not at corticostriatal projections

Since corticostriatal axons are not eliminated in an activity-dependent manner, I reasoned that the *'elimination'* signals should be activated at callosal projections, but not at corticostriatal projections. To test this idea, I virally introduced EGFP into cortical neurons to label callosal and corticostriatal axons (Fig. 5.2 A). At P6 (just prior to the start of callosal synapse elimination in CD1 mice; Fig. 3.1 I and 3.3 F-H), I evaluated Phospho-JAK2 staining on EGFP-positive projections in the contralateral cortex and ipsilateral striatum (Fig. 5.2 B). Phospho-JAK2 staining is higher on callosal projections than on corticostriatal projections (Fig. 5.2 C). This suggests that JAK2 is activated preferentially at callosal connections, which are the connections that are to be eliminated.

JAK2 signaling does not affect corticostriatal synapse refinement

Thus far, we have shown that inactive corticostriatal projections are not developmentally eliminated (Fig. 5.1). I have shown that the *'elimination'* signal, JAK2 is preferentially activated at callosal projections relative to corticostriatal ones (Fig. 5.2). Next, I asked whether JAK2 signaling can drive the elimination of corticostriatal synapses as well. To do so, I virally introduced Synaptophysin-mCherry (Sphy-mCherry), which labels presynaptic terminals, and EGFP into the left cortical hemisphere of $SOCS3^{fl/fl}$ (Control) and Emx1-Cre, $SOCS3^{fl/fl}$ (SOCS3 KO) mice (Fig. 5.3 A). I then quantified the density and size of Sphy-mCherry puncta in the striatum at P19. The Sphy-mCherry density and size were not different in SOCS3 KO mice relative to Control mice (Fig. 5.3 B and C). This suggests that the loss of SOCS3 does not affect corticostriatal synapses. This result is in contrast to our findings with callosal synapses where the loss of SOCS3 (Emx1-

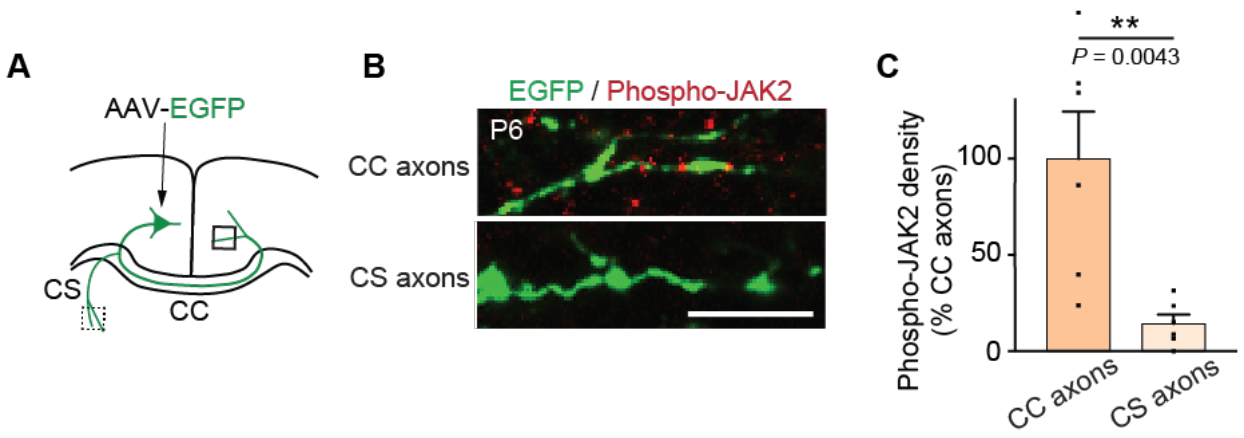

FIGURE 5.2. JAK2 is activated at callosal projections, but not at corticostriatal projections. (A) Schematic of experiments. AAV-EGFP was injected into the left cingulate cortex of CD1 mice at P0. Coronal sections were prepared at P6 and immunostained for Phospho-JAK2. Images of callosal projections (CC; in the contralateral cortex – indicated by the solid-lined black box) and corticostriatal projections (CS; in the striatum – indicated by the dash-lined black box) were taken. (B) Confocal images of Phospho-JAK2 staining on EGFP-positive CC and CS projections. Scale bar: 5 μm

(C) Quantification of Phospho-JAK2 puncta density on EGFP-positive axons. Data shown as % Phospho-JAK2 puncta density on CC axons. Phospho-JAK2 puncta density is higher on CC projections than on CS projections. Mean ± SEM. n = 6 fields from 3 mice. Mann-Whitney test.

.

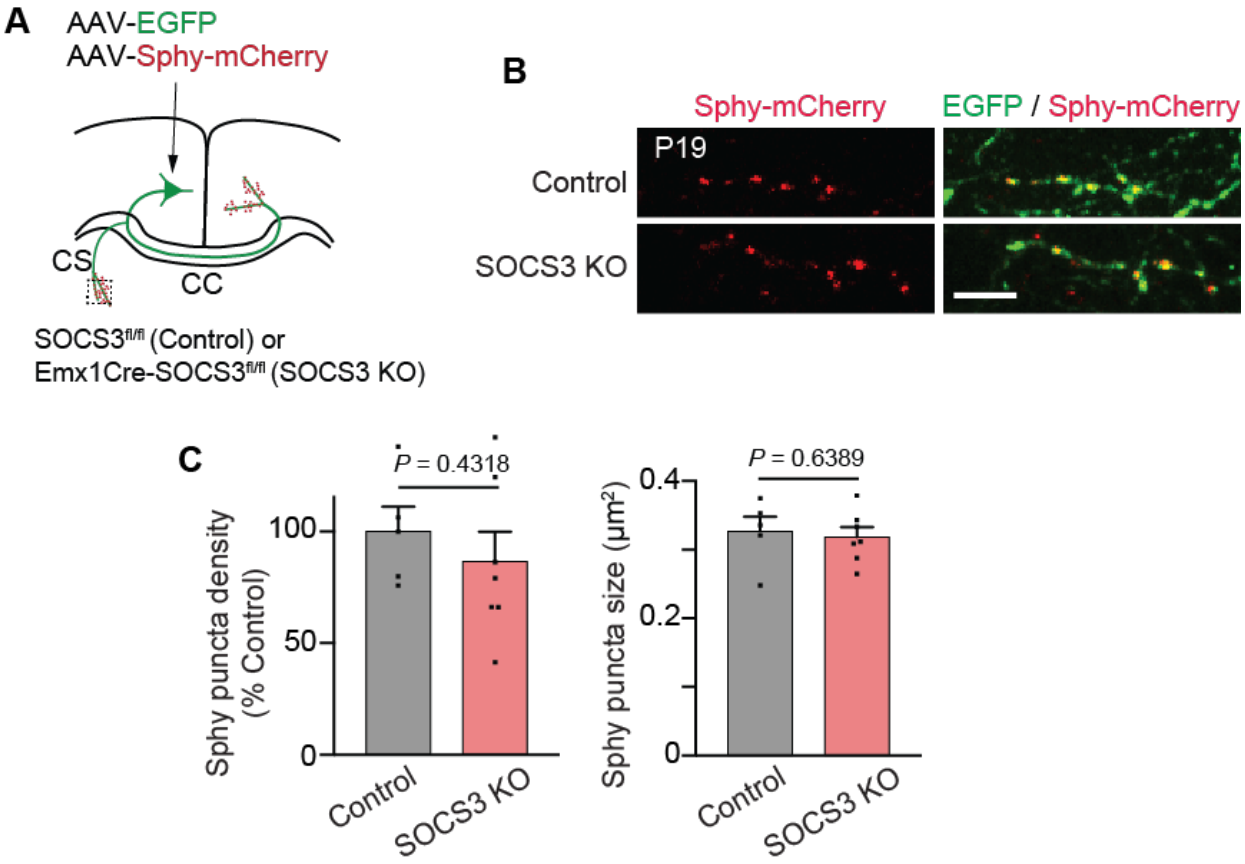

FIGURE 5.3. JAK2 signaling does not affect corticostriatal synapses.

(A) Schematic of experiments. SOCS3$^{fl/fl}$ mice were crossed to Emx1-Cre to knockout SOCS3 in all cortical neurons (SOCS3 KO). AAV-EGFP + AAV-Synaptophysin-mCherry (Sphy-mCherry) were injected into the left cingulate cortex of Control and SOCS3 KO mice at P5. Sphy-mCherry labelled presynaptic terminals were imaged in the striatum at P19 (dash-lined boxed area).

(B) Confocal images from EGFP/Synaptophysin-mCherry in Control and SOCS3 KO mice.

(C) Quantification of the density (number per axon area) and size of Synaptophysin-mCherry puncta. Sphy puncta density shown as % relative to that in Control. Mean ± SEM. n = 5 fields from 3 mice, Control; 7 fields from 3 mice, SOCS3 KO. Mann-Whitney test. Scale bar, 5 μm.

Cre, SOCS3$^{fl/fl}$) results in fewer synapses (Fig. 3.10). These results support the notion that JAK2 kinase is a projection-specific *'elimination'* signal.

The mechanisms that confer JAK2 signaling its projection specificity remains to be elucidated. It is possible that: 1) JAK2 kinase itself is preferentially localized to the callosal axon; 2) The *'punishment'* signal, from other active neurons, signals in the cortex and not in the striatum; and/or 3) Striatal connections are protected by a *'stabilization'* signal. However, it is clear that JAK2 signaling is highly regulated at a subcellular level. This tight subcellular control of JAK2 signaling allows the neuron to selectively regulate and appropriately modify synapses that are involved in information transfer to and from different regions.

5.2.2 JAK2 kinase is an *'elimination'* signal for retinogeniculate projections

The elimination of inactive inputs occurs in many other brain regions outside the cingulate cortex (Penn et al., 1998; Buffelli et al., 2003; Kano and Hashimoto, 2009; Yasuda et al., 2011). Thus, Pyk2 and JAK2 kinase may also regulate the refinement of connections in these other brain regions. Work in the lab has shown that JAK2 kinase regulates the eye-specific segregation in the dorsal lateral geniculate nucleus (dLGN). The dLGN, which is initially binocularly innervated by retinal ganglion cells (RGCs), undergoes activity-dependent refinement to become monocularly innervated during development (Godement et al., 1984; Sretavan and Shatz, 1986). Work in the lab demonstrated that the suppression of JAK2 kinase activity in RGCs impaired eye-specific segregation (data not shown; M. Yasuda). AAVs encoding JAK2DN (the dominant-negative form of JAK2) and EGFP was injected into one eye to suppress JAK2 signaling. EGFP only was injected as control. Inputs from the other eye were labeled with CF594-conjugated cholera toxin subunit B (CTB). At P15 (after the completion of eye-specific segregation), we found that the loss of JAK2 kinase signaling resulted in significantly more overlap between the inputs from both eyes (more overlap between EGFP and CTB positive inputs) relative to controls. No difference in the overlap was detected at P3, before eye segregation. This suggests that the loss

of JAK2 signaling impaired the elimination of RGC axons without affecting axon targeting (data not shown; M. Yasuda). These findings indicate that JAK2 serves as an *'elimination'* signal in multiple brain regions. Further experiments are needed to test if Pyk2 also regulates the refinement of other brain regions.

Taken together, this suggests that JAK2 is a projection-specific but brain region non-specific *'elimination'* signal. While multiple brain regions may employ the same *'elimination'* signals, different projections made by the same neuron may utilize different *'elimination'* signaling mechanisms to allow the neuron to selectively regulate specific projections.

5.3 *'Elimination'* signals and the regulation of microglial-mediated synaptic pruning

We have demonstrated that Pyk2 is necessary for synapse elimination (Fig. 3.2, 3.5 and 3.6). Pyk2 drives synaptic elimination most likely via the activation of JAK2, a Pyk2 interacting kinase (Fig. 3.8, 3.9 and 3.10). *However, the means by which Pyk2 and JAK2 kinase signaling ultimately results in synapse elimination is still unknown*. Rapidly accumulating evidence suggests that microglia, the resident immune cells of the brain, play critical roles in the removal of synapses during development, plasticity and disease (Schafer and Stevens, 2015). The importance of microglia in developmental elimination was demonstrated in the retinogeniculate system. Microglia engulfed synapses in an activity-dependent manner and disruption of microglial function impaired eye-specific segregation (Schafer et al., 2012).

At a molecular level, complement proteins, the classic *'eat me'* signal drive microglial engulfment of some synapses. Complement proteins label a subset of retinogeniculate synapses during peak pruning in the dLGN, targeting them for elimination. Mice lacking any one of these proteins demonstrate lasting defects in eye segregation and synapse refinement (Schafer et al., 2012). Another *'eat me'* signal is externalized phosphatidylserine (PTS). PTS is a phospholipid, normally maintained asymmetrically on the inner leaflet of the plasma membrane. In the dLGN,

externalized PTS is highest during peak pruning. *In vitro* microglia-driven synapse elimination is dependent on external PTS (Scott-Hewitt et al., 2020). A current model of microglial engulfment proposes that the secreted complement protein, C1q interacts with external PTS (enriched on synapses to be eliminated) and tags specific synapses for microglial engulfment (Scott-Hewitt et al., 2020).

While *'eat me'* signals promote microglial engulfment, a *'don't eat me'* signal, CD47 is thought to prevent microglial engulfment of active synapses (Lehrman et al., 2018). Mice lacking CD47 exhibited increased microglial engulfment of retinogeniculate inputs and reduced synapse numbers in the dLGN (Lehrman et al., 2018). Thus, *'eat me'* and *'don't eat me'* signals serve as molecular tags to appropriately drive or deter microglial engulfment of synapses. However, how the expression of *'eat me'* and *'don't eat me'* signals is regulated by neurons is unknown.

I hypothesize that the *'elimination'* signals, *Pyk2 and/or JAK2 determine inactive synapses for microglial engulfment by upregulating 'eat me' (e.g. external PTS) and downregulating 'don't eat me' (e.g. CD47) signals* (Fig. 5.4). Consistent with this idea, JAK2 and Pyk2 signaling have been implicated in the regulation of several pro-inflammatory genes (Di Liberto et al., 2018; Murphy et al., 2019). To determine if Pyk2 and JAK2 regulate microglial engulfment of synapses, I am currently examining microglial engulfment of synapses as well as the expression of *'eat me'* (external PTS) and *'don't eat me'* (CD47) signals in Pyk2 and JAK2 manipulated mice.

'Elimination' signals may act by detecting levels of neuronal activity and accordingly tagging inactive synapses for microglial engulfment. However, microglial engulfment accounts for a portion of inputs that are eliminated. Therefore, there are other mechanisms through which Pyk2 and JAK2 may drive synaptic elimination during developmental refinement. These include: 1) Astrocytic engulfment. Astrocytes have been reported to phagocytose and prune retinogeniculate synapses during refinement. Impaired astrocytic function results in improper eye-specific segregation. Additionally, it is proposed that astrocytes, like microglia, recognize *'eat me'* signals

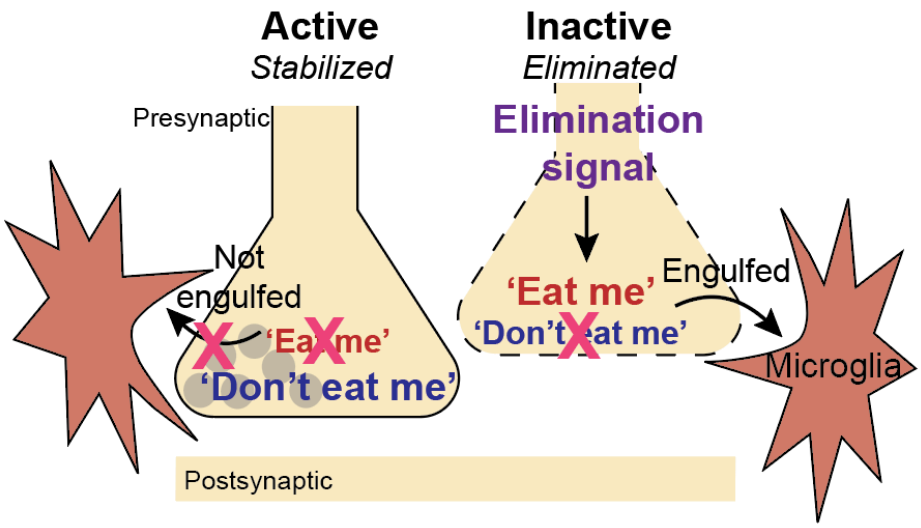

FIGURE 5.4. Proposed model for the mechanism by which *'elimination'* signals regulate microglial engulfment during developmental refinement.

'Elimination' signals active at inactive synapses upregulate *'eat me'* and downregulate *'don't eat me'* signals. These tag inactive synapses for removal via microglial engulfment. The *'elimination'* signal is not active at active synapses. Therefore, active synapses express *'don't eat me'* and are protected from microglial engulfment.

to appropriately remove synapses (Chung et al., 2013). Thus, I will also examine astrocytic engulfment of synapses in Pyk2 and JAK2 manipulated; and 2) Cytoskeletal rearrangement. Inactive inputs in the neuromuscular junction and hippocampus are eliminated via retraction, a process regulated by cytoskeletal proteins (Sanes and Lichtman, 1999; Luo, 2002; Yasuda et al., 2011). Pyk2 is known to activate RhoA, an actin regulating protein that has been implicated in axon retraction (Takeuchi et al., 2015; Lee et al., 2019). I will determine the role of RhoA in developmental synapse elimination by expressing a dominant negative form of RhoA (to suppress RhoA function) in callosal neurons and evaluating synapse elimination. I will also test if suppressing RhoA function rescues JAK2-driven synapse elimination.

5.4 The *'punishment'* signal

The work done in this thesis and by others have established that developmental synaptic elimination is an activity and competition-dependent process (Sretavan et al., 1984, Penn et al., 1998; Buffelli et al., 2003; Kano and Hashimoto, 2009; Yasuda et al., 2011). Inactive inputs are eliminated only in the presence of other active ones (Fig. 3.1). The *'elimination'* signals Pyk2 and JAK2 are active at inactive synapses, but only in the presence neuronal activity (Fig. 3.7 and 3.11). These findings suggest the existence of a *'punishment'* signal from active synapses that drives the elimination of inactive ones (Fig. 1.2). The existence of a *'punishment'* signal has long been speculated at the NMJ (Lichtman and Colman, 2000). However, the identity and mechanism through which this signal functions have remained elusive.

To serve as a *'punishment'* signal, several criteria should be met. The *'punishment'* signal should: 1) be activated in the presence of neuronal activity; 2) signal intersynaptically, likely originating from active synapses and targeting inactive ones; 3) activate *'elimination'* signals; and 4) drive synaptic elimination. The *'punishment'* signal may be pre or postsynaptic in origin. The model I propose suggests that the *'punishment'* signal more likely to be postsynaptic in origin (Fig. 1.5) based on data suggesting that the suppression of postsynaptic neuronal activity impairs

presynaptic callosal axon development (Mizuno et al., 2010). Additionally, it is thought that coordinated pre and postsynaptic activity is necessary for synapse development (Katz and Shatz, 1996). In accordance with these criteria, several molecules, including the brain-derived neurotrophic factor (BDNF), Semaphorin and Arc, may serve as *'punishment'* signals.

The idea that BDNF and Semaphorin may act as a *'punishment'* signal comes from studies on synaptic refinement in the cerebellum. The retrograde signaling of BDNF and Sema7A from the postsynaptic Purkinje cell, drives presynaptic climbing fiber elimination during development. The Purkinje cell specific knockdown of BDNF or Sema7A impairs climbing fiber synapse elimination. A similar impairment occurs when the BDNF receptor, TrkB or the Sema7A receptor, PlxnC1 is knocked down in climbing fibers (Uesaka et al., 2014; Choo et al., 2017). Additionally, BDNF and Sema7A are expressed and regulated in an activity-dependent manner (Tao et al., 2002; Inoue et al., 2018).

Similar to BDNF and Sema7A, Arc signaling within the Purkinje cell is necessary for presynaptic climbing fiber elimination (Mikuni et al., 2013). However, plasticity studies in the cortex has increased the appeal of Arc as a candidate *'punishment'* signal. To maintain balance in the brain, the potentiation of one synapse may lead to the depression of neighboring synapses. Recent work has implicated Arc in this process. It is proposed that Arc, initially positioned near potentiated spines, will translocate to neighboring spines and weaken them (El-Boustani et al., 2018). In the context of developmental elimination, this suggests that Arc signaling could be activated at the more active synapse and then be translocated to inactive ones to *'punish'* inactive synapses.

These molecules offer a good starting point into identifying the *'punishment'* signal. To identify the *'punishment'* signal, I will perform an *in vitro* screen using Pyk2 activation as a readout. I have shown that Pyk2 is activated (detected by immunostaining for Phospho-Pyk2) in cultured neurons in an activity and competition-dependent manner (Fig. 3.7). The level of Pyk2 activation

in response to the application or overexpression of these candidate molecules and others would further aid in identifying the elusive *'punishment'* signal.

5.5 Functional importance of proper callosal and hippocampal refinement

Proper synaptic development is critical for proper brain function. In this thesis, I have focused on determining the molecular mechanisms regulating the refinement of hippocampal projections (Chapter 2) and callosal projections (Chapters 3 and 4). Using what we now know about the signals that regulate synaptic refinement, we can now ask – *how is the proper developmental refinement of hippocampal and callosal projections important for brain function?* We have already begun to address this question in this thesis via electrophysiology. We showed that impaired SIRPα phosphorylation and function in hippocampal neurons affects synaptic transmission (as shown by impaired mEPSCs; Fig 2.4). I also developed a fiber fraction method to functionally assess callosal refinement (Fig. 3.3). Using this method, I showed that aberrant callosal refinement, driven by impaired Pyk2, JAK2 and SIRPα signaling, resulted in electrophysiologically-detectable changes in callosal drive (Fig. 3.5, 3.6, 3.9, 4.1, and 4.3). However, how the improper refinement of callosal and hippocampal synapses affect brain function at a *behavioral level* are unknown.

Functionally, callosal projections are thought to allow information transfer between and coordinate the activity of the two cortical hemispheres (Suarez et al., 2014). Human patients and mouse models with impaired corpus callosum (agenesis of corpus callosum or changes in callosal size and organization) often demonstrate behavioral phenotypes associated with ASD. These include impaired social interaction and communication as well as repetitive behaviors (Silverman et al., 2010; Lau et al., 2013). Additionally, mice with impaired bilateral connectivity also exhibit defects in motor coordination and sensorimotor integration (Faraji et al., 2018; Dominguez-Iturza et al., 2019). Relative to the callosum, the role of hippocampal circuits in behavior is better characterized. Behaviors associated with the hippocampus include learning and memory, spatial

navigation, social behavior and emotional processing. Loss of Neuroligin-Neurexin, molecules implicated in the strengthening of hippocampal synapses, results in impaired spatial memory and increased repetitive behavior (Etherton et al., 2009; Blundell et al., 2010). Mice lacking the cytoplasmic region of SIRPα exhibit depression-like behavior in response to stress (Ohnishi et al., 2010). It is to be noted that in these studies, the mice used are often genetically manipulated in multiple cell types across different neurodevelopmental stages. Hence, the behavioral consequences of the activity-dependent refinement of callosal and hippocampal connections, specifically, are still unknown.

To determine how the impaired refinement of callosal and hippocampal circuits affect behavior, Pyk2, JAK2 or SIRPα would have to be disrupted in a cell type and temporal-specific manner. I plan to do so using the conditional KO mouse lines used in this thesis in combination with AAV or transgenic Cre lines. Various behaviors implicated in impaired callosal or hippocampal circuitry as well as ASD and schizophrenia, diseases associated with impaired synaptic refinement, can be evaluated in these mice. These include social interaction behaviors (three chamber sociability and social novelty test), learning and memory (Morris water maze and fear conditioning) as well as sensory and motor tests.

5.6 Conclusion

The brain is a remarkably dynamic organ that can learn from, adapt and react to the external environment to appropriately modify the behavior of the organism. As a result, the synaptic networks that make up the brain is complex. Despite the complexity, synaptic connections in the brain develop with a great deal of precision. Discovering how synapses develop in such a precise manner is important to both our fundamental understanding of the brain and its function as well as our ability to approach and design treatments for neuropsychiatric disorders. Of the different stages of synaptic development, synaptic refinement is interesting as it is regulated by both genetically encoded molecular signals (nature) as well as neuronal activity

and sensory experience (nurture). In that regard, the work in this thesis has uncovered the molecular signals that regulate synaptic refinement and characterized how neuronal activity regulates these molecules to appropriately refine synaptic connections. This work also offers insight into how different activity-dependent molecular signals may interact and coordinate with one another to ensure precise synaptic development. Together, this work established the molecular bridges that link neuronal activity to synaptic connectivity, thus, furthering our understanding of brain development and function.

5.7 Experimental procedures

Mouse strains

CD1 mice (Charles River), C57Bl/6, Emx1-Cre, and SOCS3$^{fl/fl}$ mice (Jackson) were used in this study. Both male and female mice were used. No differences have been detected between male and female mice. Mice were housed in OptiMICE cages (4–5 mice per cage) with a 12-h/12-h light/dark cycle. The housing room temperature was 22 ± 1 °C. Mice were allowed *ad libitum* access to food and water. All animal care and experiments were performed in accordance with the institutional guidelines and approved by the Institutional Animal Care and Use Committees at Boston Children's Hospital.

Plasmid constructs and *in utero* electroporation

As previously described in section 3.5.

Axon density analysis

For the analysis of corticostriatal axon density in the brains expressing EGFP in callosal neurons, 50 μm-thick frozen sections were cut and mounted on glass slides. Images including the corticostriatal projections were taken with a 4x lens on an Olympus BX63 epi-fluorescence microscope using cellSens Dimensions software to obtain unsaturated images. Focus was

adjusted to obtain the highest EGFP signal intensity in the electroporated hemisphere. Images were then analyzed with ImageJ software. To quantify the corticostriatal axon density, the total EGFP fluorescence intensity of a 200-μm length of corticostriatal axon bundle in the electroporated hemisphere was divided by the total value of the EGFP intensity in the cingulate cortex of the electroporated hemisphere.

Brain fixation

Mice were euthanized and perfused transcardially with PBS followed by 4% paraformaldehyde/PBS. Brains were removed and post-fixed with 4% paraformaldehyde/PBS for 16 hours. After cryoprotection in 30% sucrose/PBS, brains were frozen in OCT embedding compound.

Immunohistochemistry

Immunohistochemistry was performed as described (Yasuda et al., 2011). 16 μm coronal sections were cut on a cryostat. Sections were blocked in blocking buffer (2% BSA, 2% goat serum, 0.1% Triton X-100 in PBS and 1mM sodium orthovanadate) for 1 hour, followed by incubation with primary antibodies in blocking buffer at 4°C for 16 hours. Sections were washed 3 times in PBS, and secondary antibodies in blocking buffer were applied for 2 hours at RT. Antibodies and dilution used were: Phospho-JAK2 (Millipore, 1:200), Images were taken with sequential scanning using a confocal microscope (Zeiss LSM700; 40X objective). 16-bit images at a 1024 x 1024 pixel resolution were obtained. All images were acquired with identical acquisition settings which include laser power, gain and offset.

For Phospho-JAK2 density calculation (Fig. 5.2): Images were analyzed using FIJI. The number of Phospho-JAK2 positive puncta on EGFP-positive callosal and corticostriatal axons was calculated. The density of Phospho-JAK2 positive puncta was calculated by dividing the number of Phospho-JAK2 positive puncta on EGFP-positive axons with EGFP-positive axon area. The

images used to quantify Phospho-JAK2 staining on callosal and on corticostriatal axons were taken from the same coronal section.

For Sphy-mCherry analysis (Fig. 5.3): Images were analyzed using FIJI. The EGFP and mCherry intensity in uninfected cortical regions was calculated as the background signal and subtracted from each image. The number and size of Sphy-mCherry positive puncta on EGFP-positive axons was calculated. The density of Sphy-mCherry positive puncta was calculated by dividing the number of Sphy-mCherry positive puncta on EGFP-positive axons with EGFP-positive axon area.

Stereotaxic viral injection

P0.5–1 C57Bl/6, SOCS3$^{fl/fl}$ or Emx1-Cre; SOCS3$^{fl/fl}$ pups were anesthetized by hypothermia. 600 nl of viral solution was stereotactically injected (100 nL/min) into the left cortex using the following coordinates: 1.2 mm anterior from lambda, 0.4 mm lateral from midline, 0.4 mm ventral from the skull surface. Viruses injected were 1 x 10^{12} gc/ml AAV-EGFP (Fig. 5.2) or 1 x 10^{12} gc/ml AAV-EGFP and 1 x 10^{12} gc/ml AAV-Synaptophysin-mCherry (Fig. 5.3).

Statistical analysis

Statistical analyses were performed using GraphPad Prism software. Statistical test used was the Mann-Whitney test. All data are mean ± s.e.m. *P* values are indicated in the figures.

Appendix I.

Supplemental figures

Figure S1. Establishment of an *in utero* electroporation-based *in vivo* system to study activity-dependent synapse refinement, related to Figure 3.1.

(A) Schematic of co-electroporation. A mixed solution of EGFP and mCherry encoded plasmids (1:1) was injected into the left ventricle of E13.5 mouse embryos, and electrical pulses were applied (50-ms pulses of 40–43 V with 950-ms intervals, five times). At P10, coronal brain sections were prepared to examine the expression patterns of EGFP and mCherry.

(B) A representative confocal image from a coronal section of cingulate cortex from an electroporated brain (P10). EGFP and mCherry were almost always co-expressed in cingulate neurons (98.7 ±1.6%; n = 3 mice). Scale bar: 10 μm.

(C) After *in utero* electroporation of EGFP at E13.5, coronal sections were prepared at P10 and stained for the neuronal marker NeuN, the astrocytic marker GFAP, or the microglial marker Iba1. All EGFP-expressing cells were NeuN positive (and GFAP and Iba1 negative), indicating that the electroporated cells are neurons and not astrocytes or microglia. This data was reproduced in 3 independent experiments. Scale bar, 10 μm.

(D) To determine which cortical neurons were targeted by electroporation, an EGFP-expressing vector was electroporated, and then 20-μm coronal brain sections were prepared at P5 and stained for the callosal projection neuron marker SATB2 (red). 88.86 ± 4.6 % of EGFP expressing neurons were SATB2 positive (n = 364 cells from 5 mice). With our electroporation setting (see methods), 19.1 ± 1.0 % of callosal projecting neurons were EGFP positive (electroporated). Thus, our electroporation condition predominantly introduces genes into ~20% of the callosal projection neurons in layer V. Scale bar, 20 μm.

(E and F) Methods of axon density quantification in electroporated brains. To quantify the intensity of the callosal axon bundle, a box (200 μm in length) was placed adjacent to the midline, contralateral to the electroporated hemisphere (red box in E). The EGFP signal intensity was quantified from the boxed area using the plot profiling-menu in ImageJ to obtain an intensity profile plot (F). The background, measured from the areas without axons (above and below the axon bundles), was subtracted, and the area of the plot (shaded area) was quantified as the intensity of callosal axon bundles. To quantify the electroporation efficiency, the total EGFP intensity in the entire cingulate cortex (white-lined area in E) of the electroporated hemisphere was measured,

FIGURE S1 (Continued)

again using the plot profiling-menu in ImageJ. The axon density was then calculated by dividing the intensity of callosal axon bundles by the intensity of the electroporated cells. Scale bar in E, 200 μm.

(G and H) Suppression of neural activity using the DREADD system induces developmental callosal axon elimination. (G) Schematic of experiments. A hM4Di-expressing plasmid was co-electroporated with an EGFP-expressing plasmid by *in utero* electroporation at E13.5. From P3 to P15, electroporated pups were treated with CNO twice a day to suppress the activity of hM4Di expressing neurons. Brains were then collected from the CNO treated and untreated control mice at P15. (H) Example images of EGFP signals in the coronal sections from control- and CNO-treated hM4Di-electroporated brains at P15. Boxed areas are magnified in the bottom panels. The axon density in the CNO treated group was significantly decreased relative to the non-treated group (52.3 ± 4.9%; $P < 0.05$ by Student's *t*-test), indicating that suppressing activity with the DREADD system induces callosal axon elimination. n = 6 mice. Scale bars, 200 μm (upper), 50 μm (lower).

(I) Examination of cell death by TUNEL staining. EGFP, TTLC, SOCS3DN and JAK2WT electroporated cells were TUNEL-negative, indicating that the electroporation of these plasmids did not induce cell death. The positive control was a DNase 1-treated cortical section. These data were reproduced in 2 independent experiments. Scale bar, 10 μm.

FIGURE S1 (Continued)

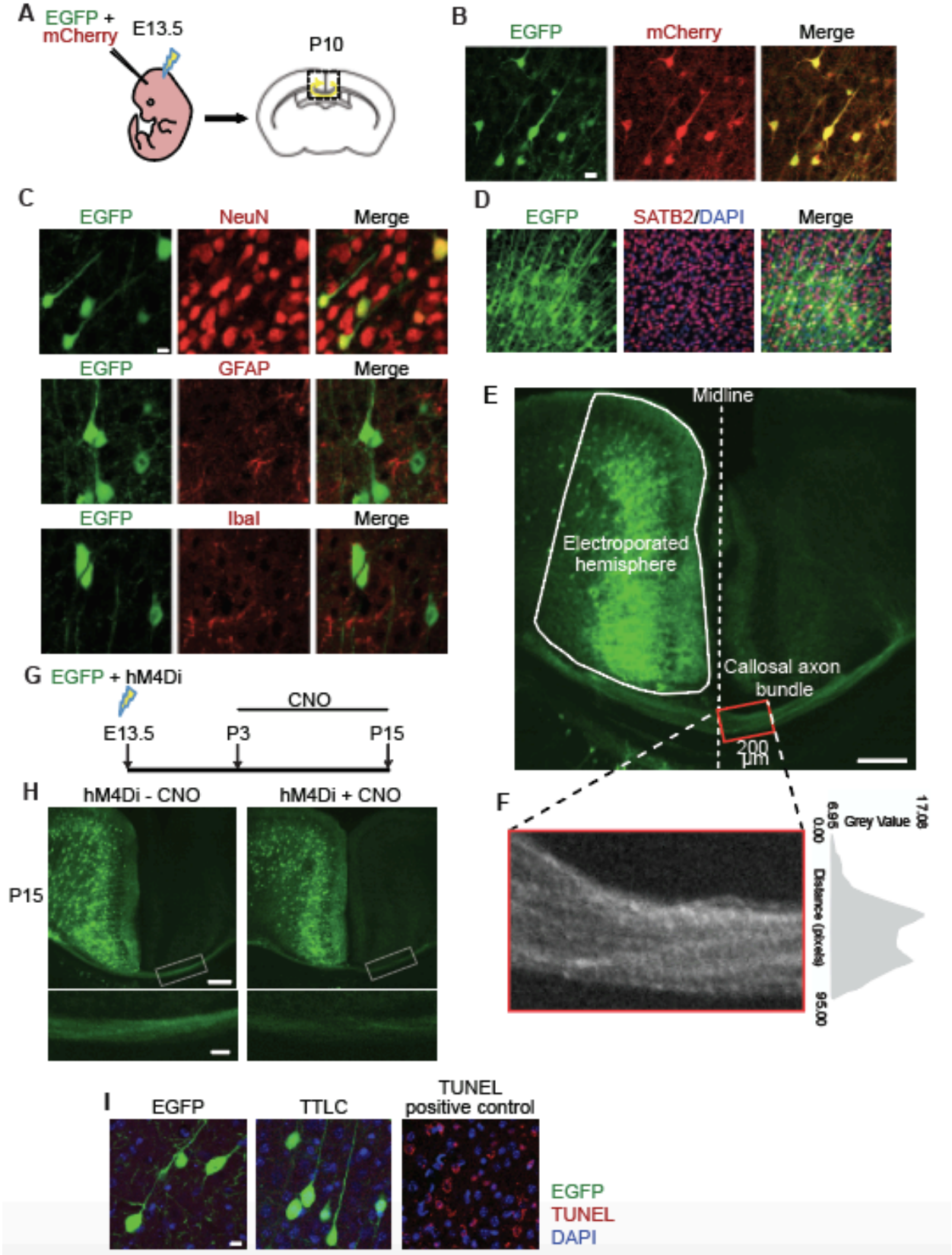

References

Alblas, J., Honing, H., de Lavalette, C.R., Brown, M.H., Dijkstra, C.D., and van den Berg, T.K. (2005) Signal regulatory protein α ligation induces macrophage nitric oxide production through JAK/STAT- and phosphatidylinositol 3-kinase/Rac1/NAPDH oxidase/H2O2-dependent pathways. *Mol. Cell Biol*. **25**. 7181-7192

Armbruster, B. N., Li, X., Pausch, M. H., Herlitze, S., Roth, B. L. (2007). Evolving the lock to fit the key to create a family of G protein-coupled receptors potently activated by an inert ligand. *Proc Natl Acad Sci U S A*. **104**, 5163-8

Atapattu, L., Saha, N., Llerena, C., Vail, M. E., Scott, A. M., Nikolov, D. B., Lackmann, M., and Janes, P. W. (2012) Antibodies binding the ADAM10 substrate recognition domain inhibit Eph function. *J. Cell Sci*. **125**, 6084–6093

Babon, J. J., Kershaw, N. J., Murphy, J. M., Varghese, L. N., Laktyushin, A., Young, S. N., Lucet, I. S., Norton, R. S., Nicola, N. A. (2012). Suppression of cytokine signaling by SOCS3: characterization of the mode of inhibition and the basis of its specificity. *Immunity*. **36**, 239–250

Bading, H., Greenberg, M. E. (1991). Stimulation of protein tyrosine phosphorylation by NMDA receptor activation. *Science.* **253**, 912-914

Bain, J., Plater, L., Elliott, M., Shpiro, N., Hastie, C.J., McLauchlan, H., Klevernic, I., Arthur, J.S., Alessi, D.R., Cohen, P. (2007) The selectivity of protein kinase inhibitors: a further update. *Biochem J*. **408**, 297-315

Barclay, A.N. and van den Berg, T.K. (2013) The interaction between signal regulatory protein alpha (SIRPα) and CD47: Structure, function and therapeutic target. *Annu. Rev. Immunol*. **32**. 25-50

Bartos, J. A., Ulrich, J. D., Li, H., Beazely, M. A., Chen, Y., MacDonald, J. F., Hell, J. W. (2010). Postsynaptic clustering and activation of Pyk2 by PSD-95. *J. Neurosci.* **30(2)**, 449-463.

Bemben, M.A., Shipman, S.L., Hirai, T., Herring, B.E., Li, Y., Badger, J.D., Nicoll, R.A., Diamond, J.S., and Roche, K.W. (2013) CaMKII phosphorylation of neuroligin-1 regulates excitatory synapses. *Nat. Neurosci*. **17**, 56-64

Bemben, M. A., Nguyen, T. A., Li, Y., Wang, T., Nicoll, R. A., Roche, K. W. (2019). Isoform-specific cleavage of neuroligin-3 reduces synapse strength. *Mol. Psych.* **24**, 145-160

Bian, Z., Shi, L., Guo, Y-L., Lv, Z., Tang, C., Niu, S., Tremblay, A., Venkataramani, M., Culpepper, C., Li, L., Zhou, Z., Mansour, A., Zhang, Y., Gewirtz, A., Kidder, K., Zen, K., and Liu, Y. (2016) CD47-Sirpα interaction and IL-10 constrain inflammation-induced macrophage phagocytosis of healthy self-cells. *Proc. Acad. Natl. Sci. USA*. E5434-E5443

Blundell, J., Blaiss, C. A., Etherton, M. R., Espinosa, F., Tabuchi, K., Walz, C., Bolliger, M. F., Sudhof, T. C., Powell, C. M. (2010). Neuroligin-1 deletion results in impaired spatial memory and increased repetitive behavior. *J. Neurosci.* **30**, 2115-2129

Browning, M. D., Huganir, R., and Greengard, P. (1985) Protein phosphorylation and neuronal

function. *J. Neurochem*. **45**, 11–23

Buffelli, M., Burgess, R. W., Feng, G., Lobe, C. G., Lichtman, J. W., Sanes, J. R. (2003). Genetic evidence that relative synaptic efficacy biases the outcome of synaptic competition. *Nature*. **424**, 430-434

Cheadle, L., Tzeng., C. P., Kalish, B. T., Harmin, D. A., Rivera, S., Ling, E., Nagy, M. A., Hrvatin, S., Hu, L., Stroud, H., Burkly, L. C., Chen, C., Greenberg, M. E. (2018). Visual experience-dependent expression of Fn14 is required for retinogeniculate refinement. *Neuron.* **99**, 525-539

Chia, P. H., Li, P., and Shen, K. (2013) Cellular and molecular mechanisms underlying presynapse formation. *J. Cell Biol*. **203**, 11–22

Chiba, T., Yamada, M., Sasabe, J., Terashita, K., Shimoda, M., Matsuoka, M., and Aiso, S. (2009) Amyloid-β causes memory impairment by disturbing the JAK2/STAT3 axis in hippocampal neurons. *Mol. Psychiatry*. **14**, 206–222

Choo, M., Miyazaki, T., Yamazaki, M., Kawamura, M., Nakazawa, T., Zhang, J., Tanimura, A., Uesaka, N., Watanabe, M., Sakimura, K., Kano, M. (2017). Retrograde BDNF to TrkB signaling promotes synapse elimination in the developing cerebellum. *Nat. Commun.* **8**:195

Chung, W-S., Clarke, L. E., Wang, G. X., Stafford, B. K., Sher, A., Chakraborty, C., Joung, J., Foo, L. C., Thompson, A., Chen, C., Smith, S. J., Barres, B. A. (2013). Astrocytes mediate synapse elimination through MEGF10 and MERTK pathways. *Nature*. **504**, 394-400

Conant, K., Wang, Y., Szklarczyk, A., Dudak, A., Mattson, M. P., Lim, S. T. (2010). Matrix metalloproteinase-dependent shedding of intercellular adhesion molecule-5 occurs with long-term potentiation. *Neuroscience*. **166**, 508-521

Costain, G., Lionel., A. C., Merico, D., Forsythe, P., Russell, K., Lowther, C., Yuen, T., Husted, J., Stavropoulos, D. J., Speevak, M., Chow, E. W. C., Marshall., C. R., Scherer, S. W., Bassett, A. S. (2013). Pathogenic rare copy number variants in community-based schizophrenia suggest a potential role for clinical microarrays. *Human Mol Genetics*. **22**, 4485-4501

Croker, B. A., Krebs, D. L., Zhang, J. -G., Wormald, S., Willson, T. A., Stanley, E. G., Robb, L., Greenhalgh, C. J., Förster, I., Clausen, B. E., Nicola, N. A., Metcalf, D., Hilton, D. J., Roberts, A. W., Alexander, W. S. (2003). SOCS3 negatively regulates IL-6 signaling in vivo. *Nat Immunol.* **4**, 540–545

Dabrowski, A., Terauchi, A., Strong, C., and Umemori, H. (2015) Distinct sets of FGF receptors sculpt excitatory and inhibitory synaptogenesis. *Development*. **142**, 1818–1830

Datwani, A., McConnell, M. J., Kanold, P. O., Micheva, K. D., Busse, B., Shamloo, M., Smith, S. J., Shatz, C. J. (2009). Classical MHC1 molecules regulate retinogeniculate refinement and limit ocular dominance plasticity. *Neuron*. **64**, 463-470

De-Fraja, C., Conti, L., Magrassi, L., Govoni, S., Cattaneo, E. (1998). Members of the JAK/STAT proteins are expressed and regulated during development in the mammalian forebrain. *J Neurosci Res.* **54**, 320-30

Di Liberto, G., Pantelyushin, S., Kreutzfeldt, M., Page, N., Musardo, S., Coras, R., Steinbach, K., Vincenti, I., Bogna, K., Linger, T., Salinas, G., Lin-Marq, N., Staszewski, O., Costa Jordão, M. J., Wagner, I., Egervari, K., Mack, M., Bellone, C., Blümcke, I., Prinz, M., Pinschewer, D. D., Merkler, D. (2018). Neurons under T cell attack coordinate phagocyte-mediated synaptic stripping. *Cell*. **175**, 1-14

Dikic, I., Tokiwa, G., Lev, S., Courtneidge, S. A., Schlessinger, J. (1996). A role for Pyk2 and Src in linking G-protein-coupled receptors with MAP kinase activation. *Nature*. **383**, 547-550.

Dominguez-Iturza, N., Lo, A. C., Shah, D., Armendariz, M., Vannelli, A., Mercaldo, V., Trusel, M., Li, K. W., Gastaldo, D., Santos, A. R., Callaerts-Vegh, Z., D'Hooge, R., Mameli, M., Van der Linden, A., Smit, A. B., Achsel, T., Bagni, C. (2019). The autism and schizophrenia associated protein CYFIP1 regulates bilateral brain connectivity and behavior. *Nat. Commun.* **10**, 3454

Dourlen, P., Fernandez-Gomez, F. J., Dupont, C., Grenier-Boley, B., Bellenguez, C., Obriot, H., Caillierez, R., Sottejeau, Y., Chapuis, J., Bretteville, A., Abdelfettah, F., Delay, C., Malmanche, N., Soininen, H., Hiltunen, M., Galas, M-C., Amouyel, P., Sergeant, N., Buee, L., Lambert, J-C., Dermaut, B. (2016). Functional screening of Alzheimer risk loci identifies *PTK2B* as an *in vivo* modulator and early marker of Tau pathology. *Mol. Psych.* **22**, 874-883

Echegoyen, J., Neu, A., Graber, K. D., Soltesz, I. (2007). Homeostatic plasticity studied using in vivo hippocampal activity-blockade: synaptic scaling, intrinsic plasticity and age-dependence. *PLoS One*. **2**, e700

El-Boustani, S., Ip, J. P. K., Breton-Provencher, V., Knott, G. W., Okuno, H., Bito, H., Sur, M. (2018). Locally coordinated synaptic plasticity of visual cortex neuron in vivo. *Science.* **360**, 1349-1354

Etherton, M. R., Blaiss, C. A., Powell, C. M., Sudhof, T. C. (2009). Mouse neurexin-1α causes correlated electrophysiological and behavioral changes consistent with cognitive impairments. *Proc. Natl. Acad. Sci. U S A*. **106**, 17998-18003

Fame, R. M., MacDonald, J. L., Macklis, J. D. (2011). Development, specification, and diversity of callosal projection neurons. *Trends Neurosci.* **34**, 41–50

Faraji, J., Karimi, M., Lawrence, C., Mohajerani, M. H., Metz, G. A. S. (2018). Non-diagnostic symptoms in a mouse model of autism in relation to neuroanatomy: the BTBR strain reinvestigated. *Translational Psych.* **8**, 234

Feng, J., Witthuhn, B. A., Matsuda, T., Kohlhuber, F., Kerr, I. M., Ihle, J. N. (1997). Activation of Jak2 catalytic activity requires phosphorylation of Y1007 in the kinase activation loop. *Mol Cell Biol.* **17**, 2497–2501

Fiala, J. C., Feinberg, M., Popov, V., Harris, K. M. (1998). Synaptogenesis via dendritic filopodia in developing hippocampal area CA1. *J. Neurosci.* **18(21)**, 8900-8911

Fox, M. A., and Umemori, H. (2006) Seeking long-term relationship: Axon and target communicate to organize synaptic differentiation. *J. Neurochem*. **97**, 1215–1231

Fujioka, Y., Matozaki, T., Noguchi, T., Iwamatsu, A., Yamao, T., Takahashi, N., Tsuda, M., Takada, T., and Kasuga, M. (1996) A novel membrane glycoprotein, SHPS-1, that binds the SH2-domain-containing protein tyrosine phosphatase SHP-2 in response to mitogens and cell adhesion. *Mol. Cell. Biol*. **16**, 6887–99

Galbaugh, T., Feeney, Y.B., and Clevenger, C.V. (2010) Prolactin receptor-integrin cross-talk mediated by SIRPα in breast cancer cells. *Mol. Cancer Res*. **8(10)**. 1413-1424

Godement, P., Salaün, J., Imbert, M. (1984). Prenatal and postnatal development of retinogeniculate and retinocollicular projections in the mouse. *J Comp Neurol.* **230**, 552-75.

Giralt., A., Brito, V., Chevy, Q., Simonnet, C., Otsu, Y., Cifuentes-Diaz, C., de Pins, B., Coura, R., Alberch, J., Gines, S., Poncer, J-C., Girault, J-A. (2017). Pyk2 modulates hippocampal excitatory synapses and contributes to cognitive deficits in a Huntington's disease model. *Nat. Commun.* 8:15592

Grigonis, A. M., Murphy, E. H. (1994). The effects of epileptic cortical activity on the development of callosal projections. *Dev Brain Res.* **77**, 251–255

Guilluy, C., Brégeon, J., Toumaniantz, G., Rolli-Derkinderen, M., Retailleau, K., Loufrani, L., Henrion, D., Scalbert, E., Bril, A., Torres, R. M., Offermanns, S., Pacaud, P., Loirand, G. (2010). The Rho exchange factor Arhgef1 mediates the effects of angiotensin II on vascular tone and blood pressure. *Nat Med.* **16**, 183–190

Gunner, G., Cheadle, L., Johnson, K., Ayata, P., Badimon, A., Mondo, E., Nagy, M. A., Liu, L., Bemiller, S. M., Kim, K-W., Lira, S. A., Lamb, B. T., Tapper, A. R., Ransohoff, R. M., Greenberg, M. E., Schaefer, A., Schafer, D. P. (2019). Sensory lesioning induces microglial synapse elimination via ADAM10 and fractalkine signaling. *Nat. Neurosci.* **22**, 1075-1088

Hamada, J., Okumura, N., Inagaki, M., Taniguchi, H., Nakahata, Y., Sano, S. I., and Nagai, K. (2004) Tyrosine phosphorylation of BIT on photic stimulation in the rat retina. *FEBS Lett*. **557**, 204–208.

Hashimoto, K., and Kano, M. (2013) Synapse elimination in the developing cerebellum. *Cell. Mol. Life Sci*. **70**, 4667–4680

Holm, C.K., Engman, S., Sulniute, R., Matozaki, T., Oldenborg, P-A., and Lundberg, P. (2016) Lack of SIRPα phosphorylation and concomitantly reduced SHP-2-PI3K-Akt2 signaling decrease osteoblast differentiation. *Biochem. Biophys. Res. Commun*. **478**. 268-273

Hong, Y. K., Park, S., Litvina, E. Y., Morales, J., Sanes, J. R., Chen, C. (2014). Refinement of the retinogeniculate synapse by bouton clustering. *Neuron*. **84**, 332-339

Hooks, B. M., Chen, C. (2006). Distinct roles for spontaneous and visual activity in remodeling of the retinogeniculate synapse. *Neuron*. **52**, 281-291

Hooks, B. M., Chen, C. (2008). Vision triggers an experience-dependent sensitive period at the retinogeniculate synapse. *J Neurosci*. **28**, 4807-17

Howell, B. W., Cooper, J. A. (1994). Csk suppression of Src involves movement of Csk to sites of Src activity. *Mol Cell Biol*. **14**, 5402-11

Hsin, H., Kim, M. J., Wang, C-F., Sheng, M. (2010). Proline-rich tyrosine kinase 2 regulates hippocampal long-term depression. *J. Neurosci.* **30(36)**, 11983-11993.

Hsu, W-L., Ma, Y-L., Hsieh, D-Y., Liu, Y-C., Lee, E. H. Y. (2014). STAT1 negatively regulates spatial memory formation and mediates the memory-impairing effect of Aβ. *Neuropsychopharmacology*. **39**, 746-758

Hubel, D. H., Wiesel, T. N. (1970). The period of susceptibility to the physiological effects of unilateral eye closure in kittens. *J. Physiol.* **206**, 419-436

Hubel, D. H., Wiesel, T. N., LeVay, S., Barlow, H. B., Gaze, R. M. (1977). Plasticity of ocular dominance columns in monkey striate cortex. *Philos. Trans. R. Soc. Lond. B. Biol. Sci.* **278**, 377-409

Huttenlocher, P. R. (1979). Synaptic density in human frontal cortex – developmental changes and effects of aging. *Brain Res*. **163**, 195-205

Ichikawa, R., Hashimoto, K., Miyazaki, T., Uchigashima, M., Yamasaki, M., Aiba, A., Kano, M., Watanabe, M. (2016). Territories of heterologous inputs onto Purkinje cell dendrites are segregated by mGluR1-dependent parallel fiber synapse elimination. *Proc. Natl. Acad. Sci. U S A.* **113**, 2282-7

Innocenti, G. M., Ansermet, F., Parnas, J. (2003). Schizophrenia, neurodevelopment and corpus callosum. *Mol Psychiatry*. **8**, 261–274

Inoue, N., Nishizumi, H., Naritsuka, H., Kiyonari, H., Sakano, H. (2018). Sema7A/PlxnC1 signaling triggers activity-dependent olfactory synapse formation. *Nat. Commun.* **9**, 1842

Janes, P. W., Saha, N., Barton, W. A., Kolev, M. V., Wimmer-Kleikamp, S. H., Nievergall, E., Blobel, C. P., Himanen, J. P., Lackmann, M., and Nikolov, D. B. (2005) Adam meets Eph: An ADAM substrate recognition module acts as a molecular switch for ephrin cleavage in trans. *Cell*. **123**, 291–304

Johnson, E. M., Craig, E. T., Yeh, H. H. (2007). TrkB is necessary for pruning at the climbing fibre-Purkinje cell synapse in the developing murine cerebellum. *J. Physiol.* **582**, 629-46

Johnson-Venkatesh, E. M., and Umemori, H. (2010) Secreted factors as synaptic organizers. Eur. *J. Neurosci*. **32**, 181–190

Kakegawa, W., Mitakidis, N., Miura, E., Abe, M., Matsuda, K., Takeo, Y. H., Kohda, K., Motohashi, J., Takahashi, A., Nagao, S., Muramatsu, S., Watanabe, M., Sakimura, K., Aricescu, A. R., Yuzaki, M. (2015). Anterograde C1ql1 signaling is required in order to determine and maintain a single-winner climbing fiber in the mouse cerebellum. *Neuron*. **85**. 316-29

Kano, M., Hashimoto, K., Chen, C., Abeliovich, A., Aiba, A., Kurihara, H., Watanabe, M., Inoue, Y., Tonegawa, S. (1995). Impaired synapse elimination during cerebellar development in PKCγ mutant mice. *Cell*. **83**, 1223-1231

Kano, M., Hashimoto, K., Watanabe, M., Kurihara, H., Offermanns, S., Jiang, H., Wu, Y., Jun K., Shin, H-S., Inoue, Y., Simon, M. I., Wu, D. (1998). Phospholipase Cβ4 is specifically involved in climbing fiber synapse elimination in the developing cerebellum. *Proc. Natl. Acad. Sci. U S A.* **95**, 15724-15729

Kano, M., Hashimoto, K. (2009). Synapse elimination in the central nervous system. *Curr Opin Neurobiol*. **19**, 154-161

Kano, M., Nakayama, H., Hashimoto, K., Kitamura, K., Sakimura, K., Watanabe, M. (2013). Calcium-dependent regulation of climbing fibre synapse elimination during postnatal cerebellar development. *J. Phyiol.* 3151-3158

Kasai, H., Fukuda, M., Watanabe, S., Hayashi-Takagi, A., and Noguchi, J. (2010) Structural dynamics of dendritic spines in memory and cognition. *Trends Neurosci*. **33**, 121–129

Katz, L. C. and Shatz, C. J. (1996) Synaptic activity and the construction of cortical circuits. *Science*. **274**, 1133

Keil, E., Finkenstädt, D., Wufka, C., Trilling, M., Liebfried, P., Strobl, B., Müller, M., Pfeffer, K. (2014). Important scaffold function of the Janus kinase 2 uncovered by a novel mouse model harboring a Jak2 activation-loop mutation. *Blood*. **123**, 520–529

Kim, E. J., Juavinett, A. L., Kyubwa, E. M., Jacobs, M. W., Callaway, E. M. (2015). Three types of cortical layer 5 neurons that differ in brain-wide connectivity and function. *Neuron*. **88**, 1253-1267

Kim, J., Lilliehook, C., Dudak, A., Prox, J., Saftig, P., Federoff, H. J., and Lim, S. T. (2010) Activity-dependent α-cleavage of nectin-1 is mediated by a disintegrin and metalloprotease 10 (ADAM10). *J. Biol. Chem*. **285**, 22919–22926

Kharitonenkov, A, Chen, Z., Sures, I., Wang, H., Schilling, J., and Ullrich, A. (1997) A family of proteins that inhibit signalling through tyrosine kinase receptors. *Nature*. **386**, 181–186

Ko, J., Soler-Llavina, G. J., Fuccillo, M. V., Malenka, R. C., Sudhof, T. C. (2011). Neuroligins/LRRTMs prevent activity- and Ca2+/calmodulin-dependent synapse elimination in cultured neurons. *J. Cell. Biol.* **194**, 323-334.

Kohno, T., Matsuda, E., Sasaki, H., Sasaki, T. (2008). Protein-tyrosine kinase CAKβ/Pyk2 is activated by binding Ca^{2+}/calmodulin to FERM F2 α2 helix and thus forming its dimer. *Biochem. J.* **410**, 513-523

Kralovics, R., Passamonti, F., Buser, A.S., Teo, SS., Tiedt, R., Passweg, J.R., Tichelli, A., Cazzola, M., and Skoda, R.C. (2005) A gain-of-function mutation of JAK2 in myeloproliferative disorders. *N. Engl. J. Med*. **352**, 1779–1790

Kumar, S. S., Huguenard, J. R. (2001). Properties of excitatory synaptic connections mediated by the corpus callosum in the developing rat neocortex. *J Neurophysiol*. **86**, 2973-85

Lambert, J., Ibrahim-Verbaasm C., Harold, D., et al. (2013). Meta-analysis of 74,046 individuals identifies 11 new susceptibility loci for Alzheimer's disease. *Nat. Genet.* **45,** 1452-1458

Le, D. A., Wu, Y., Huang, Z., Matsushita, K., Plesnila, N., Augustinack, J. C., Hyman, B. T., Yuan, J., Kuida, K., Flavell, R. A., Moskowitz, M. A. (2002). Caspase activation and neuroprotection in caspase-3-deficient mice after in vivo cerebral ischemia and in vitro oxygen glucose deprivation. *Proc Natl Acad Sci U S A*. **99**, 15188-93

Lee, H., Brott, B. K., Kirkby, L. A., Adelson, J. D., Cheng, S., Feller, M. B., Datwani, A., Shatz, C. J. (2014). Synapse elimination and learning rules co-regulated by MHC class I H2-Db. *Nature*. **509**, 195–200

Lee, S., Salazar, S. V., Cox, T. O., Strittmatter, S. M. (2019). Pyk2 signaling through Graf1 and RhoA GTPase is required for amyloid-β oligomer triggered synapse loss. *J. Neurosci.* **39**, 1910-1929

Lehrman, E. K., Wilton, D. K., Litvina, E. Y., Welsh, C. A., Chang, S. T., Frouin, A., Walker, A. J., Heller, M. D., Umemori, H., Chen, C., Stevens, B. (2018). CD47 protects synapses from excess microglia-mediated pruning during development. *Neuron*. **100**, 120-134.

Lev, S., Moreno, H., Martinez, R., Canoll, P., Peles, E., Musacchio, J. M., Plowman, G. D., Rudy, B., Schlessinger, J. (1995). Protein tyrosine kinase Pyk2 involved in Ca^{2+}-induced regulation of ion channel and MAP kinase functions. *Nature.* **376**, 737-745

Lau, Y. C., Hinkley, L. B. N., Bukshpun, P., Strominger, Z. A., Wakahiro, M. L. J., Baron-Cohen, S., Allison, C., Auyeung, B., Jeremy, R. J., Nagarajan, S. S., Sherr, E. H., Marco, E. J. (2013). Autism traits in individuals with agenesis of the corpus callosum. *J. Autism Dev. Disord.* **43**, 1106-18

Li, Z., Sheng, M. (2003). Some assembly required: the development of neuronal synapses. *Nat. Rev. Mol. Cell Biol.* **4**, 833-841

Lichtman, J.W., Colman, H. (2000). Synapse elimination and indelible memory. *Neuron*. **25**, 269-278

Lipska, B. K., Halim, N. D., Segal, P. N. and Weinberger, D. R. (2002) Effects of reversible inactivation of the neonatal ventral hippocampus on behavior in the adult rat. *J. Neurosci*. **22**, 2835–42.

Liu, K., Tedeschi, A., Park, K. K., He, Z. (2011). Neuronal intrinsic mechanisms of axon regeneration. *Annu Rev Neurosci.* **34**, 131–152.

Liu, S.Q., Alkema, P.K., Tieche, C., Tefft, B.J., Liu, D.Z., Li, Y.C., Sumpio, B.E., Caprini, J.A., and Paniagua, M. (2005) Negative regulation of monocyte adhesion to arterial elastic laminae by signal regulatory protein α and src homology 2 domain-containing protein-tyrosine phosphatase-1. *J. Biol. Chem*. **280**. 39294-39301

Lois, C., Hong, E. J., Pease, S., Brown, E. J., Baltimore, D. (2002) Germline transmission and tissue-specific expression of transgenes delivered by lentiviral vectors. *Science*. **295**, 868-72

Londino, J. D., Gulick, D., Isenberg, J. S., and Mallampalli, R. K. (2015) Cleavage of signal regulatory protein α (SIRPα) enhances inflammatory signaling. *J. Biol. Chem*. **290**, 31113–31125

Louros, S. R., Hooks, B. M., Litvina, L., Carvalho, A. L., Chen, C. (2014). A role for stargazing in experience-dependent plasticity. *Cell Reports*. **7**, 1614-1625

Lu, Y. M., Roder, J. C., Davidow, J., and Salter, M. W. (1998) Src activation in the induction of longterm potentiation in CA1 hippocampal neurons. *Science*. **279**, 1363-1367

Luo, L. (2002). Actin cytoskeleton regulation in neuronal morphogenesis and structural plasticity. *Annu. Rev. Cell. Dev. Biol.* **18**, 601-35

Maness, P. F. (1992). Nonreceptor protein tyrosine kinases associated with neuronal development. *Dev Neurosci.* **14**, 257–70

Maruyama, T., Kusakari, S., Sato-Hashimoto, M., Hayashi, Y., Kotani, T., Murata, Y., Okazawa, H., Oldenborg, P. A., Kishi, S., Matozaki, T., and Ohnishi, H. (2012) Hypothermia-induced tyrosine phosphorylation of SIRPα in the brain. *J. Neurochem*. **121**, 891–902

Matsuda, T., Cepko, C. L. (2007). Controlled expression of transgenes introduced by in vivo electroporation. *Proc Natl Acad Sci U S A*. **104**, 1027-32

Matsuno, H., Okabe, S., Mishina, M., Yanagida, T., Mori, K., Yoshihara, Y. (2006). Telencephalin slows spine maturation. *J. Neurosci.* **26(6)**, 1776-1786

Meyer, F., Louilot, A. (2012) Early prefrontal functional blockade in rats results in schizophrenia-related anomalies in behavior and dopamine. *Neuropsychopharmacology*. **37**, 2233-43

Michaluk, P., Wawrzyniak, M., Alot, P., Szczot, M., Wyrembek, P., Mercik, K., Medvedev, N., Wikczek, E., De Roo, M., Zuschratter, W., Muller, D., Wilczynski, G. M., Mozrzymas, J. W., Stewart, M. G., Kaczmarek, L., Wlodarczyk, J. (2011). Influence of matrix metalloproteinase MMP-9 on dendritic spine morphology. *J. Cell. Sci.* **124**, 3369-3380

Mikuni, T., Uesaka, N., Okuno, H., Hirai, H., Deisseroth, K., Bito, H., Kano, M. (2013). Arc/Arg3.1 is a postsynaptic mediator of activity-dependent synapse elimination in the developing cerebellum. *Neuron*. **78**, 1024-1035

Mizuno, H., Hirano, T., Tagawa, Y. (2007). Evidence for activity-dependent cortical wiring: formation of interhemispheric connections in neonatal mouse visual cortex requires projection neuron activity. *J Neurosci*. **27**, 6760–6770

Mizuno, H., Hirano, T., Tagawa, Y. (2010) Pre-synaptic and post-synaptic neuronal activity supports the axon development of callosal projection neurons during different post-natal periods in the mouse cerebral cortex. *Eur. J. Neurosci.* **31**, 410-424

Motegi, S., Okazawa, H., Ohnishi, H., Sato, R., Kaneko, Y., Kobayashi, H., Tomizawa, K., Ito, T.,

Honma, N., Buhring, H-J., Ishikawa, O., and Matozaki, T. (2003) Role of the CD47-SHPS-1 system in regulation of cell migration. *EMBO J*. **22**. 2634-2644

Murata, S., Usuda, N., Okano, A., Kobayashi, S., Suzuki, T. (2000). Occurrence of a transcription factor, signal transducer and activators of transcription 3 (Stat3), in the postsynaptic density of the rat brain. *Brain Res. Mol. Brain. Res.* **78**, 80-90

Murphy, J. M., Jeong, K., Rodriguez, Y. A. R., Kim, J-H., Ahn, E-Y. E., Lim, S-T. S. (2019). FAK and Pyk2 activity promote TNF-α and IL-1β-mediated pro-inflammatory gene expression and vascular inflammation. *Sci. Rep.* **20**, 7617

Nagappan-Chettiar, S., Johnson-Venkatesh, E. M., and Umemori, H. (2017) Activity-dependent proteolytic cleavage of cell adhesion molecules regulates excitatory synaptic development and function. *Neurosci. Res*. **116**, 60–69

Nagappan-Chettiar, S., Johnson-Venkatesh, E. M., and Umemori, H. (2018). Tyrosine phosphorylation of the transmembrane protein SIRPα: Sensing synaptic activity and regulating ectodomain cleavage for synapse maturation. *J. Biol. Chem.* **293**, 12026-12042

Nagy, V., Bozdagi, O., Matynia, A., Balcerzyk, M., Okulski, P., Dzwonek, J., Costa, R. M., Silva, A. J., Kaczamarek, L., Huntley, G. W. (2006). Matrix metalloproteinase-9 is required for hippocampal late-phase long-term potentiation and memory. *J. Neurosci*. **26(7)**, 1923-1934

Nakahata, Y., Okumura, N., Shima, T., Okada, M., and Nagai, K. (2000) Light-induced tyrosine phosphorylation of BIT in the rat suprachiasmatic nucleus. *J. Neurochem*. **74**, 2436–2444

Narushima, M., Uchigashima, M., Yagasaki, Y., Harada, T., Nagumo, Y., Uesaka, N., Hashimoto, K., Aiba, A., Watanabe, M., Miyata, M., Kano, M. (2016). The metabotropic glutamate receptor subtype 1 mediates experience-dependent maintenance of mature synaptic connectivity in the visual thalamus. *Neuron*. **91**, 1097-1109

Neznanov, N., Neznanova, L., Kondratov, R.V., Burdelya, L., Kandel, E.S., O'Rourke, D.M., Ullrich, A., and Gudkov, A.V. (2003) Dominant negative form of signal-regulatory protein-α (SIRPα/SHPS-1) inhibits tumor necrosis factor-mediated apoptosis by activation of NF-κB. *J. Biol. Chem*. **278**. 3809-3815

Nicolas, C. S., Peineau, S., Amici, M., Csaba, Z., Fafouri, A., Javalet, C., Collett, V. J., Hildebrandt, L., Seaton, G., Choi, S. L., Sim, S. E., Bradley, C., Lee, K., Zhuo, M., Kaang, B. K., Gressens, P., Dournaud, P., Fitzjohn, S. M., Bortolotto, Z. A., Cho, K., and Collingridge, G. L. (2012) The JAK/STAT pathway is involved in synaptic plasticity. *Neuron*. **73**, 374–390

Niimura, M., Moussa, R., Bissoon, N., Ikeda-Douglas, C., Milgram, N. W., and Gurd, J. W. (2005) Changes in phosphorylation of the NMDA receptor in the rat hippocampus induced by status epilepticus. *J. Neurochem*. **92**, 1377–1385

Noutel, J., Hong, Y. K., Leu, B., Kang, E., Chen, C. (2011). Experience-dependent retinogeniculate synapse remodeling is abnormal in MeCP2-deficient mice. *Neuron*. **70**, 35-42

Ohnishi, H., Murata, T., Kusakari, S., Hayashi, Y., Takao, K., Maruyama, T., Ago, Y., Koda, K., Jin, F.-J., Okawa, K., Oldenborg, P.-A., Okazawa, H., Murata, Y., Furuya, N., Matsuda, T., Miyakawa, T., and Matozaki, T. (2010) Stress-evoked tyrosine phosphorylation of signal regulatory protein regulates behavioral immobility in the forced swim test. *J. Neurosci*. **30**, 10472–10483

Paul, L. K., Brown, W. S., Adolphs, R., Tyszka, J. M., Richards, L. J., Mukherjee, P., Sherr, E. H. (2007). Agenesis of the corpus callosum: genetic, developmental and functional aspects of connectivity. *Nat Rev Neurosci.* **8**, 287–299

Peixoto, R. T., Kunz, P. A., Kwon, H., Mabb, A. M., Sabatini, B. L., Philpot, B. D., and Ehlers, M. D. (2012) Transsynaptic signaling by activity-dependent cleavage of Neuroligin-1. *Neuron*. **76**, 396–409

Penn, A. A., Riquelme, P. A., Feller, M. B., Shatz, C. J. (1998) Competition in retinogeniculate patterning driven by spontaneous activity. *Science*. **279**, 2108-2112

Penzes, P., Buonanno, A., Passafaro, M., Sala, C., and Sweet, R. A. (2013) Developmental vulnerability of synapses and circuits associated with neuropsychiatric disorders. *J. Neurochem*. **126**, 165–182

Pietrasanta, M., Restani, L., Cerri, C., Olcese, U., Medini, P., Caleo, M. (2014). A switch from inter-ocular to inter-hemispheric suppression following monocular deprivation in the rat visual cortex. *Eur J Neurosci.* **40**, 2283–2292

Polizzotto, M. N., Bartlett, P. F., Turnley, A. M. (2000). Expression of "suppressor of cytokine signaling" (SOCS) genes in the developing and adult mouse nervous system. *J Comp Neurol*. **423**, 348–358

Reiss, K., Maretzky, T., Ludwig, A., Tousseyn, T., De Strooper, B., Hartmann, D., and Saftig, P. (2005) ADAM10 cleavage of N-cadherin and regulation of cell-cell adhesion and β-catenin nuclear signalling. *EMBO J*. **24**, 742–752

Rogers, N. M., Sharifi-Sanjani, M., Csanyi, G., Pagano, P. J., Isenberg, J. S. (2014). Thrombospondin-1 and CD47 regulation of cardiac, pulmonary and vascular responses in health and disease. *Matrix Biol.* **37**, 92-101

Saito, T., Nakatsuji, N. (2001). Efficient gene transfer into the embryonic mouse brain using in vivo electroporation. *Dev Biol*. **240**, 237–246

Saito, T. (2006). In vivo electroporation in the embryonic mouse central nervous system. *Nat Protoc*. **1**, 1552-1558

Salazar, S. V., Cox, T. O., Lee, S., Brody, A. H., Chyung, A. S., Haas, L. T., Strittmatter, S. M. (2019). Alzheimer's disease risk factor Pyk2 mediates amyloid-β-induced synaptic dysfunction and loss. *J. Neurosci.* **39(4)**, 758-772

Sanes, J.R. and Lichtman, J.W. (1999) Development of the vertebrate neuromuscular junction. *Annu. Rev. of Neurosci*. **22**, 389–442

Santini, E., Huynh, T. N., MacAskill, A. F., Carter, A. G., Pierre, P., Ruggero, D., Kaphzan, H., and Klann, E. (2013) Exaggerated translation causes synaptic and behavioural aberrations associated with autism. *Nature*. **493**, 411–415

Sasaki, A., Yasukawa, H., Suzuki, A., Kamizono, S., Syoda, T., Kinjyo, I., Sasaki, M., Johnston, J. A., Yoshimura, A. (1999). Cytokine-inducible SH2 protein-3 (CIS3/SOCS3) inhibits Janus tyrosine kinase by binding through the N-terminal kinase inhibitory region as well as SH2 domain. *Genes to Cells*. **4**, 339–351

Schafer, D. P., Lehrman, E. K., Kautzman, A. G., Koyama, R., Mardinly, A. R., Yamasaki, R., Ransohoff, R. M., Greenberg, M. E., Barres, B. A., Stevens, B. (2012). Microglia sculpt postnatal neural circuits in an activity and complement-dependent manner. *Neuron*. **74**, 691-705

Schafer, D. P., Stevens, B. (2015). Microglia function in central nervous system development and plasticity. *Cold Spring Harb. Perspect. Biol.* **7**:a020545

Scott-Hewitt, N., Perrucci, F., Morini, R., Erreni, R., Mahoney, M., Witkowska, A., Carey, A., Faggiani, E., Schuetz, L. T., Mason, S., Tamborini, M., Bizzotto, M., Passoni, L., Filipello, F., Jahn, R., Stevens, B., Matteoli, M. (2020). Local externalization of phosphatidylserine mediates developmental synaptic pruning by microglia. *EMBO. J.* e105380

Sekar, A., Bialas, A. R., De Rivera, H., Davis, A., Hammond, T. R., Kamitaki, N., Tooley, K., Presumey, J., Baum, M., Van Doren, V., Genovese, G., Rose, S. A., Handsaker, R. E., Daly, M. J., Carroll, M. C., Stevens, B., and McCarroll, S. A. (2016) Schizophrenia risk from complex variation of complement component 4. *Nature*. **530**, 177–183

Sellgren, C. M., Gracias, J., Watmuff, B., Biag., J.D., Thanos, J. M., Whittredge, P. B., Fu, T., Worringer, K., Brown, H. E., Wang, J., Kaykas,, A., Karmacharya, R., Goold, C. P., Sheridan, S. D., Perlis, R. H. (2019). Increased synapse elimination by microglia in schizophrenia patient-derived models of synaptic pruning. *Nat. Neurosci.* **22(3)**, 374-385

Shen K, Scheiffele P. (2010) Genetics and cell biology of building specific synaptic connectivity. *Annu. Rev. of Neurosci*. **33**, 473–507

Shimoda, K., Feng, J., Murakami, H., Nagata, S., Watling, D., Rogers, N. C., Stark, G. R., Kerr, I. M., Ihle, J. N. (1997). Jak1 plays an essential role for receptor phosphorylation and Stat activation in response to granulocyte colony-stimulating factor. *Blood*. **90**, 597-604

Shuai, K., Liu, B. (2003). Regulation of JAK-STAT signalling in the immune system. *Nat Rev Immunol*. **3**, 900–911

Siddiqui, T. J., and Craig, A. M. (2011) Synaptic organizing complexes. *Curr. Opin. Neurobiol*. **21**, 132–143

Silverman, J. L., Yang, M., Lord, C., Crawley J. N. (2010) Behavioral phenotyping assays for mouse models of autism. *Nat. Rev. Neurosci.* **11**, 490-502

Smith R.E., Patel, V., Seatter, S.D., Deehan, M.R., Brown, M.H., Brooke, G.P., Goodridge, H.S.,

Howard, C.J., Rigley, K.P., Harnett, W., and Harnett, M.M. (2003) A novel MyD-1 (SIRP-1α) signaling pathway that inhibits LPS-induced TNFα production by monocytes. *Blood*. **102**. 2532-2540

Sonderegger, P., Matsumoto-Miyai, K. (2014). Activity-controlled proteolytic cleavage at the synapse. *Trends Neurosci.* **38(8)**, 413-423

Sretavan, D. W., Shatz, C. J. (1986). Prenatal development of cat retinogeniculate axon arbors in the absence of binocular interactions. *J Neurosci*. **6**, 990-1003

Stevens, B., Allen, N. J., Vazquez, L. E., Howell, G. R., Christopherson, K. S., Nouri, N., Micheva, K. D., Mehalow, A. K., Huberman, A. D., Stafford, B., Sher, A., Litke, A. M., Lambris, J. D., Smith, S. J., John, S. W. M., Barres, B. A. (2007). The classical complement cascade mediates CNS synapse elimination. *Cell*. **131**, 1164-1178

Stofega, M. R., Wang, H., Ullrich, A., and Carter-Su, C. (1998) Growth hormone regulation of SIRP and SHP-2 tyrosyl phosphorylation and association. *J. Biol. Chem*. **273**, 7112–7117

Stofega, M.R., Argetsinger, L.S., Wang, H., Ullrich, A., and Carter-Su, C. (2000) Negative regulation of growth hormone receptor/JAK2 signaling by signal regulatory protein alpha. *J. Biol. Chem*. **275**, 28222-28229

Suarez, R., Fenlon, L. R., Marek, R., Avitan, L., Sah, P., Goodhill, G. J., Richards, L. J. (2014). Balanced interhemispheric cortical activity is required for correct targeting of the corpus callosum. *Neuron.* **82**, 1289-1298

Suzuki, K., Hayashi, Y., Nakahara, S., Kumazaki, H., Prox, J., Horiuchi, K., Zeng, M., Tanimura, S., Nishiyama, Y., Osawa, S., Sehara-Fujisawa, A., Saftig, P., Yokoshima, S., Fukuyama, T., Matsuki, N., Koyama, R., Tomita, T., and Iwatsubo, T. (2012) Activity-dependent proteolytic cleavage of Neuroligin-1. *Neuron*. **76**, 410–422

Takada, T., Matozaki, T., Takeda, H., Fukunaga, K., Noguchi, T., Fujioka, Y., Okazaki, I., Tsuda, M., Yamao, T., Ochi, F., and Kasuga, M. (1998) Roles of the complex formation of SHPS-1 with SHP-2 in insulin-stimulated mitogen-activated protein kinase activation. *J. Biol. Chem*. **273**, 9234-9242

Takaoka, A., Tanaka, N., Mitani, Y., Miyazaki, T., Fujii, H., Sato, M., Kovarik, P., Decker, T., Schlessinger, J., Taniguchi, T. (1999). Protein tyrosine kinase Pyk2 mediates JAK-dependent activation of MAPK and Stat1 in IFN-γ, but not IFN-α, signaling. *EMBO J.* **18**, 2480-2488

Takeuchi, S., Katoh, H., Negishi, M. (2015). Eph/ephrin reverse signaling induces axonal retraction through RhoA/ROCK pathway. *J. Biochem.* **158**, 245-252

Tang, G., Gudsnuk, K., Kuo, S. H., Cotrina, M. L., Rosoklija, G., Sosunov, A., Sonders, M. S., Kanter, E., Castagna, C., Yamamoto, A., Yue, Z., Arancio, O., Peterson, B. S., Champagne, F., Dwork, A. J., Goldman, J., and Sulzer, D. (2014) Loss of mTOR-dependent macroautophagy causes autistic-like synaptic pruning deficits. *Neuron*. **83**, 1131–1143

Tao, X., West, A. E., Chen, W. G., Corfas, G., Greenberg, M. E. (2002). A calcium-responsive transcription factor, CaRF, that regulates neuronal activity-dependent expression of BDNF. *Neuron*. **33**, 383-395

Terauchi, A., Johnson-Venkatesh, E.M., Bullock, B., Lehtinen, M., Umemori, H. (2016) Retrograde fibroblast growth factor 22 (FGF22) signaling regulates insulin-like growth factor 2 (IGF2) expression for activity-dependent synapse stabilization in the mammalian brain. *eLife*. **5**, e12151

Terauchi, A., Johnson-Venkatesh, E. M., Toth, A. B., Javed, D., Sutton, M. A., and Umemori, H. (2010) Distinct FGFs promote differentiation of excitatory and inhibitory synapses. *Nature*. **465**, 783–787

Terauchi, A., Timmons, K. M., Kikuma, K., Pechmann, Y., Kneussel, M., and Umemori, H. (2015) Selective synaptic targeting of the excitatory and inhibitory presynaptic organizers FGF22 and FGF7. *J. Cell Sci*. **128**, 281–292

Tezuka, T., Umemori, H., Akiyama, T., Nakanishi, S., Yamamoto, T. (1999). PSD-95 promotes Fyn-mediated tyrosine phosphorylation of the N-methyl-D-aspartate receptor subunity NR2A. *Proc Natl Acad Sci U S A*. **96**, 435-40

Timms, J. F., Carlberg, K., Gu, H., Chen, H., Kamatkar, S., Nadler, M. J. S., Rohrschneider, L. R., and Neel, B. G. (1998) Identification of major binding proteins and substrates for the SH2-containing protein tyrosine phosphatase SHP-1 in macrophages. *Mol. Cell. Biol.* **18**, 3838–3850

Toth, A. B., Terauchi, A., Zhang, L. Y., Johnson-Venkatesh, E. M., Larsen, D. J., Sutton, M. A., and Umemori, H. (2013) Synapse maturation by activity-dependent ectodomain shedding of SIRPα. *Nat. Neurosci*. **16**, 1417–1425

Uesaka, N., Uchigashima, M., Mikuni, T., Nakazawa, T., Nakao, H., Hirai, H., Aiba, A., Watanabe, M., Kano, M. (2014). Retrograde semaphorin signaling regulates synapse elimination in the developing mouse brain. *Science*. **344**, 1020-1023

Umemori, H., Hayashi, T., Inoue, T., Nakanishi, S., Mikoshiba, K., and Yamamoto, T. (1999) Involvement of protein tyrosine phosphatases in activation of the trimeric G protein Gq/11. *Oncogene.* **18**, 7399–402

Umemori, H., and Sanes, J. R. (2008) Signal regulatory proteins (SIRPS) are secreted presynaptic organizing molecules. *J. Biol. Chem*. **283**, 34053–34061

Ungureanu, D., Saharinen, P., Junttila, I., Hilton, D. J., Silvennoinen, O. (2002). Regulation of Jak2 through the ubiquitin-proteasome pathway involves phosphorylation of Jak2 on Y1007 and interaction with SOCS-1. *Mol Cell Biol*. **22**, 3316-26

Varoqueaux, F., Aramuni, G., Rawson, R. L., Mohrmann, R., Missler, M., Gottmann, K., Zhang, W., Sudhof, T. C., Brose, N. (2006). Neuroligins determine synapse maturation and function, *Neuron*. **51(6)**, 741-754

Waites, C. L., Craig, A. M., and Garner, C. C. (2005) Mechanisms of vertebrate synaptogenesis. *Annu. Rev. Neurosci*. **28**, 251–274

Xie, J., Allen, K. H., Marguet, A., Berghorn, K. A., Bliss, S. P., Navratil, A. M., Guan, J. L., Roberson, M. S. (2008). Analysis of the calcium-dependent regulation of proline-rice tyrosine kinase 2 by gonadotropin-releasing hormone. *Mol. Endocrinol.* **22**, 2322-2335

Yasuda, M., Umemori, H. (2009). Synapse formation in the mammalian central nervous system. In: Hortsch, M., Umemori, H. (Eds.), The Sticky Synapse: Cell adhesion molecules and their role in synapse formation and maintenance. Springer, New York, pp. 85-106

Yasuda, M., Johnson-Venkatesh, E. M., Zhang, H., Parent, J. M., Sutton, M. A., and Umemori, H. (2011) Multiple forms of activity-dependent competition refine hippocampal circuits *in vivo*. *Neuron*. **70**, 1128–1142

Yu, C. R., Power, J., Barnea, G., O'Donnell, S., Brown, H. E., Osborne, J., Axel, R., Gogos, J. A. (2004). Spontaneous neural activity is required for the establishment and maintenance of the olfactory sensory map. *Neuron*. **42**, 553–566

Yuste, R., Bonhoeffer, T. (2004). Genesis of dendritic spines: insights from ultrastructural and imaging studies. *Nature*. **5**, 24-34

Zhao, H., and Agazie, Y. M. (2015) Inhibition of SHP2 in basal-like and triple-negative breast cells induces basal-to-luminal transition, hormone dependency, and sensitivity to anti-hormone treatment. *BMC Cancer*. **15**, 109

Zhuang, J., Wei, Q., Lin, Z., Zhou, C. (2015). Effects of ADAM10 deletion on notch-1 signaling pathway and neuronal maintenance in adult mouse brain. *Gene.* **555**, 150-158